

**Facilitating Emergency Vehicle Passage in Congested Urban Areas
Using Multi-agent Deep Reinforcement Learning**

DISSERTATION

Submitted in Partial Fulfillment of
the Requirements for
the Degree of

DOCTOR OF PHILOSOPHY (Transportation Systems)

at the

NEW YORK UNIVERSITY
TANDON SCHOOL OF ENGINEERING

by

Haoran Su

**Facilitating Emergency Vehicle Passage in Congested Urban Areas
Using Multi-agent Deep Reinforcement Learning**

DISSERTATION

Submitted in Partial Fulfillment of
the Requirements for
the Degree of

DOCTOR OF PHILOSOPHY (Transportation Systems)

at the

NEW YORK UNIVERSITY
TANDON SCHOOL OF ENGINEERING

by

Haoran Su

Microfilm or other copies of this dissertation are obtainable from

UMI Dissertation Publishing

ProQuest CSA

789 E. Eisenhower Parkway

P.O. Box 1346

Ann Arbor, MI 48106-1346

Vita

Haoran Su was born in 1995 in Wuxi, China. He earned dual Bachelor's degrees in Civil Engineering and Computer Science in 2017, followed by a Master of Science in Systems Engineering in 2018, all from University of California, Berkeley. In Fall 2018, he started his doctoral studies in the Transportation Systems program at the Tandon School of Engineering, New York University. He is affiliated with the C2SMARTER Center, a Tier-1 University Transportation Research Center designated by the United States Department of Transportation. His research focuses on enhancing emergency vehicle passage in congested urban areas through multi-agent reinforcement learning methods.

Acknowledgements

I would like to express my deepest gratitude to my advisors, Professor Joseph Y.J. Chow and Professor Li Jin, for their patience, guidance, and inspiration, without which this dissertation would not have been possible. Their guidance and encouragement have shaped not only this dissertation but also my growth as a researcher and as an individual.

To my colleagues at C2SMARTER—Yueshuai He, Saeid Rasulkhani, Gyugeun Yoon, Ted Pantelidis, Qi Liu, Srushti Rath, Xi Xiong, Yu Tang, Qian Xie, and others—you have made this journey both meaningful and memorable.

Special thanks to my co-author and my mentor at Siemens, Yaofeng Desmond Zhong, for an inspiring summer internship that culminated in the honor of presenting our work at NeurIPS and AAI.

I would also like to acknowledge the financial support by Dwight David Eisenhower Transportation Fellowship, C2SMARTER, NSFC Project 62103260, SJTU UM Joint Institute, and J.Wu&J.Sun Endowment Fund.

My parents are my role models and my best friends. Though I have been frustrated and struggling, they never doubt what I could achieve. Every storm runs out of rain and I am sincerely proud to be your son.

I still remember the reviews received for my very first manuscript: *"this work makes very trivial contributions to academics or the society."* I hope this dissertation can be of a little help when it comes to saving patients and fighting fires or crimes in the future.

Haoran Su

To my parents
for your constant love and support.

ABSTRACT**Facilitating Emergency Vehicle Passage in Congested Urban Areas Using
Multi-agent Deep Reinforcement Learning**

by

Haoran Su**Advisors: Prof. Joseph Y.J. Chow, Ph.D.,P.E. and Prof. Li Jin, Ph.D.****Submitted in Partial Fulfillment of the Requirements for
the Degree of Doctor of Philosophy (Transportation Systems)****January 2025**

Emergency Response Time (ERT) serves as a pivotal metric of urban resiliency and public safety, encapsulating a city's capacity to respond promptly and effectively to medical, fire, and crime emergencies. Over the last decade, increasing urbanization and traffic congestion have severely exacerbated ERT, undermining emergency management systems and public trust. In New York City (NYC), average ERT for medical emergencies has surged by 72% from 7.89 minutes in 2014 to 14.27 minutes in 2024, with over 50% of delays attributable to prolonged Emergency Vehicle (EMV) travel times. These escalating

delays have dire consequences: every minute of delay during a stroke can lead to the loss of 2 million brain cells, and survival rates for cardiac arrest diminish by 7–10% per minute. This underscores the urgency of addressing EMV travel inefficiencies through advanced routing and traffic management strategies.

This dissertation responds to these critical challenges by advancing the state of EMV facilitation through three substantive contributions. First, it introduces *EMVLight*, a decentralized multi-agent reinforcement learning (MARL) framework that dynamically integrates EMV routing and adaptive traffic signal pre-emption. *EMVLight* leverages real-time traffic data and decentralized coordination between agents to optimize EMV travel paths while reducing disruptions to non-EMV traffic. Experimental results demonstrate a 42.6% reduction in EMV travel times and a 23.5% decrease in the average travel time for non-EMVs across synthetic and real-world traffic networks.

Second, the dissertation develops the *Dynamic Queue-Jump Lane (DQJL)* system, which employs Multi-Agent Proximal Policy Optimization (MAPPO) to enable coordinated lane-clearing maneuvers in mixed-traffic environments comprising autonomous and human-driven vehicles. By dynamically forming queue-jump lanes in response to real-time traffic conditions, DQJL minimizes lane-change maneuvers and reduces EMV travel times by up to 40%, with benefits amplified under higher autonomous vehicle penetration rates.

Third, the dissertation conducts an equity-focused evaluation of Emergency Medical Services (EMS) accessibility in NYC, integrating demographic, infrastructural, and traffic data to uncover disparities in response times across boroughs. Findings reveal systemic inequities, with Staten Island experiencing the longest delays due to sparse signalized intersections, while Manhattan, despite its dense network, faces severe congestion. The study proposes actionable interventions, including optimized EMS station placements,

improved intersection configurations, and equitable resource allocation, to address these disparities.

Collectively, these contributions provide a robust foundation for enhancing EMV mobility, reducing response times, and ensuring equitable access to emergency services. The methodologies and insights presented herein offer significant implications for policymakers, transportation engineers, and urban planners, advancing the development of safer, more efficient, and resilient urban transportation systems.

Keywords: Emergency Response Time, Multi-Agent Reinforcement Learning, Traffic Signal Pre-emption, Dynamic Queue-Jump Lane, Emergency Medical Services, Urban Resiliency, Transportation Equity.

Table of Contents

Vita	iii
Acknowledgements	iv
Abstract	vi
List of Figures	xv
List of Tables	xviii
1 Introduction	1
1.1 Background and Motivation	1
1.2 Research Challenges	4
1.3 Dissertation Contributions and Summary	7
2 EMVLight: a Multi-agent Reinforcement Learning Framework for an Emer-	
gency Vehicle Decentralized Routing and Traffic Signal Control System	11
2.1 Introduction	11
2.2 Literature Review	16
2.3 Preliminaries	19
2.4 Methodology	25
2.5 Experimentation	37
2.6 Results and Discussion	43

	x
2.7 Summary	57
3 Dynamic Queue-jump Lane for Emergency Vehicles: a Multi-agent Proximal Policy Optimization Approach	59
3.1 Introduction	59
3.2 Literature Review	62
3.3 Dynamic Queue Jump Lanes in Mixed Traffic	69
3.4 Multi-Agent Learning for DQJLs	77
3.5 Experimental Setup	85
3.6 Results and Discussion	89
3.7 Summary	104
4 Intersection-Aware Assessment of EMS Accessibility in NYC: A Data-Driven Approach	106
4.1 Introduction	106
4.2 Related Works	109
4.3 Methodology	114
4.4 Results	124
4.5 Discussion	132
4.6 Summary	139
5 Conclusions	141
5.1 Research Findings	141
5.2 Limitations and Future Directions	144
5.3 Closing Remarks	147
A Appendix for Chapter 1	185

	xi
A.1 Implementation Details	185
A.2 Hyperparameters	187
A.3 Emergency Lane in SUMO	187
B Appendix for Chapter 2	189
B.1 Network Details for CAVs	189
B.2 SUMO Configurations	192
C Appendix for Chapter 3	195
C.1 Demographic maps	195

List of Figures

1.1	NYC 911 End-to-End ERTs for July 2014 and July 2024, across all incident categories.	3
1.2	NYC 911 EMV travel times for July 2014 and July 2024, across all incident categories.	4
2.1	Traffic movements of a four-way two-lane bidirectional intersection. . .	20
2.2	<i>Top</i> : 8 signal phases; <i>Left</i> : phase #2 illustration; <i>Right</i> : phase #5 illustration.	21
2.3	A demonstration of an emergency lane for EMV passage. <i>Top</i> : the EMV has to follow the congested queue due to insufficient emergency capacity; <i>Bottom</i> : the EMV is traversing on the yielded emergency lane due to sufficient emergency capacity.	24
2.4	EMVLight routing (top) vs conventional Dijkstra’s routing (bottom). . .	28
2.5	Types of agents through the EMV’s passage to the destination.	32
2.6	Overview of MA2C framework for EMVLight’s navigation and traffic signal control.	35

2.7	<i>Left</i> : the synthetic grid $_{5 \times 5}$. Origin and destination for EMV are labeled. <i>Right</i> : an intersection illustration in SUMO, the teal area are inductive loop detected area.	38
2.8	Emergency-capacitated Synthetic Grid $_{5 \times 5}$. Segments towards intersections highlighted by blue have emergency capacities.	40
2.9	Manhattan $_{16 \times 3}$: a 16-by-3 traffic network in Hell's Kitchen area. Origin and destination for the EMV dispatching are labeled. <i>Left</i> : on Google Map; <i>Right</i> : in SUMO simulator.	41
2.10	Hangzhou $_{4 \times 4}$: a 4-by-4 irregular and asymmetric network. Origin and destination for the EMV dispatching are labeled. <i>Left</i> : on Google Map; <i>Right</i> : in SUMO simulator.	42
2.11	T_{EMV} convergence by learning-based dynamic routing strategies on Manhattan $_{16 \times 3}$	49
2.12	T_{avg} convergence by learning-based dynamic routing strategies on Manhattan $_{16 \times 3}$	49
2.13	T_{EMV} convergence by learning-based dynamic routing strategies on Hangzhou $_{4 \times 4}$	51
2.14	T_{avg} convergence by learning-based dynamic routing strategies on Hangzhou $_{4 \times 4}$	51
2.15	EMV's routing choice on Emergency-capacitated Synthetic Grid $_{5 \times 5}$ based on EMVLight. Emergency lane established for EMV passage on segments highlighted in green, and not established on segments in red.	52
2.16	EMV's routing choice on config 1 of Emergency-capacitated Synthetic Grid $_{5 \times 5}$ under MP-based benchmarks.	53
2.17	The corresponding route selected by (a) W+static+MP, (b) W+dynamic+MP, (c) EMVLight on Hangzhou $_{4 \times 4}$. Distance and T_{EMV} for the selected path are indicated. The lowest values are highlighted in bold.	54

2.18	EMV's route choice on Hangzhou _{4×4} with replaced primary (a) and secondary (b) agents.	55
2.19	Reward convergence with and without fingerprint. Experiments are conducted on Config 1 synthetic grid _{5×5}	56
3.1	Illustration of a DQJL formation: Green vehicles are CAVs and yellow ones are HDVs. HDVs yields and CAVs perform coordinated lane changes for a DQJL.	65
3.2	An alternative DQJL formation, where the EMV will change lane once.	66
3.3	Comparison of EMV travel time (a) and reward (b) per episode achieved by learning-based methods.	93
3.4	Reward convergence with and without parameter sharing for CAVs.	104
4.1	EMS Stations (Blue) and Hospitals (Red) in NYC.	115
4.2	All NYC streets following NYC Street Centerline.	116
4.3	Signalized intersections layout in Brooklyn and Queens	117
4.4	Census tracts in Staten Island. Each polygon represents a census tract.	118
4.5	Population distribution of NYC census tracts.	119
4.6	Travel time distributions for EMS stations across different α values.	127
4.7	Travel time distributions for Hospital across different α values.	128
4.8	EMV travel time trend based on 911 NYC End-to-End.	129
4.9	EMS travel time heatmap, with heated regions highlighting the vulnerable regions.	131
4.10	Population covered by EMS accessibility as a function of τ	133
4.11	Synthetic Grid _{5×5} and the inner 9 intersections are observed for intersection delay.	137

	xv
4.12 Amount of time to pass intersections for EMVs.	138
4.13 Population coverage function against τ with $\alpha = 7.5s \cdot m^2$	138
A.1 A blue light device approaching an intersection with the sublane model activated.	188
C.1 Population of 65+ years old distribution of NYC census tracts	196
C.2 Median age distribution of NYC census tracts.	197
C.3 Median income distribution of NYC census tracts	198
C.4 Poverty percentage distribution of NYC census tracts	199

List of Tables

- 2.1 Time complexities of the proposed routing heuristic and the dynamic shortest-path approach. M can be arbitrarily set to determine the updating frequency. The larger M is, the shorter selected route can be. 28
- 2.2 Configuration for Synthetic Grid_{5×5}. Peak flow is assigned from 400s to 800s and non-peak flow is assigned out of this period. For Config. 1 and 2, the vehicles enter the grid from North and South, and exit toward East and West. 39
- 2.3 EMV travel time in the four configurations of Synthetic Grid_{5×5}. Lower value indicates better performance and the lowest values are highlighted in bold. 44
- 2.4 Average travel time for all vehicles which have completed trips in the four configurations of Synthetic Grid_{5×5}. 44
- 2.5 EMV travel time in the four configurations of Synthetic Grid_{5×5} with an emergency capacity co-efficient of 0.25. 46
- 2.6 Average travel time for all vehicles which have completed trips in the four configurations of Synthetic Grid_{5×5} with an emergency capacity coefficient of 0.25. 47

2.7	T_{EMV} and T_{avg} for Manhattan _{16×3} . The average travel time without the presence of EMVs (1649.64) is retrieved from data.	48
2.8	T_{EMV} and T_{avg} for Gudang _{4×4} . The average travel time without the presence of EMVs (764.08) is retrieved from data.	50
2.9	Ablation studies on pressure-based reward design and agent types. Experiments are conducted on Hangzhou _{5×5} . The lowest value are highlighted in bold.	55
2.10	EMVLight's performance on Emergency-capacitated Synthetic Grid _{5×5} with Configuration 1 given different values of β	57
3.1	Performance for all methods on evaluation metrics in the Two-Lane Roadway across different penetration rates. Bold values indicate the best performance.	90
3.2	Performance metrics on the Three-Lane Roadway across different penetration rates. Bold values indicate the best performance.	93
3.3	Performance metrics on the Four-Lane Roadway across different penetration rates. Bold values indicate the best performance.	95
3.4	Performance metrics on the Two-Lane Roadway across varying traffic densities. Bold values indicate the best performance.	96
3.5	Performance metrics on the Three-Lane Roadway across varying traffic densities. Bold values indicate the best performance.	98
3.6	Performance metrics on the Four-Lane Roadway across varying traffic densities. Bold entries indicate best performance.	100
3.7	Effects of different α values on EMV passage time and lane-change maneuvers on the Three-Lane Roadway with 15 veh/lane/min and 50% CAV penetration rate.	102

	xviii
4.1	Number of EMS Stations and Hospitals by boroughs in NYC 114
4.2	Total area, population and population density for boroughs and NYC. . . 123
4.3	Summary of travel time [mins] for EMS stations, hospitals, and combined (Overall) given different α values. 126
4.4	Statistics for actual travel time (T_{actual}) based on 911 End-to-End reports. The ratio $T_{actual}/T_{simulated}$ compares actual travel time to simulated travel time for overall medical service when $\alpha = 15 \text{ s} \cdot \text{m}^2$ 130
A.1	Hyper-parameters selected for RL-based methods. 187
B.1	Parameter summary for MAPPO-DQJL simulations 194

Chapter 1

Introduction

In this chapter, we present the background and motivations underpinning this dissertation in Section 1.1, providing a comprehensive overview of the problem domain and its significance. Section 1.2 identifies the key research challenges that this work aims to address, highlighting gaps in the existing literature and practical constraints. Finally, Section 1.3 outlines the major contributions and structure of this dissertation.

1.1 Background and Motivation

Emergency Response Time (ERT) is a critical metric for assessing urban resiliency and public safety, reflecting a city's capacity to respond promptly and effectively to a diverse range of emergencies, including medical incidents, fire outbreaks, and criminal activities. Shorter ERTs are indicative of well-coordinated emergency response systems, efficient infrastructure, and sufficient resource allocation. Conversely, delays in ERT exacerbate the severity of incidents, increasing risks to human life and property.

Over the past decade, urban centers have faced mounting challenges in maintaining

optimal ERT levels, primarily due to increasing traffic congestion. As urban populations grow and vehicular density escalates, the mobility of Emergency Vehicles (EMVs) is increasingly compromised. This trend has led to significant delays in emergency response, with profound implications for public health and safety. Prolonged ERTs correlate with higher mortality rates in critical medical cases, more extensive damage during fire incidents, and reduced effectiveness in deterring or containing criminal activities. Collectively, these factors undermine public trust in emergency management systems.

Taking New York City (NYC) as an illustrative case, Fig. 1.1 presents the end-to-end ERT for all emergency incident types, comparing data from July 2014 to July 2024, as reported in the NYC 911 End-to-End Response Time dataset [1]. The values annotated above each bar represent the average ERT (minutes), with the percentage increase over the ten-year period highlighted in red for each incident type. Notably, ERTs have increased significantly across all categories, with non-critical and non-life-threatening cases experiencing the most severe delays.

Among the various stages of emergency response, spanning from incident reporting to on-scene arrival, the increased travel time of EMVs accounts for over 50% of the observed growth in ERT within NYC, as illustrated in Fig. 1.2. This escalation is primarily attributed to worsening traffic congestion in NYC. In 2024, INRIX, a global traffic analytics service, identified NYC as the most congested city globally [2], with drivers enduring an average of 101 hours annually in traffic delays—a significant increase compared to the 91 hours recorded in 2014, marking a ten-hour rise over the decade.

The implications of delayed emergency responses are severe. For instance, a stroke victim loses approximately 2 million brain cells for every minute of delayed medical intervention [3], while survival rates during cardiac arrest decline by 7–10% with each minute of delay [4]. Despite having designated rights-of-way on urban roads, EMVs

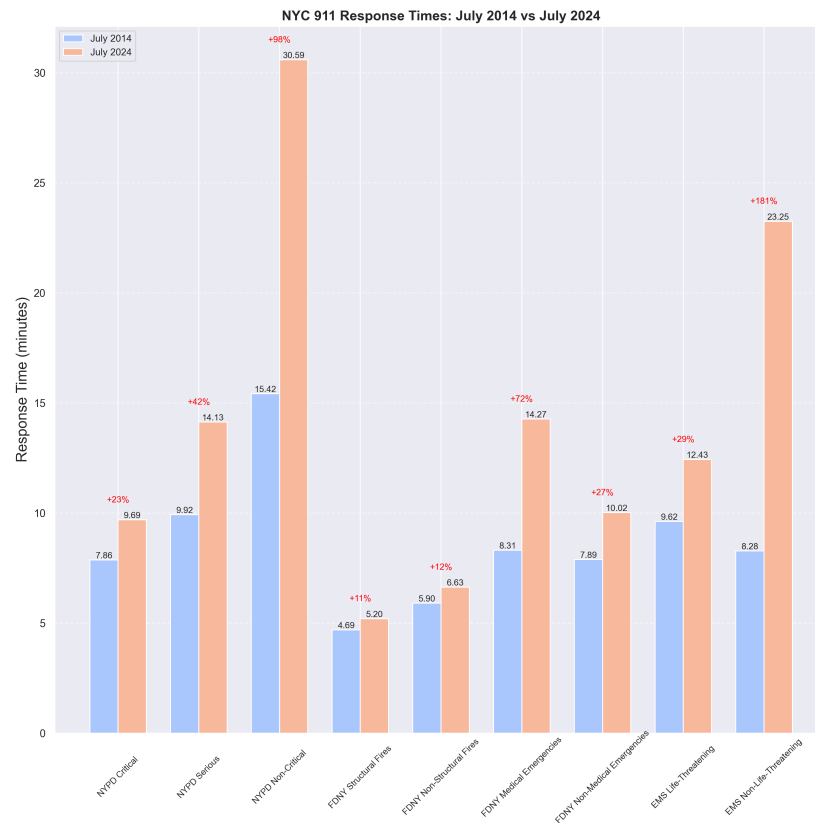


Figure 1.1: NYC 911 End-to-End ERTs for July 2014 and July 2024, across all incident categories.

face mounting challenges in navigating through increasingly congested streets to reach emergency scenes in a timely manner.

Escalating traffic congestion not only impedes the mobility of EMVs but also undermines their capacity to meet critical response time benchmarks, thereby compounding risks to public health and safety. This alarming trend underscores the pressing need for innovative strategies to facilitate the mobility of EMVs, ensuring that life-saving interventions can be delivered without avoidable hindrance.

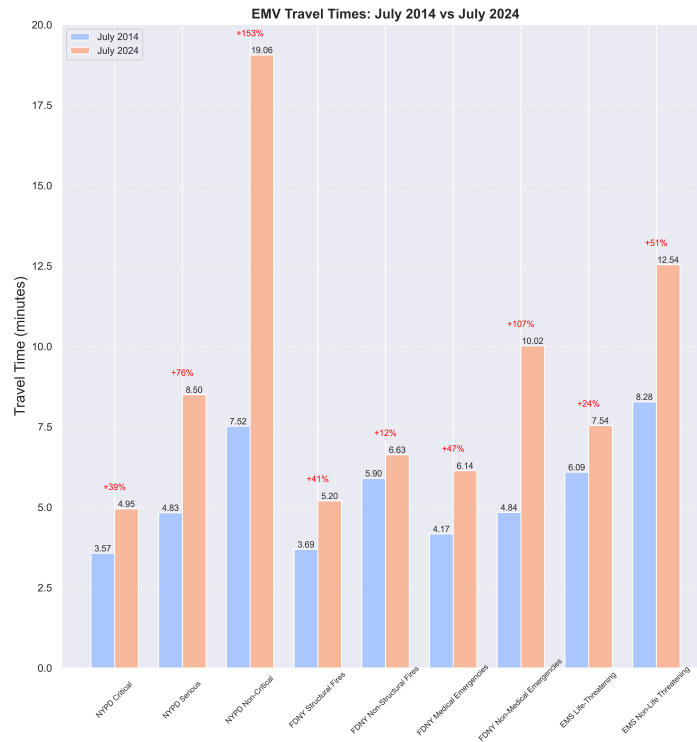


Figure 1.2: NYC 911 EMV travel times for July 2014 and July 2024, across all incident categories.

1.2 Research Challenges

1.2.1 Coupling of EMV Navigation and Traffic Signal Pre-emption

Efficient EMV passage in urban traffic networks presents two interrelated challenges: dynamically routing EMVs under time-dependent traffic conditions and coordinating traffic signal pre-emption to minimize delays for both EMVs and non-EMVs.

The first challenge arises from the inherently dynamic nature of urban traffic, where congestion levels fluctuate across road segments in real time. As an EMV progresses through the network, its routing decisions must be continuously updated to account

for evolving traffic conditions. Traditional approaches, such as recalculating shortest paths at every intersection, are computationally expensive and fail to meet the real-time requirements of EMV passage. Therefore, an efficient and adaptive routing algorithm is essential to ensure timely and computationally feasible updates to the EMV's route.

The second challenge concerns the coordination of traffic signals to achieve dual objectives: prioritizing EMV passage while minimizing network-wide disruptions for non-EMVs. Conventional methods often focus exclusively on reducing EMV travel time, disregarding the broader impact on non-EMVs. Vehicles along an EMV's path are often required to stop or pull over, yet the absence of clear and coordinated guidance from traffic signals frequently results in unnecessary delays. Moreover, non-EMVs at adjacent intersections may experience additional disruptions due to the lack of coordination in addressing the cascading delays caused by EMV pre-emption. Addressing this challenge requires traffic signals to operate collaboratively across the network, balancing the urgent need for EMV prioritization with minimizing delays for non-EMVs.

Compounding these challenges are the stochastic and unpredictable characteristics of urban traffic, which introduce significant uncertainties into both routing and signal control decisions. These uncertainties are further exacerbated by the cascading disruptions caused by EMV pre-emption, which ripple through the traffic network and amplify congestion. Addressing these issues necessitates a holistic approach capable of dynamically adapting to real-time traffic conditions, coordinating actions across the network, and accounting for the inherent uncertainties of urban traffic environments. Chapter 2 aims to address these challenges.

1.2.2 Intra-link Movement for EMV

From a microscopic perspective, the intra-link traversal of EMVs poses significant challenges. While traffic laws mandate yielding the right-of-way to EMVs, and most drivers instinctively comply, their uncoordinated and unpredictable maneuvers often result in suboptimal outcomes, especially on congested roadways. This lack of coordination leads to inefficiencies and delays that undermine the effectiveness of emergency responses.

Despite advancements in vehicle-to-everything (V2X) technologies designed to enhance EMV mobility, sirens remain the primary tool relied upon in practice. However, traditional siren systems frequently fail to provide sufficient warning time to other drivers, particularly in heavily congested traffic conditions. Furthermore, ambiguity regarding which route should be cleared often causes confusion, delaying the EMV's progress. These uncertainties exacerbate delays and contribute to accident rates that are 4 to 17 times higher [5], along with increased collision severity [6]. These factors not only hinder EMV traversal but also pose additional risks to traffic safety, highlighting the urgent need for effective solutions.

Current lane-clearing strategies in emergency scenarios predominantly rely on mixed-integer linear programming (MILP) formulations. While these approaches offer theoretical insights, they often oversimplify real-world traffic dynamics and fail to provide actionable decisions in real time. The reliance on computationally intensive models makes them unsuitable for dynamic, time-sensitive scenarios. Additionally, these methods struggle to account for the stochastic nature of traffic flows, unexpected driver behaviors, and the cascading disruptions caused by lane-clearing maneuvers.

The core challenge, therefore, is how to quickly establish a cleared and easy-to-manuever route for EMV passage on a road segment while minimizing additional distur-

bances for non-EMVs. Addressing this challenge requires innovative strategies capable of capturing real-time traffic information, managing uncertainties, and delivering computationally efficient solutions that can infer optimal actions within milliseconds. Meeting this need is critical for ensuring timely and safe EMV traversal through congested urban traffic. Chapter 3 focuses on providing a solution.

1.3 Dissertation Contributions and Summary

This dissertation addresses the aforementioned challenges associated with efficient EMV passage in congested urban areas, adopting a comprehensive approach that spans network-level EMV route optimization to intra-link EMV passage strategies. By systematically reducing EMV travel time and mitigating downstream traffic disturbances, the proposed methods aim to enhance emergency response efficiency. Furthermore, a qualitative case study on the emergency accessibility of NYC is conducted to evaluate the potential of the proposed solutions in a real-world setting. The research topics explored in this dissertation represent some of the earliest contributions in EMV passage, addressing critical gaps between theoretical concepts and their practical applications in real-world scenarios.

1.3.1 EMVLight

Chapter 2 introduces *EMVLight*, a decentralized multi-agent reinforcement learning (MARL) framework that addresses two critical challenges mentioned above: dynamically routing EMVs under time-dependent traffic conditions and coordinating traffic signal pre-emption to minimize delays for both EMVs and non-EMVs. Dynamic EMV routing is particularly challenging due to the evolving nature of road congestion, which requires

real-time updates to routing decisions without the computational burden of recalculating shortest paths at every intersection. Similarly, traffic signal pre-emption must balance the need to prioritize EMVs along their routes while ensuring network-wide efficiency, a task that demands coordinated adjustments across the entire traffic network. To address these challenges, *EMVLight* models each intersection as an autonomous agent capable of optimizing local traffic flow and coordinating with neighboring agents to facilitate EMV passage. The framework incorporates three key contributions: a mathematical model for emergency lane formation, which evaluates road segment capacity and dynamically re-locates lanes to enable full-speed EMV travel; a decentralized path-finding algorithm that leverages real-time traffic information to adapt EMV routes efficiently; and an integrated MARL approach that jointly optimizes EMV routing and traffic signal control through specialized agents with tailored reward functions. Experimental results demonstrate that *EMVLight* achieves up to a 42.6% reduction in EMV travel time and a 23.5% decrease in the average travel time for all vehicles, significantly outperforming existing methods across both synthetic and real-world traffic networks for this problem.

1.3.2 MAPPO-DQJL

Chapter 3 introduces dynamic queue-jump lanes (DQJLs) as a novel intra-link coordination strategy designed to expedite EMV passage through congested road segments. Extending the traditional concept of queue-jump lanes (QJLs) used in bus operations, DQJLs dynamically form lanes during an EMV’s approach or traversal, leveraging V2X communication technologies to coordinate connected autonomous vehicles (CAVs) while accounting for non-connected human-driven vehicles (HDVs). To address the inherent complexity of mixed traffic environments, we model DQJL formation as a partially observable Markov decision process (POMDP), which captures both the controllable be-

havior of CAVs and the stochastic, unpredictable nature of HDVs. To optimize the DQJL formation process, we develop a multi-agent proximal policy optimization algorithm (MAPPO-DQJL) that employs centralized training with decentralized execution, enabling CAVs to efficiently coordinate lane-clearing maneuvers while minimizing disruptions to all non-EMVs. This framework effectively balances the dual objectives of reducing EMV passage time and reducing disturbance to overall traffic, demonstrating scalability across varying CAV penetration rates and traffic densities in multilane roadways. Through extensive SUMO-based simulations, the proposed framework is validated, achieving up to 39.8% reduction in EMV passage times and up to 55.7% reduction in lane-changing maneuvers compared to baseline methods, with particularly pronounced benefits under scenarios of increasing CAV adoption. These contributions address critical gaps in current EMV passage strategies, providing a robust and scalable solution for integrating DQJLs into EMV management systems.

1.3.3 EMS Accessibility Study of NYC

Chapter 4 presents a comprehensive intersection-aware EMS accessibility model to address the critical challenge of EMS accessibility in congested urban environments, focusing on NYC as a case study. By integrating road network characteristics, intersection density, and population demographics, the proposed model provides a granular evaluation of EMS accessibility, identifying vulnerable regions where response times exceed critical benchmarks. The study introduces a novel metric that incorporates intersection-induced delays into travel time calculations, capturing the complexities of urban traffic networks more realistically. Additionally, it highlights the disparities in EMS coverage across NYC boroughs, with significant accessibility gaps in Staten Island, Queens, and parts of Manhattan. The implementation of *EMVLight*, introduced in Chapter 2, is further

explored to demonstrate its potential in reducing intersection delays, improving hospital accessibility, and ensuring that over 95% of NYC residents are served within the benchmark response time. These contributions lay a robust foundation for advancing emergency traffic management strategies and guiding urban planning decisions aimed at equitable and efficient EMS accessibility.

1.3.4 Dissertation Outline

The remainder of this dissertation is organized as follows. Chapter 2 introduces *EMV-Light*, a multi-agent reinforcement learning framework for EMV decentralized routing and traffic signal control. Chapter 3 proposes MAPPO-DQJL, an innovative approach that facilitates intra-link EMV movements through cooperative and efficient lane-clearing strategies. Chapter 4 presents a case study on EMS accessibility in New York City, providing valuable insights into the potential impacts of deploying *EMV-Light* in real-world settings. Finally, Chapter 5 concludes with a summary of research contributions, a discussion of research limitations, and potential directions for future work.

Chapter 2

EMVLight: a Multi-agent Reinforcement Learning Framework for an Emergency Vehicle Decentralized Routing and Traffic Signal Control System¹

2.1 Introduction

Emergency vehicles (EMVs) include ambulances, fire trucks, and police cars, which respond to critical events such as medical emergencies, fire disasters, and public security crisis. Emergency response time is the key indicator of a city's incidents management

¹This chapter has been published in Transportation Research Part C: Emerging Technologies, and can be referenced as: Su, H., Zhong, Y. D., Chow, J. Y., Dey, B., & Jin, L. (2023). EMVLight: A multi-agent reinforcement learning framework for an emergency vehicle decentralized routing and traffic signal control system. *Transportation Research Part C: Emerging Technologies*, 146, 103955.

ability and resiliency. Reducing response time saves lives and prevents property losses. For instance, Berdowski et al. [7] indicated that the survivor rate from a sudden cardiac arrest without treatment drops 7% - 10% for every minute elapsed, and there is barely any chance to survive after 8 minutes. EMV travel time, the time interval for an EMV to travel from a rescue station to an incident site, accounts for a major portion of the emergency response time. However, overpopulation and urbanization have exacerbated road congestion, making it more challenging to reduce the average EMV travel time. Records [8] have shown that even with a decline in average emergency response time, the average EMV travel time increased from 7.2 minutes in 2015 to 10.1 minutes in 2021 in New York City, an approximately 40% increase over six years even accounting for post-Covid traffic conditions. Therefore, there is a severe urgency and significant benefit for shortening the average EMV travel time on increasingly crowded roads.

Existing work has studied strategies to reduce the travel time of EMVs by route optimization and traffic signal pre-emption [9, 10]. Route optimization refers to the search for a time-based shortest path. The traffic network (e.g., city road map) is modeled as a graph with intersections as nodes and road segments between intersections as edges. Based on the time a vehicle needs to travel through each edge (road segment), route optimization calculates an optimal route with the minimal EMV travel time [10]. In addition, as the EMV needs to be as fast as possible, the law in most places requires non-EMVs to yield to emergency vehicles sounding sirens, regardless of the traffic signals at intersections [11]. Even though this practice gives the right-of-way to EMVs, it poses safety risks for vehicles and pedestrians at intersections [12]. To address this safety concern, existing methods [13, 14, 10, 15] have also studied traffic signal pre-emption which refers to the process of deliberately altering the signal phases at each intersection to prioritize EMV passage.

However, a major challenge for adaptive EMV operation is the coupling between EMV route optimization and traffic light pre-emption [10]. As the traffic condition constantly changes, static route optimization can potentially become suboptimal as an EMV travels through the network; i.e. the traffic is highly time-dependent and exhibits transient properties during a dispatch [16]. Moreover, traffic signal pre-emption has a significant impact on the traffic flow, which would change the fastest route as well. Thus, the optimal route should be updated with real-time traffic flow information, i.e., the route optimization should be solved in a dynamic (time-dependent) way. As an optimal route can change as an EMV travels through the traffic network, the traffic signal pre-emption would need to adapt accordingly. In other words, the subproblems of dynamic route optimization and traffic signal pre-emption are coupled and should be solved ideally simultaneously in real-time. Existing approaches have limited consideration to this coupling.

In addition, most of the existing models on emergency vehicle service have a single objective of reducing the EMV travel time [17, 18, 19, 20]. As a result, their traffic signal control strategies have an undesirable effect of increasing the travel time of non-EMVs. Non-EMVs on the path of approaching EMVs would pull over or stop, and they usually do not receive clear guidance from traffic signals on resuming their trips [21], causing unnecessary delay. Non-EMVs elsewhere are also likely indirectly and negatively impacted if adjacent intersections lack coordination to address the incurred delay [10]. Therefore, traffic signal control strategies accommodating both EMVs and non-EMVs need to be recommended.

In this chapter, we aim to perform route optimization and traffic signal pre-emption to not only reduce EMV travel time but also to reduce the average travel time of non-EMVs. In particular, we address the following two key challenges:

1. **How to dynamically route an EMV to a destination under time-dependent traffic conditions in a computationally efficient way?** As the congestion level of each road segment changes over time, the routing algorithm should be able to update the remaining route as the EMV passes each intersection. Running the shortest-path algorithm each time the EMV passes through an intersection is not efficient. A computationally efficient decentralized routing algorithm is desired.
2. **How to coordinate traffic signals to not only reduce EMV travel time but reduce the average travel time of non-EMVs as well?** To reduce EMV travel time, only the traffic signals along the route of the EMV need to be altered. However, to further reduce average non-EMV travel time, traffic signals in the whole traffic network need to cooperate.

Reinforcement learning (RL), which gained significant traction in assorted domains of traffic signal control recently, has been extensively studied and proven effective for learning stochastic traffic conditions and dealing with randomness. Thus, to tackle the above challenges, we propose **EMVLight**, a decentralized multi-agent reinforcement learning framework with a dynamic routing algorithm to control traffic signal phases for efficient EMV passage. In the proposed RL design, each intersection is an agent and each agent is responsible for deciding local traffic signal phases. Multiple agents coordinate to facilitate EMV passage as well as alleviate congestion. Our experimental results demonstrate that EMVLight outperforms traditional traffic engineering methods and existing RL methods under two metrics - EMV travel time and the average travel time of all vehicles - on different traffic configurations. We extend the preliminary work [22] by taking into account extra capacity of each road segments and the possibility of forming “emergency lanes” for full speed EMV passage. In addition, we demonstrate

EMVLight’s performance on synthetic and real-world maps with extra capacities. We also present the difference in EMV routing between EMVLight and benchmark methods with an emphasize on the number of successfully formed emergency lanes.

Our contributions are threefold. First, we capture the emergency capacity in road segments for emergencies and incidents. We also propose a mathematical model to decide whether an emergency lane can be formed for full speed EMV passage based on emergency capacity and number of vehicles of a road segment. Second, we incorporate a decentralized path-finding scheme for EMVs based on real time traffic information. Third, we propose to solve EMV routing and traffic signal control problems simultaneously in a multi-agent reinforcement learning framework. In particular, we set up different types of reinforcement learning agents based on the location of the EMV and design different rewards for each type. This leads to up to a 42.6% reduction in EMV travel time as well as an 23.5% shorter average travel time of all trips completed in the network compared with existing benchmark methods.

The rest of the paper is organized as follows. Section 2.2 reviews relevant literature. Section 2.3 introduces our definition of pressure and emergency capacity. Section 2.4 presents our EMVLight methodology, i.e., dynamic routing and reinforcement learning. Benchmark methods and experimental setup are presented in Section 2.5. Section 2.6 discussed and compared the performance of EMVLight and benchmark methods in terms of EMV travel time, average travel time of all vehicles as well as EMV route choices. We conclude in Section 2.7 and share inspirations on future directions.

2.2 Literature Review

Conventional routing optimization and traffic signal pre-emption for EMVs.

Although routing and pre-emption are coupled in reality, existing methods usually solve them separately. Many of the existing approaches leverage Dijkstra's shortest path algorithm to determine the optimal route [23, 24, 25, 26]. Nordin et al. [27] proposed an A* algorithm for ambulance routing, assuming that routes and traffic conditions are fixed and static, which fails to address the dynamic nature of real-world traffic flows. Another line of work considers the temporal dynamics of traffic flows. For instance, Ziliaskopoulos et al. [28] developed a shortest-path algorithm for time-dependent traffic networks, assuming that travel times associated with each edge are known in advance. Similarly, Musolino et al. [29] proposed routing strategies tailored to specific times of the day (e.g., peak/non-peak hours) based on historical traffic data. However, in the problem under consideration, routing and pre-emption strategies can significantly influence the travel time of each edge during the EMV passage, and the existing methods fail to handle such real-time changes effectively. Haghani et al. [18] formulated the dynamic shortest path problem as a mixed-integer programming model, and Koh et al. [30] utilized reinforcement learning (RL) for real-time vehicle navigation and routing. Related studies [31, 32, 33, 34, 35, 36, 37, 38, 39, 40] explored adaptive routing problems in various stochastic and time-dependent traffic scenarios. However, none of these works considered the coupling of traffic signal pre-emption with EMV routing or the specific context of EMV passage when solving shortest path problems.

Once an optimal route for the EMV has been determined, traffic signal pre-emption is deployed to further reduce the EMV travel time. A common pre-emption strategy is to extend the green phases of traffic signals to allow the EMV to pass through intersections

along a fixed optimal route [23, 41]. Pre-emption strategies for handling multiple EMV requests were introduced by Asaduzzaman et al. [42]. Wu et al. [43] approached the lane-clearing problem for emergency vehicles from a microscopic motion planning perspective, while Hosseinzadeh et al. [44] developed an EMV-centered traffic control scheme for multiple intersections to alleviate congestion. While these studies offer valuable insights into pre-emption strategies, they do not consider the dynamic routing of EMVs to determine the optimal path.

For a thorough survey of conventional routing optimization and traffic signal pre-emption methods, readers are referred to Lu et al. [9] and Humagain et al. [10]. It is worth noting that conventional methods prioritize EMV passage, often causing significant disturbances to traffic flow and increasing the average travel time for non-EMVs.

RL-based traffic signal control. Traffic signal pre-emption only adjusts traffic phases at intersections where an EMV travels. However, reducing congestion often requires coordinated phase adjustments at nearby intersections. The problem of coordinating traffic signals to mitigate congestion has been addressed using deep reinforcement learning (RL) in an increasing body of research. Abdulhai et al. [45] were among the first to apply Q-learning, a model-free RL method, to adaptive traffic signal control. Their work demonstrated the concept for both isolated traffic signal controllers and networks of controllers. However, as the state representation grows exponentially with the number of traffic signals, the learning process becomes computationally expensive, and their study was limited to isolated intersections. Prashanth et al. [46] introduced feature-based state representations to address the curse of dimensionality, reducing computational complexity while improving performance. El-Tantawy et al. [47] incorporated game-theoretic approaches into Q-learning, allowing agents to converge to best-response policies relative to their neighbors.

The advent of deep neural networks enabled more advanced applications of RL. Van der Pol et al. [48] integrated deep Q-networks (DQN) into traffic coordination tasks, which inspired subsequent research leveraging the Q-learning framework for traffic signal control. For instance, CoLight [49] utilized graph attentional networks to enhance communication and cooperation between traffic signals, while FRAP [50] introduced a phase competition model to improve RL-based methods. PressLight [51] incorporated the max pressure strategy [52, 53, 54, 55, 56] into reward design, achieving better results than traditional designs. ThousandLights [57] combined FRAP and PressLight to achieve city-level traffic signal control, and Zang et al. [58] employed meta-learning algorithms to accelerate Q-learning.

Actor-critic methods represent another category of RL approaches that address the scalability challenge in multi-agent settings. Aslani et al. [59] demonstrated the effectiveness of actor-critic controllers for adaptive signal control under different disruption scenarios, while Xu et al. [60] introduced a hierarchical actor-critic method to foster cooperation between intersections. Chu et al. [61] used a multi-agent independent advantage actor-critic algorithm, and Ma et al. [62] proposed a manager-worker hierarchy to manage traffic locally within actor-critic frameworks. While existing RL-based traffic control methods effectively reduce network congestion, they are not designed specifically for EMV pre-emption. In contrast, the proposed RL framework builds on state-of-the-art methods, such as max pressure, to minimize both EMV travel time and overall congestion. Moreover, the centralized training with decentralized execution paradigm enables compatibility with stochastic traffic settings while incurring minimal communication costs. Mo et al. [63] investigated traffic signal control strategies based on connected vehicle communications, illustrating the potential of RL in this domain.

For a detailed review of RL-based traffic signal control, see Noaen et al. [64] and

Wei et al. [65]. While RL methods have demonstrated effectiveness in traffic signal control, no existing studies have explicitly addressed the unique challenges posed by EMV passages or their impact on non-EMV traffic flow.

Intra-link EMV traversal strategies. Advances in vehicle-to-vehicle communication technology [66] have sparked interest in optimizing EMV traversal strategies on congested road links. Agarwal et al. [67] proposed Fixed Lane and Best Lane strategies for EMV traversal, which were further analyzed by Insaf et al. [68], showing that Fixed Lane outperforms Best Lane under conditions of low speed variance. Hannoun et al. [69, 70] developed a semi-automated warning system that instructs downstream traffic to yield using mixed-integer linear programming. This system adapts to varying connected vehicle penetration rates and is validated as computationally efficient for real-time deployment. Su et al. [71] proposed a dynamic queue-jump lane (DQJL) strategy leveraging multi-agent reinforcement learning.

2.3 Preliminaries

In this section, we introduce relevant preliminary terms and definitions which facilitate the problem formulation.

2.3.1 Traffic map, movement and signal phase

A traffic map can be represented by a graph $G(\mathcal{V}, \mathcal{E})$, with intersections as nodes and road segments between intersections as edges. We refer to a one-directional road segment between two intersections as a link. A link has a fixed number of lanes, denoted as $h(l)$ for lane l . Vehicles are allowed to switch lane between two intersections. Fig. 2.1 shows 8 links and each link has 2 lanes.

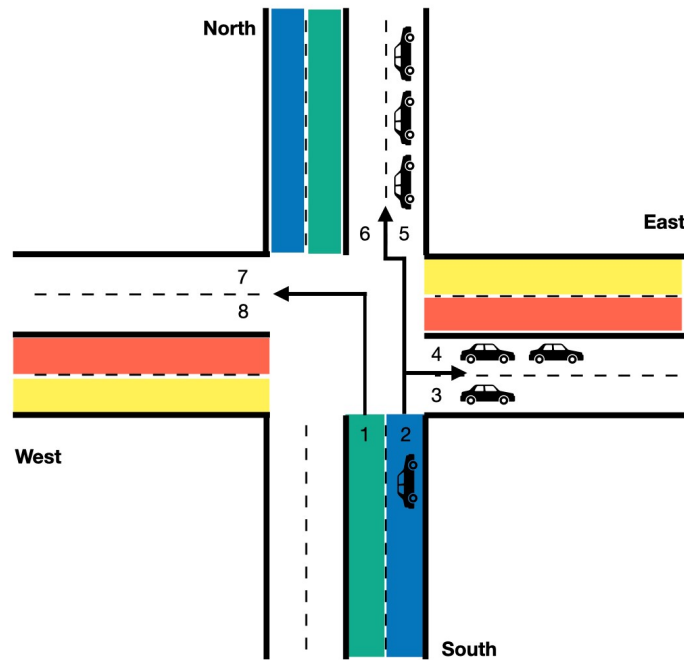


Figure 2.1: Traffic movements of a four-way two-lane bidirectional intersection.

A traffic movement (l, m) is defined as the traffic traveling across an intersection from an incoming lane l to an outgoing lane m . The intersection shown in Fig. 2.1 has 24 permissible traffic movements. As an example, vehicles on lane 1 are turning left, and vehicles on lane 2 may go straight or turn right. After turning into the link, vehicles will enter either lane. Thus, the incoming South link has the potential traffic movements of $\{(1, 7), (1, 8), (2, 5), (2, 6), (2, 3), (2, 4)\}$. The set of all permissible traffic movements of an intersection is denoted as \mathcal{M} .

A traffic signal phase is defined as the set of permissible traffic movements. As shown in Fig. 2.2, an intersection with 4 links has 8 phases.

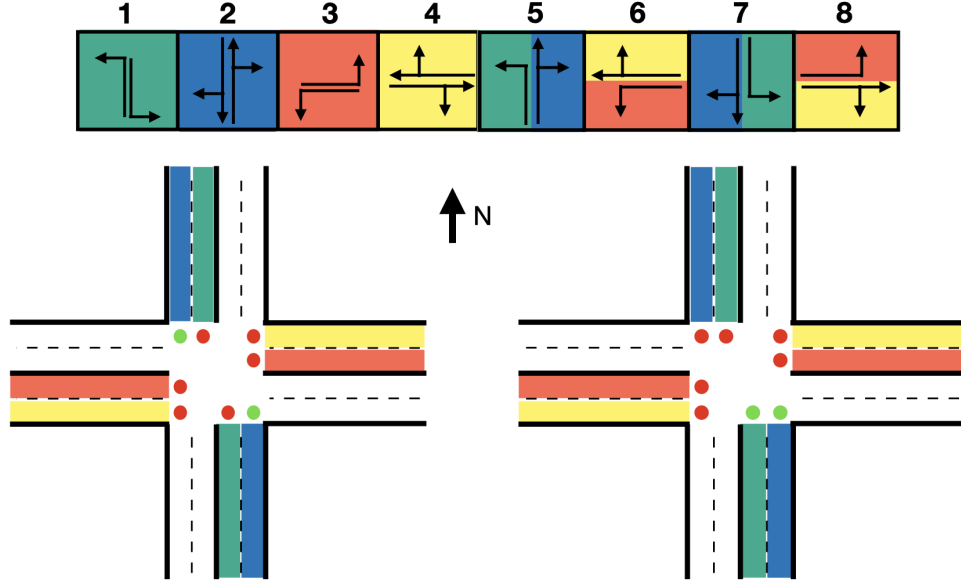


Figure 2.2: *Top*: 8 signal phases; *Left*: phase #2 illustration; *Right*: phase #5 illustration.

2.3.2 Pressure

The pressure of an incoming lane l measures the unevenness of vehicle density between lane l and corresponding outgoing lanes in permissible traffic movements. The vehicle density of a lane is $x(l)/x_{max}(l)$, where $x(l)$ is the number of vehicles on lane l and $x_{max}(l)$ is the vehicle capacity on lane l , which is related to the length of a lane. Then the pressure of an incoming lane l is

$$w(l) = \left| \frac{x(l)}{x_{max}(l)} - \sum_{\{m|(l,m) \in \mathcal{M}\}} \frac{1}{h(m)} \frac{x(m)}{x_{max}(m)} \right|, \quad (2.1)$$

where $h(m)$ is the number of lanes of the outgoing link which contains m . In Fig. 2.1, $h(m) = 2$ for all the outgoing lanes. An example for Eqn. (2.1) is shown in Fig. 2.1.

Taking the intersection's traffic conditions shown in Fig. 2.1 as an example, assuming the maximum capacity for each lane is 5 vehicles, we can calculate the lane pressure for

lane 2 to be

$$w(2) = \left| \underbrace{\frac{1}{5}}_{\text{lane 2}} - \frac{1}{2} \left(\underbrace{\frac{1}{5} + \frac{2}{5}}_{\text{lane 3 and 4}} \right) - \frac{1}{2} \left(\underbrace{\frac{3}{5} + \frac{0}{5}}_{\text{lane 5 and 6}} \right) \right| = \frac{2}{5}$$

The pressure of an intersection indicates the unevenness of vehicle density between incoming and outgoing lanes in an intersection. Intuitively, reducing the pressure leads to more evenly distributed traffic, which indirectly reduce congestion and average travel time of vehicles. EMVLight defines pressure of an intersection in EMVLight as the average of the pressure of all incoming lanes,

$$P_i = \frac{1}{|\mathcal{I}_i|} \sum_{l \in \mathcal{I}_i} w(l),$$

where \mathcal{I}_i represents the set of all incoming lanes of intersection i . According to such definition, the intersection pressure shown in Fig.2.1 is computed to be $\frac{25}{80}$.

PressLight [51] assumes that traffic movements are lane-to-lane, i.e., vehicles in one lane can only move into a particular lane in a link. Because of the lane-to-lane assumption, in PressLight, the pressure is defined per movement. PressLight defines the pressure of a movement as the difference of the vehicle density between an incoming lane l and the outgoing lane m , i.e.,

$$w^*(l, m) = \frac{x(l)}{x_{max}(l)} - \frac{x(m)}{x_{max}(m)},$$

For instance, lane 2, shown in Fig.2.1, carries $w^*(2, 3)$, $w^*(2, 4)$, $w^*(2, 5)$, $w^*(2, 6)$, $w^*(2, 7)$ and $w^*(2, 8)$. Taking the permissible traffic movement from lane 2 to lane 4 as an example, we can get the pressure for this movement as

$$w^*(2, 4) = \frac{1}{5} - \frac{2}{5} = -\frac{1}{5}$$

PressLight then defines the pressure of an intersection i as the absolute value of the sum of pressure of movements of intersection i , i.e., When calculating the pressure intersection, PressLight has

$$P_i^* = \left| \sum_{(l,m) \in \mathcal{M}_i} w^*(l,m) \right|,$$

where \mathcal{M}_i is the set of permissible traffic movements of intersection i . According to PressLight's definition of intersection pressure, Fig.2.1 shows an intersection with pressure of 6.

Pressure in our work EMVLight assumes a lane-to-link style traffic movement as vehicles can enter either lane on the target link, see Fig.2.1. Following lane pressure defined in (2.1),

Comparison The first difference between the two definitions is that $w^*(l,m)$ can be both positive or negative, but $w(l)$ can only take positive values that measures the unevenness of the vehicle density in the incoming lane and that of the corresponding outgoing lanes. We take the absolute value since the direction of pressure is irrelevant here, and the goal of each agent is to minimize this unevenness. The second difference is that at the intersection level, P_i^* takes a sum but P_i takes an average. The average is more suitable for our purpose since it scales the pressure down and the unit penalty for normal agents would be relatively large as compared to rewards for pre-emption agents (Eqn. (3)). This design puts the efficient passage of EMV vehicles at the top priority. Our experimentation results, presented in Sec.2.6 indicate the proposed pressure design produces a more robust reward signal during training and outperforms PressLight in congestion reduction.

2.3.3 Emergency capacity

A roadway segment may have additional capacity, e.g. shoulder, parking lanes, bike lanes, dedicated to providing extra space that can be used under emergencies and incidents. In the presence of EMVs, existing vehicles are allowed to pull-over or park on the shoulders temporarily, forming an *emergency lane* for the emergency vehicle to pass. An emergency lane is an lane formed between original lanes dedicated for EMV passage, see Fig.2.3 bottom. EMVs are assumed to travel freely on the emergency lane through the dense traffic. This is referred as an *emergency yielding* and non-EMVs are experiencing an *part-time shoulder use* [72].

Adaptive traffic management strategies based on part-time shoulder use, such as dynamic hard shoulder running (D-HSR) [73], have proven beneficial and cost-effective for such scenarios.

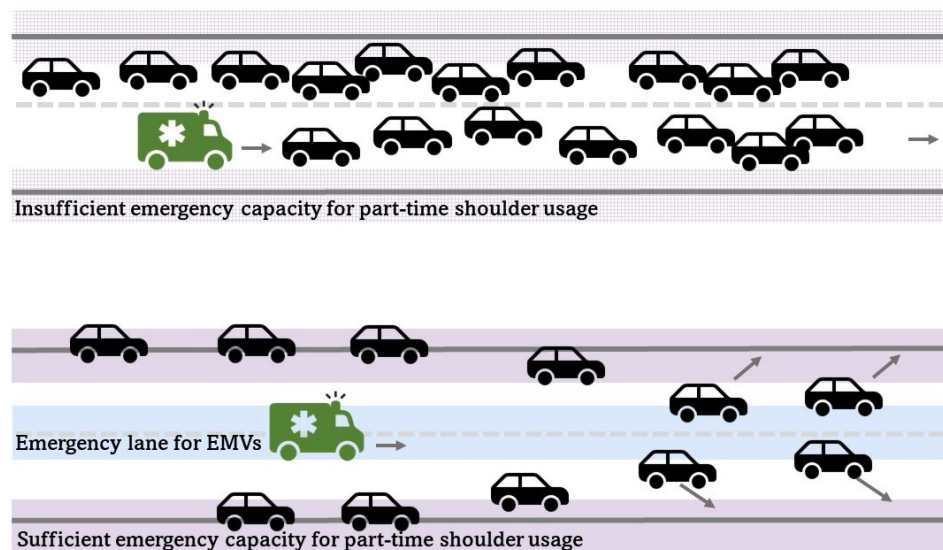


Figure 2.3: A demonstration of an emergency lane for EMV passage. *Top*: the EMV has to follow the congested queue due to insufficient emergency capacity; *Bottom*: the EMV is traversing on the yielded emergency lane due to sufficient emergency capacity.

We use an intuitive mathematical model to determine whether such an emergency lane

for EMV passage can be established. First, we define *emergency capacity* C_i^{EC} of a link i to be the additional capacity in the link for emergencies and incidents. The emergency capacity depends on the segment's shoulder width, lane width, geometric clearance and other factors. We say that a link is *emergency-capacitated* if it has a nonzero emergency capacity. In order to express the maximum number of vehicles allowed in a link, for forming an emergency lane, we assume there are n_i non-EMVs in the link i with an average speed of s_i . We also assume that the normal capacity k_i is evenly distributed among l_i lanes so that each lane has a capacity of k_i/l_i . The overall capacity of the link is then $k_i + C_i^{\text{EC}}$. To form an emergency lane for EMV passage with maximum speed, all the non-EMVs need to move out of the emergency lane. Thus the maximum number of vehicles allowed is $k_i + C_i^{\text{EC}} - k_i/l_i$. As a result, the travel speed of the EMV is

$$s_i^{\text{EMV}} = \begin{cases} s_f & n_i \leq k_i + C_i^{\text{EC}} - \frac{k_i}{l_i}, \\ s_i & \text{else,} \end{cases} \quad (2.2)$$

where s_f represents the maximum speed allowed for EMVs.

2.4 Methodology

In this section, we elaborate the methodology of EMVLight. We begin with implementing a decentralized shortest path onto EMV navigation in traffic networks, and then incorporate it into the proposed multi-class RL agent design. Subsequently, we introduce the multi-agent advantage actor-critic framework as well as the RL training workflow in details.

2.4.1 Decentralized Routing for EMVLight

Dijkstra's algorithm is an algorithm that finds the shortest path between a given node and every other nodes in a graph. The time-based Dijkstra's algorithm finds the fastest path and has been widely used for EMV routing. In order to find such a path, the EMV travel time along each link need to be estimated first and we refer to it as the *intra-link travel time*. Dijkstra's algorithm takes as input the traffic graph, the intra-link travel time and a destination, and can return the time-based shortest path as well as estimated travel time from each intersection to the destination. The latter is usually referred to as the *estimated time of arrival* (ETA) of each intersection.

In a traffic network, the intra-link travel time usually depends on the link's emergency capacity and number of vehicles in that link. In our model, this dependency is captured by EMV speed Eqn. (2.2). The intra-link travel time is then calculated as the link length divided by the EMV speed. However, traffic conditions are constantly changing and so does EMV travel time along each link. Moreover, EMV pre-emption techniques alter traffic signal phases, which will significantly change the traffic condition as the EMV travels. The pre-determined shortest path might become congested due to stochasticity and pre-emption. Thus, updating the optimal route dynamically can facilitate EMV passage. One option is to run Dijkstra's algorithm repeatedly as the EMV travels through the network in order to take into account the updated EMV intra-link travel time. However, this requires global traffic information of the entire traffic network throughout EMVs' trips. Even when a centralized controller is established to navigate the EMV, the synchronization and communication cost grows exponentially when the network size increases and the nonscability disallows the centralized scheme to be real-time for the navigation.

Decentralized routing approaches [74, 75, 76] were introduced to find the shortest

path with partial observability of the system. However, these models require network decomposition or partitioning in advance, and solve optimal paths with polynomial-bounded time complexity at best [77]. Some other approach heavily relies on V2I communication [78]. Considering the massive amount of iterations of trial-and-error in reinforcement learning, none of these decentralized routing methods provide a suitable design for a learning-based framework.

To achieve efficient decentralized dynamic routing, we extend Dijkstra’s algorithm to update the optimal route based on the updated intra-link travel times. As shown in Algorithm 1, first a pre-populating process is carried out where a standard Dijkstra’s algorithm is run to get the ETA^0 from each intersection to the destination. For each intersection, the next intersection $Next^0$ along the shortest path is also calculated. For an intersection i , the result ETA_i^0 and $Next_i^0$ are stored locally in the intersection. We assume this process can be done before the EMV leaves the dispatching hub. This is reasonable since a sequence of processes, including call-taker processing, are performed before the EMVs are dispatched. Once the pre-populating process is finished, we can update ETA and Next for each intersection efficiently in parallel in a decentralized way, since the update only depends on information of neighboring intersections. Fig. 2.4 provides an example comparing between Algorithm.1 and conventional Dijkstra’s algorithm on an 3-by-3 traffic network. The numerical value represents the ETA of each intersection, and it gets updated as described above. EMVLight, rather than solving the full shortest path like the conventional Dijkstra’s algorithm, only determines the next link to travel each iteration. A comparison of the worst-case time complexity between the EMVLight routing heuristic and a Dijkstra-based dynamic shortest path method is provided in Table 2.1. Notice that the Dijkstra’ algorithm can be implemented with a Fibonacci heap min-priority queue and solve the shortest path with a time complexity of

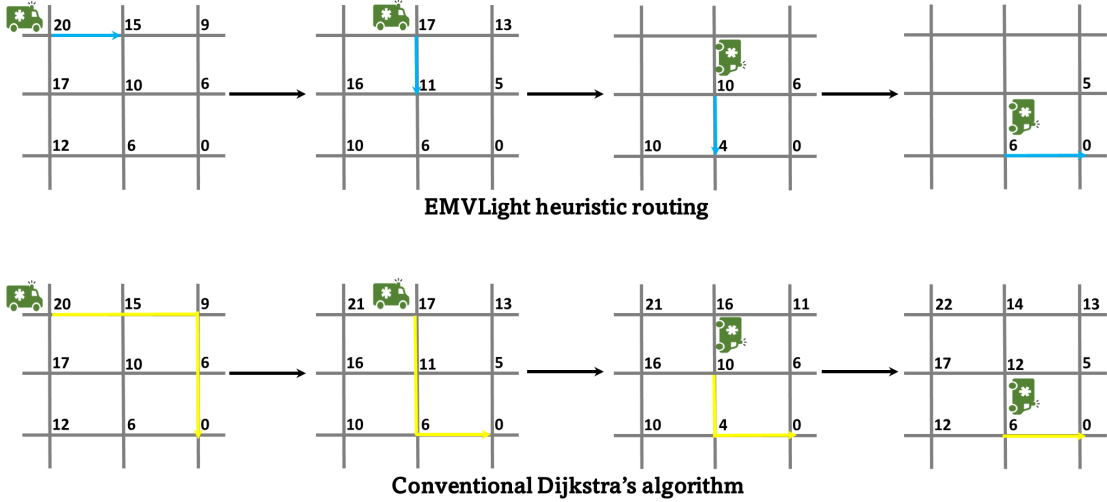


Figure 2.4: EMVLight routing (top) vs conventional Dijkstra's routing (bottom).

$\mathcal{O}(|\mathcal{V}| \log |\mathcal{V}| + |\mathcal{E}|)$ [79].

	EMVLight heuristic	Dynamic shortest-path based on Dijkstra's
Initialization	$\mathcal{O}(\mathcal{V} \log \mathcal{V} + \mathcal{E})$	-
updating	$\mathcal{O}(\mathcal{V})$	$\mathcal{O}(\mathcal{V} \log \mathcal{V} + \mathcal{E})$
updating frequency	$ \mathcal{V} $	M

Table 2.1: Time complexities of the proposed routing heuristic and the dynamic shortest-path approach. M can be arbitrarily set to determine the updating frequency. The larger M is, the shorter selected route can be.

By adopting the proposed heuristic routing algorithm, we facilitate the RL agent design, which is introduced in Sec. 2.4.2.

Remark 1. *In static Dijkstra's algorithm, the shortest path is obtained by repeatedly querying the Next attribute of each node from the origin until we reach the destination. In our dynamic Dijkstra's algorithm, since the shortest path changes, at a intersection i , we only care about the immediate next intersection to go to, which is exactly Next_i .*

2.4.2.1 Types of agents for EMV passage

When an EMV is on duty, we distinguish 3 types of traffic control agents based on EMV location and routing (Fig. 2.5). An agent is a *primary pre-emption agent* i_p if an EMV is on one of its incoming links. The agent of the next intersection $i_s = \text{Next}_{i_p}$ is referred to as a *secondary pre-emption agent*. The rest of the agents are *normal agents*. We design these types since different agents have different local goals, which is reflected in their reward designs.

2.4.2.2 Agent design

State: The state of an agent i at time t is denoted as s_i^t and it includes the number of vehicles on each outgoing lanes and incoming lanes, the distance of the EMV to the intersection, the estimated time of arrival (ETA), and which link the EMV will be routed to (Next), i.e.,

$$s_i^t = \{x^t(l), x^t(m), d_{\text{EMV}}^t[L_{ji}], \text{ETA}_i^t, \text{Next}_i^t\}, \quad (2.3)$$

where L_{ji} represents the links incoming to intersection i from its adjacent intersections $j \in \mathcal{N}_i$. With a slight abuse of notation, l and m denote the set of incoming and outgoing lanes, respectively. The vector d_{EMV}^t contains the information about the distance of an EMV to the intersection is an EMV is present. For the intersection shown in Fig. 2.1, d_{EMV}^t is a vector of four elements. In particular, for primary pre-emption agents, one of the elements represents the distance of EMV to the intersection in the corresponding link and the rest of the elements are set to -1. For all other agents, d_{EMV}^t are padded with -1.

Action: Prior work has focused on using phase switch, phase duration and phase itself as actions. In this work, we define the action of an agent as one of the 8 phases in Fig. 2.2; this enables more flexible signal patterns as compared to the traditional cyclical patterns.

Due to safety concerns, once a phase has been initiated, it should remain unchanged for a minimum amount of time, e.g. 5 seconds. Because of this, we set our MDP time step length to be 5 seconds to avoid rapid switch of phases.

Reward: PressLight has shown that minimizing the pressure is an effective way to encourage efficient vehicle passage. For normal agents, we adopt a similar idea, as shown in Eqn. 2.4a. For secondary pre-emption agents, we additionally encourage less vehicles on the link where the EMV is about to enter in order to encourage efficient EMV passage. Thus, the reward is a weighted sum of the pressure and this additional term, with a weight β , as shown in Eqn. 2.4b. For a default setting of balancing EMV navigation and traffic congestion alleviation, we choose $\beta = 0.5$. For primary pre-emption agents, we simply assign a unit penalty at each time step to encourage fast EMV passage, as shown in Eqn. 2.4c. Thus, depending on the agent type, the local reward for agent i at time t is as follows

$$r_i^t = \begin{cases} -P_i^t & i \notin \{i_p, i_s\}, \\ -\beta P_{i_s}^t - \frac{1-\beta}{|L_{i_p i_s}|} \sum_{l \in L_{i_p i_s}} \frac{x(l)}{x_{max}(l)} & i = i_s, \\ -1 & i = i_p. \end{cases} \quad \begin{matrix} (2.4a) \\ (2.4b) \\ (2.4c) \end{matrix}$$

Justification of agent design. The quantities in local agent state can be obtained at each intersection using various technologies. Numbers of vehicles on each lane ($x^t(l), x^t(m)$) can be obtained by vehicle detection technologies, such as inductive loop [80] based on the hardware installed underground. The distance of the EMV to the intersection $d_{EMV}^t[L_{ji}]$ can be obtained by *vehicle-to-infrastructure* technologies such as VANET[81], which broadcasts the real-time position of a vehicle to an intersection. Prior work by [82] and [83] have explored these technologies for traffic signal pre-emption.

The dynamic routing algorithm (Algorithm 1) can provide (ETA, Next) for each agent

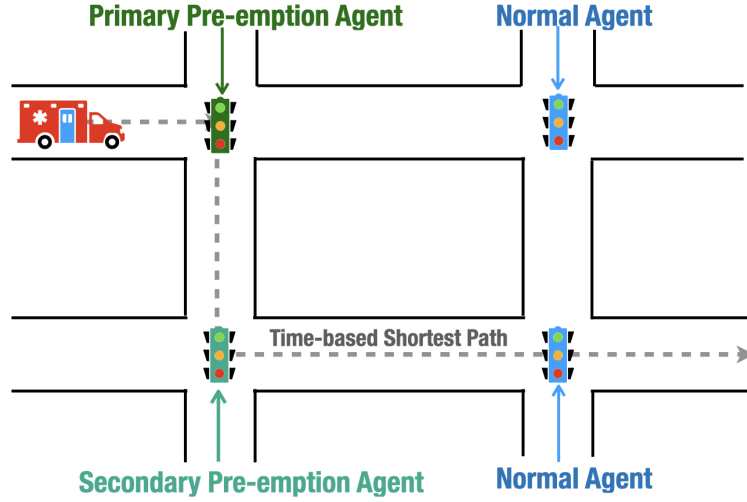


Figure 2.5: Types of agents through the EMV's passage to the destination.

at every time step. However, due to the stochastic nature of traffic flows, updating the route too frequently might confuse the EMV driver, since the driver might be instructed a new route, say, every 5 seconds. There are many ways to ensure reasonable frequency. One option is to inform the driver only once while the EMV travels on a single link. We implement it by updating the state of a RL agent $(ETA_i^{t'}, Next_i^{t'})$ at the time step when the EMV travels through half of a link. For example, if the EMV travels through a link to agent i from time step 11 to 20 in constant speed, then dynamic routing information in s_i^{16} to s_i^{20} are the same, which is $(ETA_i^{15}, Next_i^{15})$, i.e., $t' = 15$.

As for the reward design, one might wonder how an agent can know its type. As we assume an agent can observe the state of its neighbors, agent type can be inferred from the observation. This will become clearer in Section 2.4.3.

2.4.3 Multi-agent Advantage Actor-critic

We adopt a multi-agent advantage actor-critic (MA2C) framework similar to [61] to address the coupling of EMV navigating and traffic signal control simultaneously in a decentralized manner. The difference is that our local state includes dynamic routing information and our local reward encourages efficient passage of EMV. Here we briefly introduce the MA2C framework.

In a multi-agent network $G(\mathcal{V}, \mathcal{E})$, the neighborhood of agent i is denoted as $\mathcal{N}_i = \{j | j \in \mathcal{E} \text{ or } ij \in \mathcal{E}\}$. The local region of agent i is $\mathcal{V}_i = \mathcal{N}_i \cup i$. We define the distance between two agents $d(i, j)$ as the minimum number of edges that connect them. For example, $d(i, i) = 0$ and $d(i, j) = 1, \forall j \in \mathcal{N}_i$. In MA2C, each agent learns a policy π_{θ_i} (actor) and the corresponding value function V_{ϕ_i} (critic), where θ_i and ϕ_i are learnable neural network parameters of agent i .

Local Observation. In an ideal setting, agents can observe the states of every other agent and leverage this global information to make a decision. However, this is not practical in our problem due to communication latency and will cause scalability issues. We assume an agent can observe its own state and the states of its neighbors, i.e., $s_{\mathcal{V}_i}^t = \{s_j^t | j \in \mathcal{V}_i\}$. The agents feed this observation to its policy network π_{θ_i} and value network V_{ϕ_i} .

Fingerprint. In multi-agent training, each agent treats other agents as part of the environment, but the policy of other agents are changing over time. [84] introduce *fingerprints* to inform agents about the changing policies of neighboring agents in multi-agent Q-learning. [61] bring fingerprints into MA2C. Here we use the probability simplex of neighboring policies $\pi_{\mathcal{N}_i}^{t-1} = \{\pi_j^{t-1} | j \in \mathcal{N}_i\}$ as fingerprints, and include it into the input of policy network and value network. Thus, our policy network can be written as $\pi_{\theta_i}(a_i^t | s_{\mathcal{V}_i}^t, \pi_{\mathcal{N}_i}^{t-1})$ and value network as $V_{\phi_i}(s_{\mathcal{V}_i}^t, \pi_{\mathcal{N}_i}^{t-1})$, where $s_{\mathcal{V}_i}^t$ is the local observation

with spatial discount factor introduced below.

Spatial Discount Factor and Adjusted Reward. MA2C agents cooperatively optimize a global cumulative reward. We assume the global reward is decomposable as $r_t = \sum_{i \in \mathcal{V}} r_i^t$, where r_i^t is defined in Eqn. (2.4). Instead of optimizing the same global reward for every agent, here we employ the spatial discount factor α , introduced by [61], to let each agent pay less attention to rewards of agents farther away. The adjusted reward for agent i is

$$\tilde{r}_i^t = \sum_{d=0}^{D_i} \left(\sum_{j \in \mathcal{V} | d(i,j)=d} (\alpha)^d r_j^t \right), \quad (2.5)$$

where D_i is the maximum distance of agents in the graph from agent i . When $\alpha > 0$, the adjusted reward include global information, it seems this is in contradiction to the local communication assumption. However, since reward is only used for offline training, global reward information is allowed. Once trained, the RL agents can control a traffic signal without relying on global information.

Temporal Discount Factor and Return. The local return \tilde{R}_i^t is defined as the cumulative adjusted reward $\tilde{R}_i^t := \sum_{\tau=t}^T \gamma^{\tau-t} \tilde{r}_i^\tau$, where γ is the temporal discount factor and T is the length of an episode. We can estimate the local return using value function,

$$\tilde{R}_i^t = \tilde{r}_i^t + \gamma V_{\phi_i^-}(s_{\mathcal{V}_i}^{t+1}, \pi_{\mathcal{N}_i}^t | \pi_{\theta_{-i}^-}), \quad (2.6)$$

where ϕ_i^- means parameters ϕ_i are frozen and θ_{-i}^- means the parameters of policy networks of all other agents are frozen.

Network architecture and training. As traffic flow data are spatial temporal, we leverage a long-short term memory (LSTM) layer along with fully connected (FC) layers for policy network (actor) and value network (critic). Fig. 2.6 provides an overview for the MA2C frameworks for EMVLight.

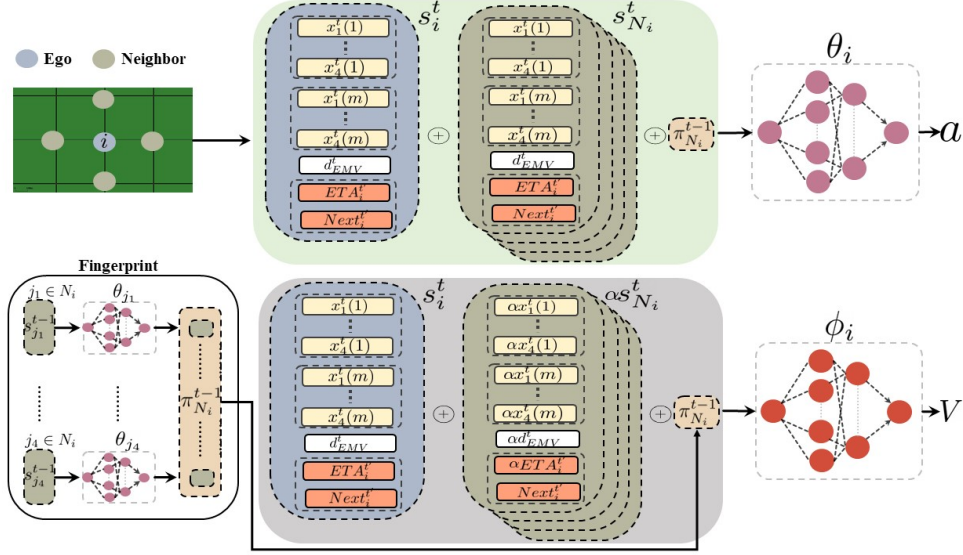


Figure 2.6: Overview of MA2C framework for EMVLight's navigation and traffic signal control.

Value loss function With a batch of data $B = \{(s_i^t, \pi_i^t, a_i^t, s_i^{t+1}, r_i^t)_{i \in \mathcal{V}}\}^{t \in \mathcal{T}}$, each agent's value network is trained by minimizing the difference between bootstrapped estimated value and neural network approximated value

$$\mathcal{L}_v(\phi_i) = \frac{1}{2|B|} \sum_B \left(\tilde{R}_i^t - V_{\phi_i}(s_{\mathcal{V}_i}^t, \pi_{\mathcal{N}_i}^{t-1}) \right)^2. \quad (2.7)$$

Policy loss function Each agent's policy network is trained by minimizing its policy loss

$$\mathcal{L}_p(\theta_i) = -\frac{1}{|B|} \sum_B \left(\ln \pi_{\theta_i}(a_i^t | s_{\mathcal{V}_i}^t, \pi_{\mathcal{N}_i}^{t-1}) \tilde{A}_i^t \right) \quad (2.8)$$

$$- \lambda \sum_{a_i \in \mathcal{A}_i} \pi_{\theta_i} \ln \pi_{\theta_i}(a_i | s_{\mathcal{V}_i}^t, \pi_{\mathcal{N}_i}^{t-1}), \quad (2.9)$$

where $\tilde{A}_i^t = \tilde{R}_i^t - V_{\phi_i}(s_{\mathcal{V}_i}^t, \pi_{\mathcal{N}_i}^{t-1})$ is the estimated advantage which measures how much better the action a_i^t is as compared to the average performance of the policy π_{θ_i} in the

state s_i^t . The second term is a regularization term that encourage initial exploration, where \mathcal{A}_i is the action set of agent i . For an intersection as shown in Fig. 1, \mathcal{A}_i contains 8 traffic signal phases.

Training algorithm Algorithm S1 shows the multi-agent A2C training process.

Algorithm S1: Multi-agent A2C Training

Input :

T	maximum time step of an episode
N_{bs}	batch size
η_{θ}	learning rate for policy networks
η_{ϕ}	learning rate for value networks
α	spatial discount factor
γ	(temporal) discount factor
λ	regularizer coefficient

Output :

$\{\phi_i\}_{i \in \mathcal{V}}$	learned parameters in value networks
$\{\theta_i\}_{i \in \mathcal{V}}$	learned parameters in policy networks

```

1 initialize  $\{\phi_i\}_{i \in \mathcal{V}}, \{\theta_i\}_{i \in \mathcal{V}}, k \leftarrow 0, B \leftarrow \emptyset$ ; initialize SUMO,  $t \leftarrow 0$ , get
    $\{s_i^0\}_{i \in \mathcal{V}}$ 
2 repeat
   /* generate trajectories */
3   foreach  $i \in \mathcal{V}$  do (in parallel)
4     sample  $a_i^t$  from  $\pi_i^t$ 
5     receive  $\tilde{r}_i^t$  and  $s_i^{t+1}$ 
6      $B \leftarrow B \cup \{(s_i^t, \pi_i^t, a_i^t, s_i^{t+1}, r_i^t)_{i \in \mathcal{V}}\}$ 
7      $t \leftarrow t + 1, k \leftarrow k + 1$ 
8   if  $t == T$  then
9     initialize SUMO,  $t \leftarrow 0$ , get  $\{s_i^0\}_{i \in \mathcal{V}}$ 
   /* update actors and critics */
10  if  $k == N_{\text{bs}}$  then
11    foreach  $i \in \mathcal{V}$  do (in parallel)
12      calculate  $\tilde{r}_i^t$  (Eqn. (4)),  $\tilde{R}_i^t$  (Eqn. (5))
13       $\phi_i \leftarrow \phi_i - \eta_{\phi} \nabla \mathcal{L}_v(\phi_i)$ 
14       $\theta_i \leftarrow \theta_i - \eta_{\theta} \nabla \mathcal{L}_p(\theta_i)$ 
15     $k \leftarrow 0, B \leftarrow \emptyset$ 
16 until Convergence

```

2.5 Experimentation

In this section, we demonstrate our RL framework using Simulation of Urban MOBility (SUMO) [85]. SUMO is an open-source traffic simulator capable of simulating both microscopic and macroscopic traffic dynamics, suitable for capturing the EMV’s impact on the regional traffic as well as monitoring the overall traffic flow. An RL-simulator training pipeline is established between the proposed RL framework and SUMO, i.e., the agents collect observations from SUMO and preferred signal phases are fed back into SUMO. Notice that in order to reflect the proposed emergency lane in Fig.3, we enable the built-in *Sublane model* [86] and *Blue light device* [87] to establish the emergency lane for EMV passage. Under this scenarios, non-EMVs pull over to the sides when the EMV is driving between, and they resume normal driving when the EMV leaves the segment, see A.3 for more details.

2.5.1 Datasets and Maps Descriptions

We conduct the following experiments based on both synthetic and real-world map.

Synthetic Grid_{5×5} We synthesize a 5×5 traffic grid, where intersections are connected with bi-directional links. Each link contains two lanes. We assume all the links have zero emergency capacity. We design 4 configurations of time-varying traffic flows, listed in Table 2.2. The origin (O) and destination (D) of the EMV are labelled in Fig. 2.7. The traffic for this map has a time span of 1200s. We dispatch the EMV at $t = 600s$ to ensure the roads are compacted when it starts travel.

Emergency-capacitated (EC) Synthetic Grid_{5×5} This map adopts the same network layout as the Synthetic Grid_{5×5} but with emergency-capacitated segments. As shown

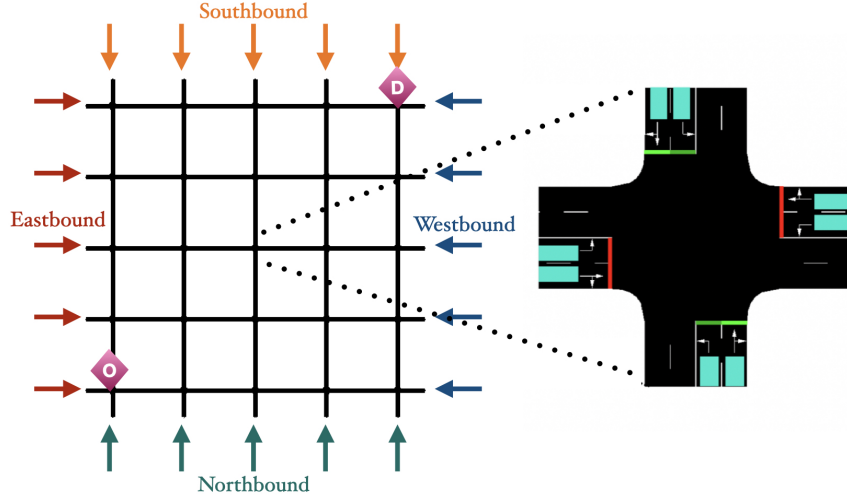


Figure 2.7: *Left*: the synthetic grid $_{5 \times 5}$. Origin and destination for EMV are labeled. *Right*: an intersection illustration in SUMO, the teal area are inductive loop detected area.

in Fig. 2.8, segments approaching intersections highlighted by blue are emergency-capacitated with $C^{EC} = 0.2k$, with k represents the normal vehicle capacity of this segment. All other segments are not emergency-capacitated.

Manhattan $_{16 \times 3}$ This is a 16×3 traffic network extracted from Manhattan Hell’s Kitchen area (Fig. 2.9) and customized for demonstrating EMV passage. In this traffic network, intersections are connected by 16 one-directional streets and 3 one-directional avenues. We assume each avenue contains four lanes and each street contains two lanes so that the right-of-way of EMVs and pre-emption can be demonstrated. We assume the emergency capacity for avenues and streets are $C_{avenue}^{EC} = 0.2k_{avenue}$ and $C_{street}^{EC} = 0.15k_{street}$, respectively. The traffic flow for this map is generated from open-source NYC taxi data. Both the map and traffic flow data are publicly available.² The origin and destination of EMV are set to be far away as shown in Fig. 2.9.

²<https://traffic-signal-control.github.io/>

Config	Traffic Flow (veh/lane/hr)		Origin	Destination
	Non-peak	Peak		
1	200	240	N,S	E,W
2	160	320		
3	200	240	Randomly generated	
4	160	320		

Table 2.2: Configuration for Synthetic Grid $_{5 \times 5}$. Peak flow is assigned from 400s to 800s and non-peak flow is assigned out of this period. For Config. 1 and 2, the vehicles enter the grid from North and South, and exit toward East and West.

Hangzhou $_{4 \times 4}$ An irregular 4×4 road network represents major avenues in Gudang sub-district in Hangzhou, China. All the road segments are bi-directional with two lanes in each direction. Both the map and traffic flow data are publicly available. We set the origin and destination for EMV routing as shown in Fig. 2.10. The emergency capacity for each segment is set as $C^{EC} = 0.2k$. Notice that this map only includes primary arterials and intersections because secondary arterials and intersections usually lack ITS infrastructure to assist EMVs’ passage. They are also hard to monitor and control, considering Hangzhou Gudang district is a densely populated area. It is common to see double parking or merchants occupying road space on these secondary roads. The associated traffic flow dataset [88] also excludes vehicle trajectories information on these secondary arterials for simplification.

2.5.2 Benchmark Methods

Due to the lack of existing RL methods for efficient EMV passage, we select traditional methods and RL methods for each subproblem and combine them to set up benchmarks.

For traffic signal pre-emption, the most intuitive and widely-used approach is the idea of extending green light period for EMV passage at each intersection which results in a

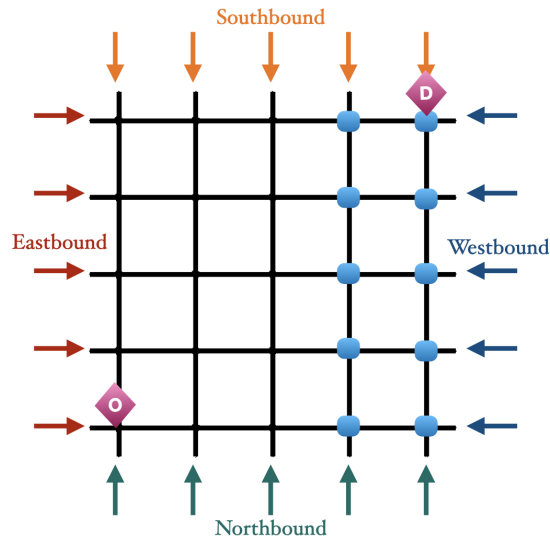


Figure 2.8: Emergency-capacitated Synthetic Grid $_{5 \times 5}$. Segments towards intersections highlighted by blue have emergency capacities.

Green Wave [89]. **Walabi (W)** [41] is an effective rule-based method that implemented Green Wave for EMVs in SUMO environment. We integrate Walabi with combinations of routing and traffic signal control strategies introduced below as benchmarks. We first present two routing benchmarks.

- **Static routing:** static routing is performed only when EMV starts to travel and the route remains fixed. We adopt A* search as the implementation of static routing since it is a powerful extension to the Dijkstra's shortest path algorithm and is used in many real-time applications.³
- **Dynamic routing:** dynamic routing updates the route by taking into account real-time information of traffic conditions. The route is then updated by repeatedly running static routing algorithms. To set up the dynamic routing benchmark, we run A* every 50s as EMV travels. The update interval is set to 50s since running

³Our implementation of A* search employs a Manhattan distance as the heuristic function.

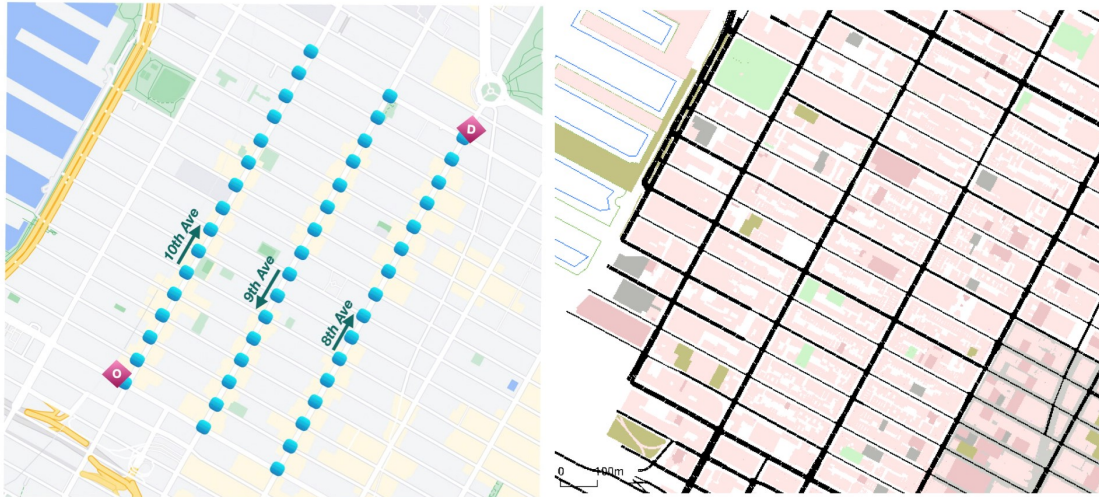


Figure 2.9: Manhattan_{16×3}: a 16-by-3 traffic network in Hell’s Kitchen area. Origin and destination for the EMV dispatching are labeled. *Left*: on Google Map; *Right*: in SUMO simulator.

the full A* to update the route is not as efficient as our proposed dynamic Dijkstra’s algorithm.

Traffic signal control benchmarks:

- **Fixed Time (FT)**: Cyclical fixed time traffic phases with random offset [90] is a policy that split all phases with an predefined green ratio. The coordination between traffic signals are predefined so it is not updated based on real-time traffic. Because of its simplicity, it is the default strategy in real traffic signal control for steady traffic flow.
- **Max Pressure (MP)**: [52] studies max pressure control and use it as the main criterion for selecting traffic signal phases. It defines pressure for each signal phases and aggressively selects the traffic signal phase with maximum pressure to smooth congestion. Hence the name Max Pressure. It is the state-of-the-art network-level signal control strategy that is not based on learning.

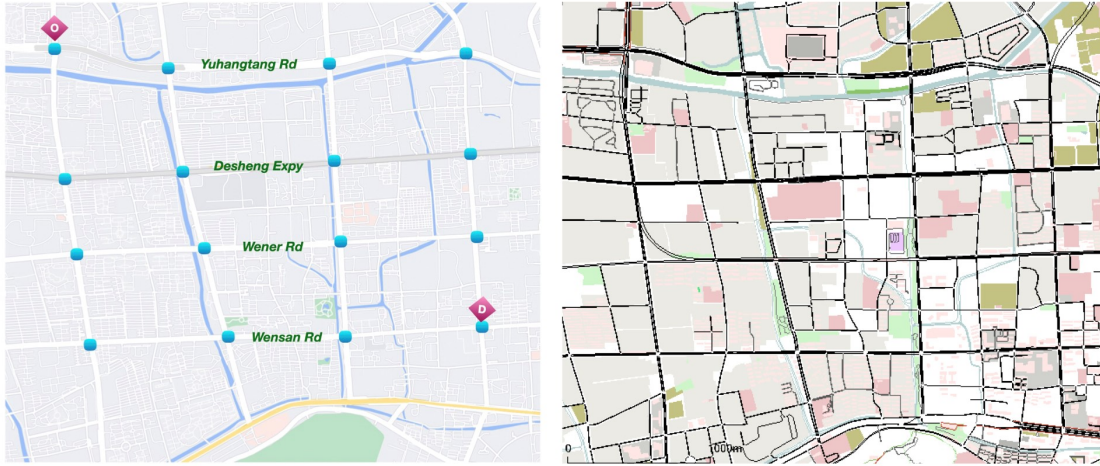


Figure 2.10: Hangzhou $_{4 \times 4}$: a 4-by-4 irregular and asymmetric network. Origin and destination for the EMV dispatching are labeled. *Left*: on Google Map; *Right*: in SUMO simulator.

- **Coordinated Deep Reinforcement Learners (CDRL)**: CDRL [48] is a Q-learning based coordinator which directly learns joint local value functions for adjacent intersections. It extends Q-learning from single-agent scenarios to multi-agent scenarios. It also employs transfer planning and max-plus coordination strategies for joint intersection coordination.
- **PressLight (PL)**: PL [51] is also a Q-learning based method for traffic signal coordination. It aims at optimizing the pressure at each intersection. However, it defines pressure for each intersection, which is slightly different from the definition in Max Pressure. Our definition of pressure Eqn. (2.4). is also different from that in PL.
- **CoLight (CL)**: CoLight [49] uses a graph-attentional-network-based reinforcement learning method for large scale traffic signal control. It adjusts queue length with information from neighbor intersections.

2.5.3 Metrics

We evaluate performance of all strategies under two metrics: *EMV travel time*, which reflects the routing and pre-emption ability, and *average travel time*, which indicates the ability of traffic signal control for efficient vehicle passage. Vehicles which have completed their trips during the simulation interval are counted when calculating the average travel time.

2.6 Results and Discussion

In this section, we demonstrate the performance of EMVLight and compare it against that of all benchmark methods on four experimentation maps. The results show a clear advantage of EMVLight under the two metrics. In addition, we illustrate the difference of underlying route selection by EMVLight and benchmark methods. We further conduct ablation studies to investigate the contribution of different components to EMVLight’s performance.

2.6.1 Performance Comparison

To evaluate the performance of the proposed EMVLight and all benchmark methods, we conduct SUMO simulation with five independent runs for each setting. Randomly generated seeds are used in learning-based methods. Means as well as standard deviations of the simulation results are reported for a full numerical assessment. The differences in simulation results for the same setting under independent SUMO runs are coming from configuration noise during generation, such as vehicles’ lengths/accelerations/lane-changing eagerness, and, for RL-based methods, random seeds for initialization.

We provide implementation details of EMVLight on different experimentation settings in A.1. Hyper-parameters choices for EMVLight and RL-based benchmarks are provided in A.2.

2.6.1.1 Synthetic Grid_{5×5} results

Method	EMV Travel Time T_{EMV} [s]			
	Config 1	Config 2	Config 3	Config 4
FT w/o EMV	N/A	N/A	N/A	N/A
W + static + FT	258.18 ± 5.32	273.32 ± 9.74	256.40 ± 6.20	240.84 ± 4.43
W + static + MP	260.22 ± 10.87	272.40 ± 10.92	265.74 ± 11.98	242.32 ± 9.48
W + static + CDRL	269.42 ± 7.32	282.20 ± 5.28	276.14 ± 2.58	280.32 ± 4.82
W + static + PL	270.68 ± 9.13	279.14 ± 9.22	281.42 ± 5.62	266.10 ± 8.32
W + static + CL	255.72 ± 4.23	272.06 ± 8.13	270.22 ± 2.81	277.12 ± 6.10
W + dynamic + FT	229.38 ± 8.28	212.87 ± 3.17	218.46 ± 4.28	220.69 ± 7s.96
W + dynamic + MP	220.48 ± 9.26	208.08 ± 12.90	212.46 ± 9.82	220.98 ± 10.62
W + dynamic + CDRL	239.84 ± 5.24	219.15 ± 8.26	211.86 ± 7.13	232.46 ± 10.16
W + dynamic + PL	243.32 ± 13.86	244.82 ± 10.52	250.12 ± 8.13	255.02 ± 12.76
W + dynamic + CL	220.12 ± 4.19	209.12 ± 4.76	224.00 ± 5.31	226.32 ± 4.13
EMVLight	195.46 ± 7.48	190.66 ± 8.28	183.12 ± 6.43	189.44 ± 8.32

Table 2.3: EMV travel time in the four configurations of Synthetic Grid_{5×5}. Lower value indicates better performance and the lowest values are highlighted in bold.

Method	Average Travel Time T_{avg} [s]			
	Config 1	Config 2	Config 3	Config 4
FT w/o EMV	353.43 ± 4.65	371.13 ± 4.58	314.25 ± 2.90	334.10 ± 3.73
W + static + FT	380.42 ± 13.35	395.17 ± 15.37	350.16 ± 13.66	363.90 ± 15.39
W + static + MP	355.10 ± 15.36	362.09 ± 16.15	318.76 ± 14.90	330.69 ± 15.52
W + static + CDRL	559.19 ± 3.60	540.81 ± 12.04	568.13 ± 13.25	568.13 ± 6.67
W + static + PL	369.52 ± 8.72	372.32 ± 16.05	339.18 ± 7.17	339.12 ± 5.33
W + static + CL	365.64 ± 14.08	380.13 ± 8.20	328.42 ± 17.52	333.74 ± 5.76
W + dynamic + FT	380.76 ± 10.70	404.81 ± 18.76	345.09 ± 11.60	358.90 ± 15.27
W + dynamic + MP	360.38 ± 10.31	365.10 ± 8.33	327.98 ± 18.90	351.62 ± 3.79
W + dynamic + CDRL	565.38 ± 16.10	544.29 ± 19.23	598.73 ± 11.01	572.22 ± 13.94
W + dynamic + PL	373.17 ± 17.98	387.25 ± 13.98	349.12 ± 16.25	330.21 ± 17.23
W + dynamic + CL	359.14 ± 9.52	370.45 ± 4.02	320.64 ± 4.10	335.27 ± 7.62
EMVLight	335.09 ± 4.13	333.28 ± 8.81	307.90 ± 3.89	321.02 ± 5.87

Table 2.4: Average travel time for all vehicles which have completed trips in the four configurations of Synthetic Grid_{5×5}.

Table 2.3 and 2.4 present the experimental results on average EMV travel time and average travel time on Synthetic Grid_{5×5}. In terms of EMV travel time T_{EMV} , the dynamic routing benchmark performs better than static routing benchmarks. This is expected since dynamic routing considers the time-dependent nature of traffic conditions and update optimal route accordingly. The best learning and non-learning benchmark methods are dynamics routing with CoLight and Max Pressure, respectively. EMVLight further reduces EMV travel time by 16% on average as compared to dynamic routing benchmarks. This advantage in performance can be attributed to the design of secondary pre-emption agents. This type of agents learns to “reserve a link” by choosing signal phases that help clear the vehicles in the link to encourage high speed EMV passage (Eqn. (2.4)).

As for average travel time T_{avg} , we first notice that the traditional pre-emption technique (W + static + FT) indeed increases the average travel time by around 10% as compared to a traditional Fix Time strategy without EMV (denoted as “FT w/o EMV” in Table 2.4), thus decreasing the efficiency of vehicle passage. Different traffic signal control strategies have a direct impact on overall efficiency. Fixed Time is designed to handle steady traffic flow. Max Pressure, as a SOTA traditional method, outperforms Fix Time and, surprisingly, nearly outperforms all RL benchmarks in terms of overall efficiency. This shows that pressure is an effective indicator for reducing congestion and this is why we incorporate pressure in our reward design. Coordinate Learner performs the worst probably because its reward is not based on pressure. PressLight doesn’t beat Max Pressure because it has a reward design that focuses on smoothing vehicle densities along a major direction, e.g. an arterial. Grid networks with the presence of EMV make PressLight less effective. CoLight achieves similar performance as Max Pressure and is the best learning benchmark method. Our EMVLight improves its pressure-based reward

design to encourage smoothing vehicle densities of all directions for each intersection. This enable us to achieve an advantage of 7.5% over our best benchmarks (Max Pressure).

2.6.1.2 Emergency-capacitated Synthetic Grid_{5×5} results

Method	EMV Travel Time T_{EMV} [s]			
	Config 1	Config 2	Config 3	Config 4
FT w/o EMV	N/A	N/A	N/A	N/A
W + static + FT	254.04 ± 7.42	260.18 ± 12.03	252.12 ± 11.03	232.47 ± 12.23
W + static + MP	233.76 ± 8.05	258.60 ± 9.06	252.74 ± 13.05	233.20 ± 8.96
W + static + CDRL	240.10 ± 8.65	266.28 ± 8.54	258.10 ± 9.27	270.43 ± 6.18
W + static + PressLight	265.28 ± 7.28	269.10 ± 6.65	270.18 ± 8.83	259.20 ± 7.13
W + static + CoLight	250.82 ± 6.73	267.08 ± 10.21	266.12 ± 4.13	270.18 ± 8.12
W + dynamic + FT	210.28 ± 8.90	206.18 ± 7.19	210.28 ± 8.81	207.64 ± 10.02
W + dynamic + MP	202.28 ± 8.54	203.20 ± 9.07	206.64 ± 7.98	210.86 ± 8.59
W + dynamic + CDRL	218.36 ± 8.12	209.28 ± 7.19	208.180 ± 10.54	230.22 ± 9.22
W + dynamic + PressLight	270.08 ± 10.20	238.10 ± 9.22	242.10 ± 6.98	248.24 ± 10.24
W + dynamic + CoLight	216.04 ± 4.91	206.12 ± 6.27	219.26 ± 6.87	223.78 ± 5.10
EMVLight	150.28 ± 7.48	158.20 ± 6.28	154.28 ± 4.19	159.28 ± 6.03

Table 2.5: EMV travel time in the four configurations of Synthetic Grid_{5×5} with an emergency capacity co-efficient of 0.25.

Table 2.5 shows T_{EMV} of all the methods implemented on the emergency-capacitated synthetic Grid_{5×5} map. By comparing Table 2.3 and Table 2.5, we conclude that the emergency-capacitated map exhibits overall shorter T_{EMV} in all configurations. For benchmark methods, the nonzero emergency capacity shorten T_{EMV} by an average of approximately 12 seconds. In particular, dynamic routing-based methods benefit more from the additional emergency capacity, resulting in an average reduction of in 16.28 seconds T_{EMV} . This is due to the adaptive nature of dynamic navigation. By comparing EMVLight and benchmark methods in Table 2.5, we observe that EMVLight reduce T_{EMV} by up to 50 seconds (25%) as compared to the best benchmark method in all configurations. The substantial difference in T_{EMV} reduction between benchmark methods and EMVLight is due to high success rate of emergency lane forming under coordination,

which is investigated further in Section 2.6.2.

Method	Average Travel Time T_{avg} [s]			
	Config 1	Config 2	Config 3	Config 4
FT w/o EMV	353.43 ± 4.65	371.13 ± 4.58	314.25 ± 2.90	334.10 ± 3.73
W + static + FT	395.28 ± 5.17	410.94 ± 9.16	365.82 ± 6.14	379.64 ± 6.21
W + static + MP	370.52 ± 6.18	375.44 ± 6.48	331.62 ± 5.92	345.13 ± 8.63
W + static + CDRL	575.28 ± 7.76	555.62 ± 10.04	574.91 ± 19.86	585.20 ± 7.53
W + static + PL	385.28 ± 12.09	380.83 ± 10.07	360.09 ± 11.62	369.72 ± 18.02
W + static + CL	382.17 ± 6.02	380.13 ± 8.21	344.19 ± 16.02	352.07 ± 4.10
W + dynamic + FT	389.12 ± 18.21	411.98 ± 15.31	353.72 ± 9.09	367.74 ± 16.82
W + dynamic + MP	370.28 ± 12.51	362.82 ± 9.05	335.10 ± 9.16	360.02 ± 17.18
W + dynamic + CDRL	575.05 ± 9.67	550.92 ± 14.06	609.26 ± 11.12	578.10 ± 12.09
W + dynamic + PL	380.29 ± 6.10	395.28 ± 5.62	359.16 ± 14.07	337.26 ± 4.96
W + dynamic + CL	366.14 ± 8.21	380.74 ± 15.84	330.44 ± 17.29	343.58 ± 14.27
EMVLight	334.96 ± 5.52	336.18 ± 17.09	309.10 ± 15.56	323.76 ± 17.24

Table 2.6: Average travel time for all vehicles which have completed trips in the four configurations of Synthetic Grid_{5×5} with an emergency capacity coefficient of 0.25.

As the EMV travels faster and more emergency lanes are formed, the average travel time of non-emergency vehicles increases. Table 2.6 shows T_{avg} with emergency capacity added. By comparing Table 2.4 and Table 2.6, we observe that with added emergency capacity, the average increase in T_{avg} for non-learning-based and learning-based benchmarks are 12.04 seconds and 7.78 seconds, respectively. Learning-based methods lead to a smaller average increase since agents gradually learn to direct non-EMVs, which are interrupted by EMV passages, to resume their trips as soon as possible. As a result, potential congested queues would not be formed on these segments, effectively reducing the overall T_{avg} .

EMVLight, surprisingly, manages to achieve nearly no increase in T_{avg} with added emergency capacity, even though more emergency lanes are formed as indicated by smaller T_{EMV} . This result shows that EMVLight is able to learn a strong traffic signal coordination strategy while navigating EMVs simultaneously. The proposed multi-class agent design demonstrates EMVLight’s capability of addressing the coupled problems of

EMV routing and traffic signal control simultaneously. EMVLight manages to prepare segments for incoming EMVs by reducing the number of vehicles on those segments and restores the impacted traffic in a timely manner after the EMV passage.

2.6.1.3 Manhattan_{16×3} results

Method	Manhattan _{16×3}	
	T_{EMV}	T_{avg}
FT w/o EMV	N/A	1649.64
W + static + FT	817.37 ± 17.40	1816.43 ± 68.96
W + static + MP	686.72 ± 19.23	917.52 ± 52.16
W + static + CDRL	702.62 ± 24.29	1247.67 ± 83.47
W + static + PL	626.88 ± 24.82	992.06 ± 47.67
W + static + CL	545.26 ± 30.21	855.28 ± 41.29
W + dynamic + FT	820.54 ± 28.86	1808.25 ± 68.04
W + dynamic + MP	632.68 ± 13.29	921.18 ± 49.29
W + dynamic + CDRL	680.62 ± 20.17	1262.39 ± 60.09
W + dynamic + PL	521.42 ± 27.62	977.62 ± 53.45
W + dynamic + CL	501.26 ± 28.71	862.94 ± 45.19
EMVLight	292.82 ± 16.23	782.13 ± 39.31

Table 2.7: T_{EMV} and T_{avg} for Manhattan_{16×3}. The average travel time without the presence of EMVs (1649.64) is retrieved from data.

Table 2.7 presents EMV travel time and average travel time of all the methods on the Manhattan_{16×3} map. In terms of T_{EMV} , dynamic routing benchmarks in general result in faster EMV passage, as expected. Compared with benchmark methods, EMVLight produces a considerably low average T_{EMV} of 292.82 seconds, which is 38% faster than the best benchmark (W+static+CL). As for T_{avg} , We have similar observation as in the synthetic maps that Max Pressure achieves a similar level of performance on reducing congestion as PressLight and beats CDRL by a solid margin of 25%. CoLight stands out among benchmarks regarding both metrics. Particularly, CoLight shortens T_{avg} by approximately one minute than Max Pressure strategies on this map.

Fig. 2.11 and Fig. 2.12 shows the learning curves of T_{EMV} and T_{avg} , respectively, in

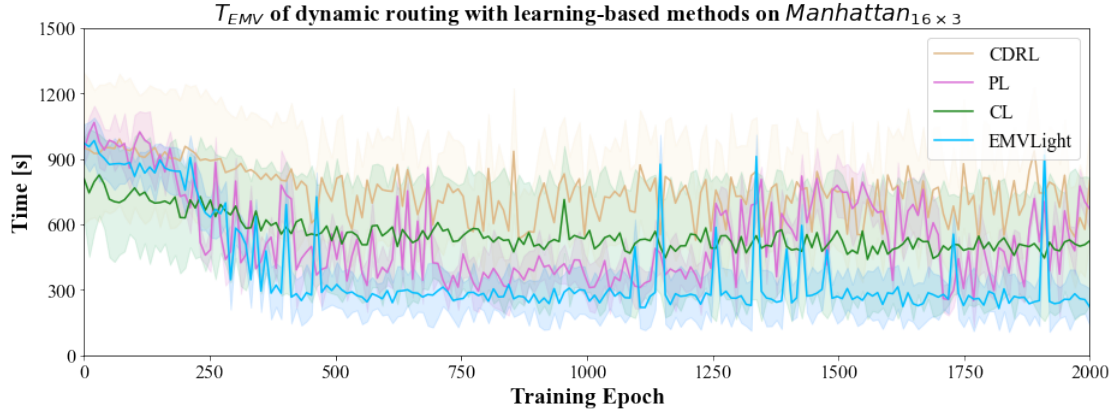


Figure 2.11: T_{EMV} convergence by learning-based dynamic routing strategies on *Manhattan*_{16×3}.

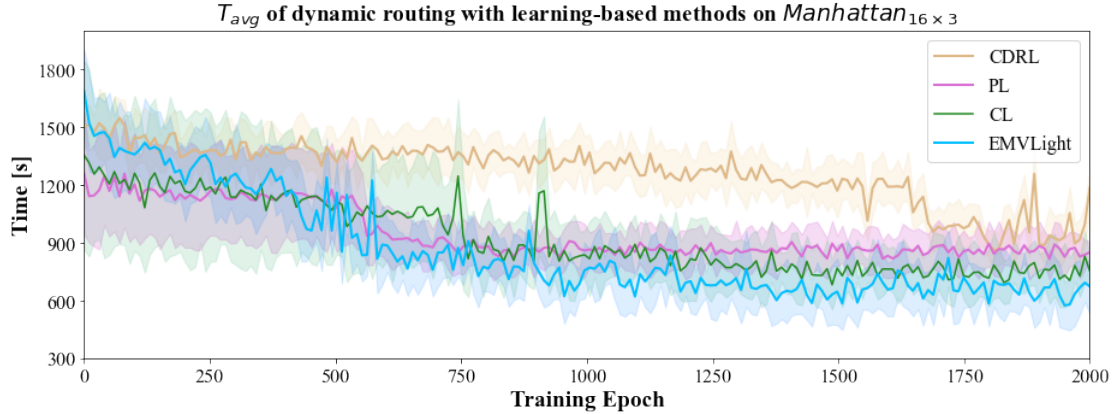


Figure 2.12: T_{avg} convergence by learning-based dynamic routing strategies on *Manhattan*_{16×3}.

the four RL methods. From both figures, we observe that EMVLight has the fastest convergence - in 500 epochs for T_{EMV} and in 1000 epochs for T_{avg} - among all four methods. In Fig. 2.11, both PressLight and CDRL struggle with converging to a stable T_{EMV} . In Fig. 2.12, CDRL converges very slowly as compared to the other three methods. Both figures shows that CDRL behaves the worst since its DQN design hardly scales with an increasing number of intersections. These learning curves demonstrate the fast and stable learning of EMVLight.

2.6.1.4 Hangzhou_{4×4} results

Method	Hangzhou _{4×4}	
	T_{EMV}	T_{avg}
FT w/o EMV	N/A	764.08
W + static + FT	466.19 ± 10.25	779.13 ± 12.90
W + static + MP	377.20 ± 14.42	404.37 ± 8.12
W + static + CDRL	409.56 ± 12.06	749.10 ± 10.02
W + static + PL	380.82 ± 6.72	425.46 ± 9.74
W + static + CL	368.20 ± 14.66	366.14 ± 8.25
W + dynamic + FT	415.63 ± 9.03	783.89 ± 10.03
W + dynamic + MP	328.42 ± 12.28	410.25 ± 6.23
W + dynamic + CDRL	401.08 ± 15.25	755.28 ± 12.82
W + dynamic + PL	321.52 ± 14.58	431.27 ± 8.24
W + dynamic + CL	319.84 ± 11.09	370.20 ± 7.13
EMVLight	194.52 ± 9.65	331.42 ± 6.18

Table 2.8: T_{EMV} and T_{avg} for Gudang_{4×4}. The average travel time without the presence of EMVs (764.08) is retrieved from data.

Table 2.8 presents T_{EMV} and T_{avg} of EMVLight and benchmark methods on Hangzhou_{4×4}. EMVLight achieves the lowest T_{EMV} of 194.52 seconds, *beating* the best benchmark (W+dynamic+CL) by 115 seconds (37%). As for T_{avg} , EMVLight also has excellent performance, exhibiting a 10% advantage over W+dynamic+CL, and a 20% advantage over W+dynamic+MP. Once again, Max Pressure *outperforms* PressLight in terms of T_{avg} . This is consistent with our observations with other maps above, suggesting Max Pressure result in great traffic signal coordination strategies to reduce overall congestion.

Based on results of all introduced experiments, Max Pressure has evinced the consistency to restrict congestion, particularly when restoring stagnant traffic after EMV passages. Consequently, Max Pressure accomplishes the comparable congestion reduction acquirement with, if not better than, RL-based strategies.

CDRL fails to learn an effective coordination strategy to manage congestion, where its T_{avg} trivially differs from Fix Time strategy’s T_{avg} . CoLight surpasses other methods by shortening T_{avg} by at least 40 seconds but it does not illustrate significant improvement

in terms of T_{EMV} from alternative benchmarks. Learning curves in Fig. 2.13 and 2.14 show that EMVLight converges in 500 epochs.

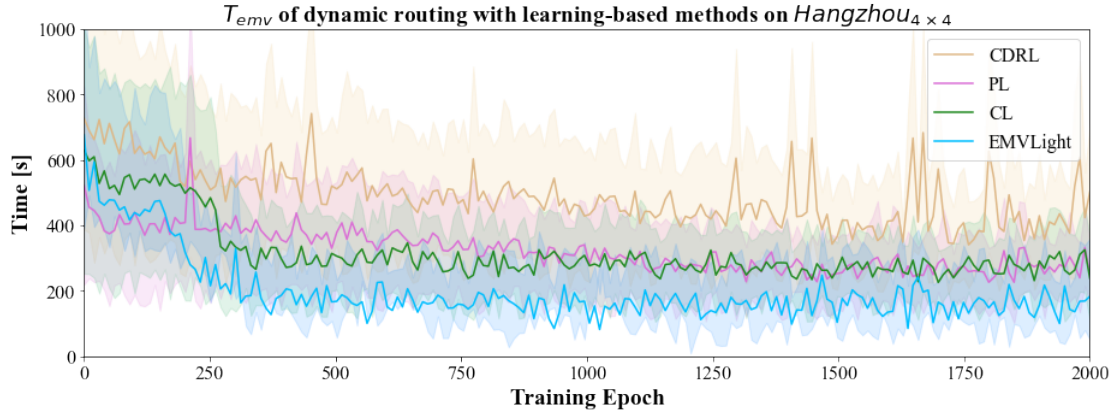


Figure 2.13: T_{EMV} convergence by learning-based dynamic routing strategies on $Hangzhou_{4 \times 4}$.

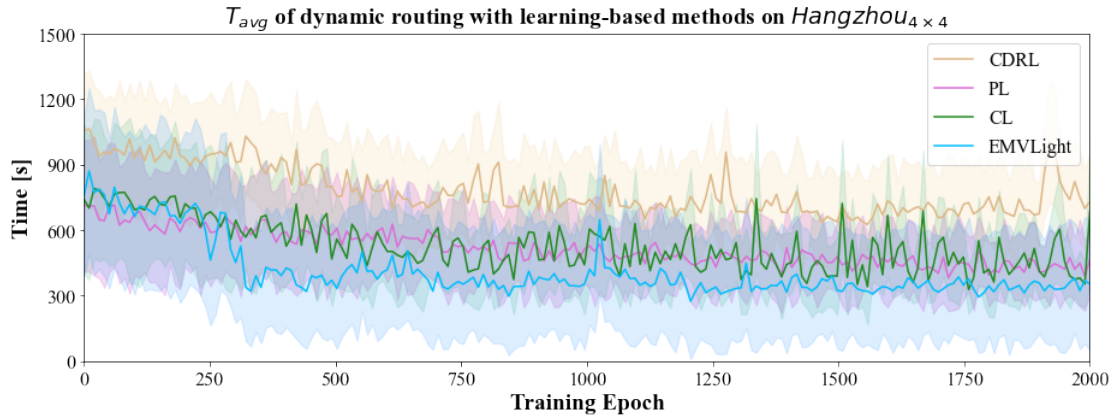


Figure 2.14: T_{avg} convergence by learning-based dynamic routing strategies on $Hangzhou_{4 \times 4}$.

2.6.2 Routing choices

In this section, we investigate the reason behind EMVLight's best performance in T_{EMV} from a routing perspective. In particular, we show how EMVLight is able to

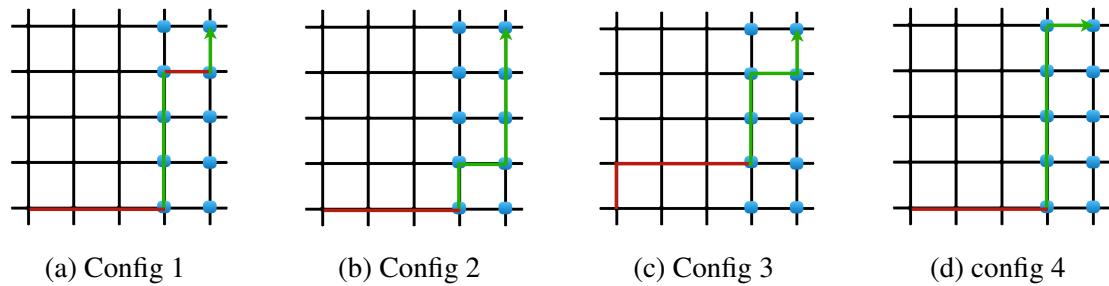


Figure 2.15: EMV’s routing choice on Emergency-capacitated Synthetic Grid $_{5 \times 5}$ based on EMVLight. Emergency lane established for EMV passage on segments highlighted in green, and not established on segments in red.

leverage emergency capacity to achieve maximum speed passage. To understand different route choices between benchmark methods and EMVLight, we analyze EMV routes on emergency-capacitated Synthetic Grid $_{5 \times 5}$ as well as Hangzhou $_{4 \times 4}$ to gain insight into the advantage of EMVLight.

Emergency-capacitated Synthetic Grid $_{5 \times 5}$ routes Routes selected by EMVLight are demonstrated in Fig. 2.15 for all four configurations. As this is a regular grid, first we notice that the length of all EMV routes are the Manhattan distance between the origin and destination. This is the shortest length possible to achieve successful EMV dispatch. The four routes confirm that EMVLight directs EMVs to enter the region in the east as soon as possible to leverage the extra emergency capacity for full speed passage. This results in 4 full speed links in Config 1 and 3 as well as 5 full speed links in Config 2 and 4.

We also present the route choices of W+static+MP and W+dynamic+MP in Config 1, of this map, as shown in Fig. 2.16. By comparing these routes with EMVLight (Fig. 2.15a), we can clearly see the benchmark method cannot actively leverage the emergency capacity, generating routes with only 1 full speed segment (Fig. 2.16a) and 2 full speed segment (Fig. 2.16b).

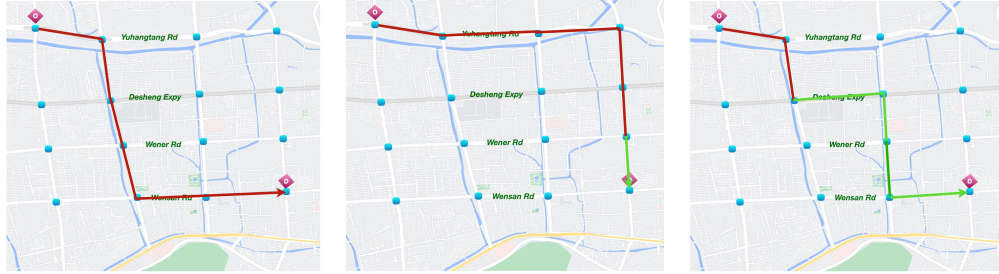


Figure 2.16: EMV's routing choice on config 1 of Emergency-capacitated Synthetic Grid_{5×5} under MP-based benchmarks.

Hangzhou_{4×4} routes Since Hangzhou_{4×4} is an irregular grid where different links have different lengths, the routes optimized by different algorithms have different total lengths. This provides another perspective on evaluating routing performance of different models. Fig. 2.17 shows EMV routes given by W+static+MP, W+dynamic+MP and EMVLight in this grid. By comparing the total distances of the three routes, we find that the route chosen by EMVLight is the longest among the three models. However, EMVLight achieves the smallest EMV travel time on this route. This is because EMVLight is able to coordinate traffic signals to leverage the emergency capacity to let the EMV travel at its maximum speed on more than half of the route, indicated by the green segments.

As for static routing (W+static+MP), it chooses a fixed route given the traffic conditions upon dispatching, favoring the shortest-in-distance route. The dynamic routing method (W+dynamic+MP) recalculate the time-based shortest path every 30 seconds as EMV travels. Most of the time, however, Max Pressure fails to reduce the number of vehicles on the upcoming links to enable an emergency lane. Fig. 2.17b shows that the emergency lane is only formed in one of the six links. EMVLight is able to further reduce EMV travel time partly because the time-based shortest path is updated in real time. More importantly, EMVLight is able to reduce the number of vehicles in upcoming links so that emergency lanes can be formed. This can be attributed to the design of

primary and secondary preemption agents in EMVLight, which will be further examined in Sec.2.6.3.1.



(a) 5.5km, $277.20 \pm 14.42s$ (b) 5.9km, $228.42 \pm 12.28s$ (c) 6.0km, **$194.52 \pm 9.65s$**

Figure 2.17: The corresponding route selected by (a) W+static+MP, (b) W+dynamic+MP, (c) EMVLight on Hangzhou_{4x4}. Distance and T_{EMV} for the selected path are indicated. The lowest values are highlighted in bold.

2.6.3 Ablation Studies

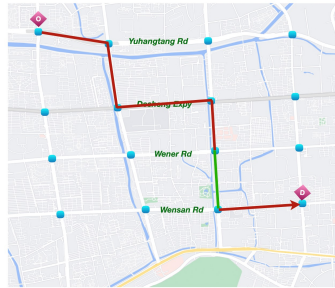
2.6.3.1 Ablation studies on reward

We propose three types of agents and design their rewards (Eqn. (2.4)) based on our improved pressure definition and heuristics. In order to see how our improved pressure definition and proposed agent types influence the results, we propose three ablation studies:

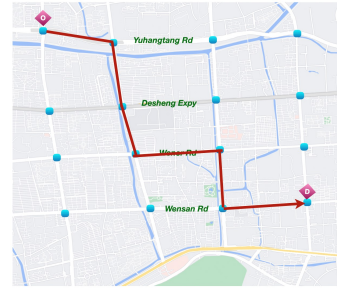
1. replacing our pressure definition by that defined in PressLight
2. replacing our pressure definition by $P_i = \sum_{l \in \mathcal{I}_i} w(l)$
3. replacing secondary pre-emption agents with normal agents
4. replacing primary pre-emption agents with normal agents

Ablations	Ablation 1	Ablation 2	Ablation 3	Ablation 4	EMVLight
T_{EMV} [s]	205.20 \pm 6.92	237.40 \pm 10.08	311.52 \pm 5.18	384.71 \pm 8.52	194.52 \pm 9.65
T_{avg} [s]	389.14 \pm 8.40	382.07 \pm 6.92	442.73 \pm 6.65	444.15 \pm 7.02	331.42 \pm 6.18

Table 2.9: Ablation studies on pressure-based reward design and agent types. Experiments are conducted on Hangzhou_{5 \times 5}. The lowest value are highlighted in bold.



(a) Without secondary agents



(b) Without primary agents

Figure 2.18: EMV’s route choice on Hangzhou_{4 \times 4} with replaced primary (a) and secondary (b) agents.

Table 2.9 shows the results of these ablations on the Hangzhou_{4 \times 4} map. We observe that PressLight-style pressure yields a slightly larger T_{EMV} but significantly increases the T_{avg} . Without secondary pre-emption agents, T_{EMV} increases by 60% since almost no “link reservation” happened. In Ablation 2, if we do not take the average while keep the sum of absolute value of lane pressures as the intersection pressure, we notice a slightly smaller T_{avg} but a 15% increase in T_{EMV} . EMVLight’s pressure design outperforms the ones in Ablation 1 and 2 and has been proven as the most suitable pressure design for this particular task. Moreover, without primary pre-emption agents, T_{EMV} increases considerably, which again proves the importance of pre-emption. We can further confirm the importance of agent designs by inspecting the selected routes in the last two ablation studies. Fig. 2.18a and 2.18b shows routes selected by EMVLight’s after replacing secondary agents and primary agents with normal agents, respectively. Even though the routes are similar as that in Fig. 2.17c, much fewer emergency lanes are successfully

formed. This failure of utilizing emergency capacity lead to the significant increase in EMV travel time as shown in Table 2.9. As we can see from the routes, EMVs barely take advantage of emergency yielding during their trips.

2.6.3.2 Ablation study on policy exchanging

In multi-agent RL, fingerprint has been shown to stabilize training and enable faster convergence. In order to see how fingerprint affects training in EMVLight, we remove the fingerprint design, i.e., policy and value networks are changed from $\pi_{\theta_i}(a_i^t | s_{\mathcal{V}_i}^t, \pi_{\mathcal{N}_i}^{t-1})$ and $V_{\phi_i}(\tilde{s}_{\mathcal{V}_i}^t, \pi_{\mathcal{N}_i}^{t-1})$ to $\pi_{\theta_i}(a_i^t | s_{\mathcal{V}_i}^t)$ and $V_{\phi_i}(\tilde{s}_{\mathcal{V}_i}^t)$, respectively. Fig. 2.19 shows the influence of fingerprint on training. With fingerprint, the reward converges faster and suffers from less fluctuation, confirming the effectiveness of fingerprints, i.e. policy exchanging.

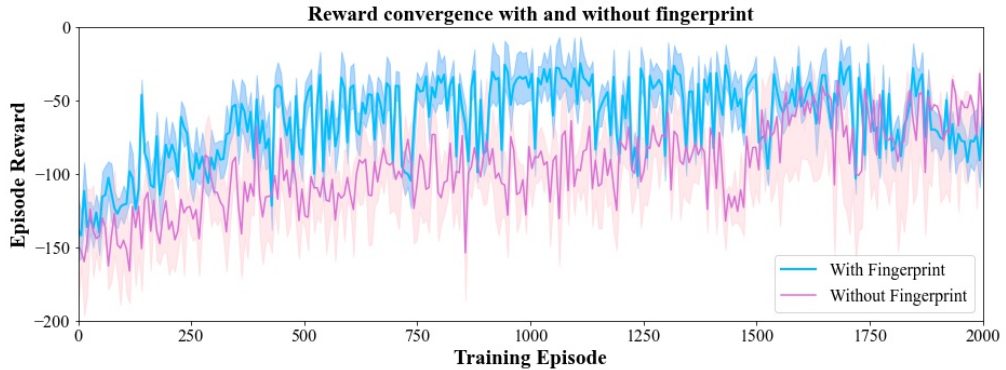


Figure 2.19: Reward convergence with and without fingerprint. Experiments are conducted on Config 1 synthetic grid_{5×5}.

2.6.4 Sensitivity Analysis on β

The value of β 's in Eqn. (2.4b) represents the weights assigned to the two tasks. When $\beta = 1$, the secondary pre-emption agents will act like normal agents and only focus on congestion alleviation. When $\beta = 0$, the secondary pre-emption agents concentrate on

emptying non-EMVs and reserve the whole segment for the approaching EMV. In order to illustrate the tradeoff, we conduct experimental runs on the emergency-capacitated synthetic Grid_{5×5} with configuration 1 as the sensitivity analysis on β , see Table 2.10. We perform 5 independent runs for each β 's value.

	0	0.25	0.5	0.75	1
T_{EMV}	119.10 ± 5.14	134.40 ± 5.83	158.20 ± 6.28	172.60 ± 5.71	185.20 ± 4.19
T_{avg}	340.23 ± 4.75	338.17 ± 7.25	334.92 ± 5.52	331.81 ± 9.28	327.10 ± 8.18

Table 2.10: EMVLight’s performance on Emergency-capacitated Synthetic Grid_{5×5} with Configuration 1 given different values of β .

As we can see from Table 2.10, T_{EMV} obtains the minimum value when β is 0 since the EMV’s path has been cleared and reserved in advance. Comparing to T_{EMV} when $\beta = 1$, we witness a 35% reduction in T_{EMV} when secondary agents effortlessly reserve the segments. Likewise, T_{avg} hits the smallest value when secondary agents shift their responsibility onto congestion reduction entirely. Under this scenario, pre-emption only happens on the segment which EMV is currently traveling on and the EMV will travel with the slowest speed since more vehicles appear ahead of its road. Although every non-EMV saves about 10 seconds for the whole trip in this case, an ambulance might delay for more than one minute and a precious life might be lost. We believe it would be the best for the traffic system administrator to decide β given the emergency of the case.

2.7 Summary

In this paper, we introduced a decentralized reinforcement learning framework, EMVLight, to facilitate the efficient passage of EMVs and reduce traffic congestion at the same time. Leveraging the multi-agent A2C framework, agents incorporate dynamic routing and cooperatively control traffic signals to reduce EMV travel time and

average travel time of non-EMVs. Our work considers the realistic settings of emergency capacitated road segments and traffic patterns before, during and after EMV passages. Extending Dijkstra's algorithm and embedding into the multi-class RL agent design, EMVLight fundamentally addresses the coupling challenge of EMV's dynamic routing and traffic signal control, filling the research gap on this particular task. Evaluated on both synthetic and real-world map, EMVLight shortens the EMV travel time and average travel time by up to 42.6% and 23.5% respectively, comparing with existing methods from traditional and learning-based traffic signal control for EMV-related managements. Both quantitative and qualitative assessments on EMVLight, including its EMV navigation as well as pre-clear and restore traffic conditions under emergency state, have concluded that EMVLight is a promising control scheme for such task.

Non-trivial future directions for this study including, but not limited to, the followings. First, the interactions among vehicles, especially under emergency, are extremely complicated. As an effort to close the gap between simulation and reality, we are motivated to extend current ETA estimation model to capture more realistic traffic patterns with EMVs so that agents are more responsive in the field tests. Second, we are looking forward to navigating multiple EMVs simultaneously in the same traffic network. The reward design for pre-emption agents (imagine two or more EMVs appears within one intersection) is worth a technical and ethical discussion. Last but not least, as one of the RL applications in the field of transportation, our method has required a massive number of updated iterations, even in the simulated environments, to achieve the desirable result. How to learn efficiently so that our trail-and-error attempts would not bring catastrophic impacts on real traffic is a critical question for all ITS RL applications.

Chapter 3

Dynamic Queue-jump Lane for Emergency Vehicles: a Multi-agent Proximal Policy Optimization Approach

3.1 Introduction

The increasing population and urbanization have made it exceedingly difficult to operate urban emergency services efficiently. Over the past decade, response times for emergency vehicles (EMVs), such as ambulances, fire trucks, and police vehicles, have worsened due to rising traffic congestion. Historical data from New York City, USA [91], shows that the number of annual emergency incidents increased from 1,114,693 in 2004 to 1,352,766 in 2014, with average response times increasing from 7 minutes 53 seconds to 9 minutes 23 seconds [92]. This represents a 20% increase in response times over a decade. Furthermore, in fiscal year 2023, the city's emergency response times worsened by an additional 82 seconds—16.1% higher than in 2019 [93]. These delays

are especially critical in life-threatening situations, such as cardiac arrests, where every minute without defibrillation reduces survival chances by 7% to 10%, with survival rates dropping sharply after 8 minutes [4].

Given the urgent need to reduce EMV response times, technological solutions must be explored to mitigate the impact of traffic congestion. One promising direction is the use of connected vehicle technologies, specifically vehicle-to-everything (V2X) communication, which allows for real-time information sharing between EMVs, non-EMVs, and traffic management systems. These systems enable EMVs to receive optimal routing information based on current traffic conditions, and they facilitate coordination between non-EMVs to clear paths for approaching EMVs.

This study focuses on a critical yet specific challenge within the focused context of intra-link movement of EMVs: the establishment of dynamic queue jump lanes (DQJL) to expedite EMV passage through congested road segments.

Definition 1 (Dynamic Queue Jump Lane). *A DQJL is a dynamically formed lane created while an EMV is approaching or en route, clearing downstream space to facilitate its passage.*

A queue jump lane (QJL) is typically used in bus operations to allow buses to bypass long queues before intersections [94, 95]. In the context of EMV movement, we introduced DQJL as in Definition 1. The formation of these lanes is facilitated by V2X technology, which enables connected and autonomous vehicles (CAVs) to coordinate their maneuvers based on real-time instructions. However, the challenge is not only to ensure rapid EMV passage but also to minimize the disruption to surrounding traffic, particularly the non-connected human-driven vehicles (HDVs), which are not directly controllable.

The task of DQJL formation is highly intricate, as it requires coordinating CAVs to

influence the behavior of HDVs indirectly, a task fraught with uncertainty due to the unpredictability of human drivers. The key objective is to minimize the time it takes for the EMV to traverse the congested segment while ensuring reduced maneuvers from non-EMVs, particularly HDVs, motivating all maneuvers to be efficient. Striking a balance between these objectives—optimizing EMV passage time while reducing the complexity of maneuvers for non-EMVs—requires sophisticated coordination strategies.

To address these challenges, we propose modeling the DQJL formation as a partially observable Markov decision process (POMDP), which allows for the incorporation of both controllable CAVs and uncontrollable HDVs. The POMDP framework enables agents (CAVs) to make real-time decisions based on partial observations of the traffic environment. We adopt a multi-agent actor-critic deep reinforcement learning approach to derive optimal coordination strategies, enabling CAVs to dynamically clear lanes for EMVs while minimizing the impact on other vehicles. This approach accounts for partial connectivity, ensuring flexibility with varying levels of CAV penetration rates in mixed traffic environments.

The contributions of this work are threefold. First, we introduce the concept of DQJL as a novel traffic management strategy, providing a scalable framework for its dynamic formation in mixed traffic environments. This framework addresses the inherent complexities of heterogeneous traffic systems by integrating both CAVs and HDVs. Second, we design a multi-agent reinforcement learning algorithm tailored to optimize DQJL formation. This algorithm leverages centralized training with decentralized execution to effectively coordinate CAVs while accounting for the stochastic and reactive behavior of HDVs, ensuring robust performance under varying traffic conditions. Finally, through extensive SUMO-based simulations, we validate the proposed system’s effectiveness. Our results demonstrate substantial improvements over baseline scenarios, achieving

significant reductions in EMV passage time (up to 39.8%) and overall lane-changing maneuvers (up to 55.7%), particularly under scenarios with increasing CAV penetration rates.

The remainder of this chapter is organized as follows. In Section 3.2, we review relevant studies on queue-jump lanes and multi-agent reinforcement learning (MARL) frameworks in connected vehicle applications. Section 3.3 formulates the DQJL problem as a partially observable Markov decision process (POMDP), differentiating between CAVs and HDVs in mixed traffic scenarios. In Section 3.4, we present our MARL-based approach for solving the DQJL problem, detailing the network architecture and learning algorithms. Section 3.5 outlines the experimental setup. In Section 3.6, we present experimental results and key insights and a conclusion is drawn in Section 3.7.

3.2 Literature Review

In this section, we discuss literature available on queue jump lane in Subsec. 3.2.1, and existing multi-agent deep reinforcement learning techniques on similar connected vehicle applications in Subsec. 3.2.2.

3.2.1 Queue Jump Lane for EMVs

Deep learning has recently demonstrated significant promise across various applications [96, 97, 98, 99, 100, 101, 102]. Queue jump lanes (QJLs) have never been used for EMV deployment and represent a novel operational strategy that leverages CAV technologies for EMV deployment. Although QJLs are relatively new, the literature already demonstrates their positive effects in reducing travel time variability, particularly when combined with transit signal priority (TSP). However, these studies are primarily

based on moving-bottleneck models for buses [94, 95, 103, 104]. We adapt this bus operation strategy for EMV deployment in our setting, given that EMVs typically travel faster than non-EMVs and can “preempt” non-EMV traffic due to their priority status.

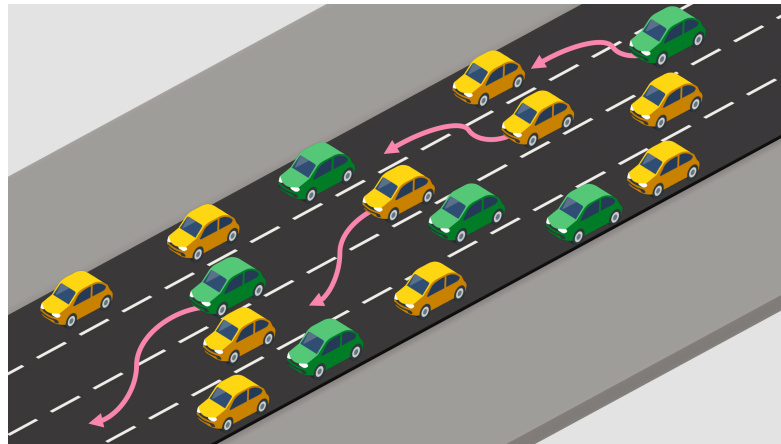
At the same time, traditional siren technologies often fail to provide adequate warning time for other vehicles, and there is frequently a lack of clarity regarding which route should be avoided [105, 106, 107]. This confusion, particularly under highly congested conditions, leads to increased delays, as mentioned earlier, and contributes to accident rates that are 4 to 17 times higher [5, 108], as well as increased collision severity [6, 109, 110], both of which can further delay EMV response times. A study by Savolainen et al. [111], utilizing data from Detroit, Michigan, confirmed the sensitivity of driver behaviors to various ITS communication methods for conveying EMV route information. Kohneh et al. [112] adopts a hybrid non-dominated sorting genetic algorithm II-particle swarm optimization (NSGAI-PSO) approach to solve the bi-objective optimization problem which minimizes EMV travel time while maximizing safety.

Wu et al. [113] proposed a lane pre-clearing strategy for normal road segments, employing cooperative driving with CAVs to maintain EMV speed while minimizing traffic disruption. Their approach formulates the problem as a bi-level optimization and employs an EMV sorting algorithm, effectively clearing lanes and identifying a linear relationship between optimal solutions and road density to improve EMV routing decisions. Hannoun et al. [69] utilized mixed-integer linear programming (MILP) to develop a static path clearance control strategy for approaching EMVs. A follow-up work [70], relying on V2X, extended the problem to larger distances by dividing roads into segments, allowing for a divide-and-conquer approach to optimization. These approaches simplify the road network into cells, approximating vehicle positions and velocities, limiting its precision and applicability to complex real-world traffic scenarios.

Moreover, the computational complexity of MILP-based approaches makes them less suited for real-time applications in dynamic traffic settings.

QJLs have not yet been studied as a dynamic control strategy, underscoring the need to account for uncertainties in realistic, non-deterministic traffic conditions, such as yielding to an approaching EMV [114, 115, 116]. To address this gap, we introduce the concept of dynamic queue jump lanes (DQJLs), as illustrated in Fig. 3.1. During the DQJL clearing process for an approaching EMV, non-EMVs are continuously monitored and instructed, enabling the rapid and safe establishment of DQJLs. Additionally, we explore the application of DQJLs in partially connected scenarios, where only a subset of vehicles are equipped with communication devices, allowing for partial communication between vehicles and infrastructure.

A related task, referred to as corridor clearance, is investigated by Suo et al. [117, 118], who propose a proximal policy optimization (PPO) method to enhance clearance between intersections. In their approach, the corridor is formed by designating a single CAV as a "splitting point", which blocks following traffic to allow the EMV to switch into a less congested lane. However, their study adopts a single-agent perspective, focusing solely on the interaction between a CAV and an EMV, thereby limiting the collaborative potential of multiple CAVs in the system. Additionally, the simulation was conducted on a simple two-lane road segment, failing to capture the more complex interactions between CAVs and background traffic in multi-lane environments. This "splitting point" design, however, suggests that DQJLs do not always have to be a straight line. Instead, they can consist of different lanes that require minimal lane-change maneuvers by the EMV. While this might slightly increase the EMV's passage time, it minimizes disruption to the surrounding traffic, see Fig. 3.2.

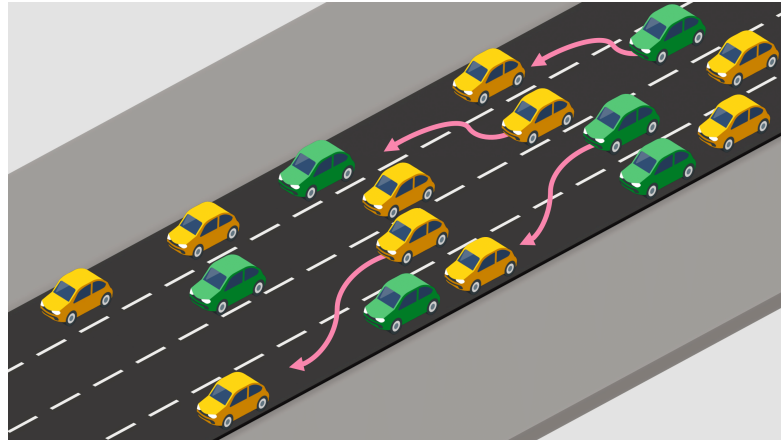


(a) Actions planning.



(b) DQJL established.

Figure 3.1: Illustration of a DQJL formation: Green vehicles are CAVs and yellow ones are HDVs. HDVs yields and CAVs perform coordinated lane changes for a DQJL.



(a) Actions planning.



(b) DQJL established.

Figure 3.2: An alternative DQJL formation, where the EMV will change lane once.

3.2.2 Multi-agent Reinforcement Learning for CAVs

The proliferation of V2X communication technologies has significantly increased the presence of CAVs, driving extensive research into multi-agent reinforcement learning (MARL) frameworks for vehicular applications [119, 120, 121, 122]. In these systems, individual vehicles are modeled as autonomous agents collaborating toward shared objectives. This paradigm offers several advantages, including decentralized decision-making, scalability, adaptability to dynamic traffic conditions, and the capacity for

collaborative learning among vehicles.

MARL in CAV scenarios presents a promising approach to addressing complex transportation challenges, particularly where traditional methods have shown limitations. Recent studies have applied MARL to various aspects of traffic management and vehicle coordination, highlighting its versatility and effectiveness. For instance, in the realm of congestion mitigation, Ha et al. [123] developed a MARL-based control model using graph convolutional networks (GCN) and deterministic policy gradient (DDPG) techniques for highway scenarios, outperforming traditional speed harmonization methods even with low CAV penetration rates. Similarly, Nakka et al. [124] applied a decentralized multi-agent deterministic policy gradient (MADDPG) approach to highway merging, successfully eliminating stop-and-go traffic.

Intersection management has also been a key focus for MARL applications [125, 126, 127, 128, 129]. Guo et al. [130] employed an enhanced monotonic value function factorisation (QMIX) algorithm to coordinate CAVs at unsignalized intersections in mixed-autonomy traffic, while Antonio et al. [131] introduced an advanced autonomous intersection management (AIM) system using MARL and Curriculum through Self-Play, significantly surpassing traditional traffic light systems in performance.

In vehicle control, Zhou et al. [132] proposed an MA2C method for lane-changing decisions in mixed traffic environments, utilizing a multi-objective reward function. Shi et al. [133] presented a cooperative longitudinal control strategy for CAVs in mixed traffic, improving both string stability and efficiency. Additionally, Chen et al. [134] addressed mixed-traffic highway on-ramp merging with a MARL framework, enabling autonomous vehicles to collaborate and adapt to human-driven vehicles (HDVs).

Beyond traffic flow management, MARL has demonstrated potential in other CAV applications [135, 136, 137]. Zhang et al. [138] developed a MARL framework for

online parking assignment in mixed CV and non-connected vehicle (NCV) environments, achieving substantial improvements over conventional methods. In the domain of robotic driving simulation, Palanisamy et al. [139] introduced MACAD-Gym, a multi-agent simulation platform for CAVs, which supports research into deep reinforcement learning (DRL)-based algorithms in complex, multi-agent environments beyond geo-fenced operational design domains.

Parada et al. [140] have proposed a MAPPO learning framework for autonomous vehicle maneuvering in the presence of EMVs. However, this study assumes a fully autonomous traffic setting and focuses primarily on collision risk avoidance. While effective for collision minimization, this design de-prioritizes the reduction of EMV passage time, which is a critical factor in emergency response. Such an approach may also not be feasible for near-term deployment in mixed autonomy environments.

These diverse applications of MARL in CAV contexts underscore its potential to revolutionize traffic management and vehicle coordination [141, 142, 143]. For those interested in a more comprehensive review of MARL frameworks for CAV applications in mixed traffic environments, Yadav et al. [144] and Dinneweth et al. [145] provide valuable insights into the current state of the art and emerging trends in this rapidly advancing field.

Despite the extensive research on MARL in CAV applications, there is currently no work that employs MARL and focuses on pre-clearing lanes for EMVs in heterogeneous traffic settings. This gap presents an exciting opportunity for this research to explore how MARL can be leveraged to optimize the formation and management of DQJLs, potentially resulting in more efficient and adaptive traffic management strategies in urban environments.

3.3 Dynamic Queue Jump Lanes in Mixed Traffic

In this section, we describe the modeling of DQJL formation as a discrete-time partially observed Markov Decision Process (POMDP) in Subsec. 3.3.1. Additionally, in Subsec. 3.3.2, we introduce two distinct agent designs for CAVs and HDVs, enabling the study of system performance under varying levels of connectivity penetration. This approach allows for a comprehensive evaluation of DQJL formation dynamics in mixed traffic environments.

3.3.1 System Modeling

We formulate the establishment of DQJLs in heterogeneous traffic as a collaborative multi-agent system. Each non-EMV is an autonomous agent, with the agent set \mathcal{N} comprising two subsets:

$$\mathcal{N} = \mathcal{N}_{\text{CAV}} \cup \mathcal{N}_{\text{HDV}} \quad (3.1)$$

DQJLs can be formed either before or when EMVs enter a road segment. To investigate interactions between EMVs and non-EMVs, we assume an EMV begins traversing a congested road segment at time t_0 , where the EMV itself is not considered an active agent but passively awaits the clearing of a path. In this scenario, CAVs leverage V2X communication capabilities, while HDVs rely solely on local sensory information. All agents collaborate to create a clear path for the EMV.

This mixed autonomy environment is modeled as a Partially Observable Markov Decision Process (POMDP), represented by the tuple $(S, A, T, R, \Omega, O, \gamma)$. In this formulation, S denotes the global state space that represents the overall traffic environment, including the positions, speeds, and states of CAVs, HDVs, and the EMV. Each agent

takes actions from the action space A , with choices such as lane changes or speed adjustments aimed at optimizing DQJL formation. The transition function $T : S \times A \rightarrow S'$ defines how the state of the environment evolves probabilistically in response to agents' actions.

The reward function R_i , specific to each agent $i \in \mathcal{N}$, balances global system-wide objectives with individual goals. Observations are partial, where Ω represents the observation space for each agent, and the observation function O maps the global state to the local observation available to each agent. Notably, the observation space and observation function differ between CAVs and HDVs, reflecting their distinct capabilities, which will be further discussed in Subsec 3.3.2. The process is further governed by a discount factor γ , which moderates the trade-off between immediate and future rewards.

3.3.2 Agent Design

This study proposes two realistic and straightforward designs for CAVs and HDVs, tailored to their respective communication, perception capabilities, and maneuverability.

3.3.2.1 Connected and Automated Vehicles (CAVs)

The POMDP for the i -th CAV agent is defined as:

$$\text{POMDP}_{\text{CAV}}^i = (S^i, A^i, T^i, R^i, \Omega^i, O^i, \gamma) \quad (3.2)$$

State Space The state space for the i -th CAV is given by:

$$S^i = \{x, y, v, d_{\text{EMV}}, l_{\text{EMV}}, d_{\text{clear}}\} \quad (3.3)$$

In this formulation, x denotes the longitudinal position of the CAV, while y refers to

the lateral position, represented as an integer indicating the lane index. The variable v describes the velocity of the CAV. The term d_{EMV} represents the longitudinal distance to the approaching EMV, and l_{EMV} denotes the lane difference with respect to the EMV. This lane difference is expressed as an integer, where positive or negative values indicate the relative lane position of the CAV compared to the EMV, allowing for multiple lane differences (e.g., $-2, -1, 0, 1$). Lastly, d_{clear} stands for the clear distance ahead, providing essential feedback for the agent to learn lane-changing strategies and evaluate the completeness of DQJL formation. Based on this design, the responsibility for effective DQJL formation predominantly rests with CAVs.

Action Space The action space for the i -th CAV is decomposed into longitudinal and lateral actions:

$$A^i = A_{long} \times A_{lat} \quad (3.4)$$

The longitudinal action space A_{long} consists of discrete control actions for speed adjustment, allowing a CAV to accelerate, decelerate, or maintain its current speed. Specifically, we discretize the action space as follows:

$$A_{long} = \{-2.5 \text{ m/s}^2, 0 \text{ m/s}^2, +1.5 \text{ m/s}^2\}.$$

Here, a negative value corresponds to deceleration, zero indicates maintaining the current speed, and a positive value corresponds to acceleration. These choices reflect representative urban driving behaviors, enabling the CAV to respond flexibly to varying traffic conditions, including the distance to the EMV (d_{EMV}) and the clear distance ahead (d_{clear}).

The lateral action space, A_{lat} , determines whether the CAV performs a lane change. It includes actions to indicate the direction of lane changes, where $A_{\text{lat}} = 1$ denotes a lane change to the right, $A_{\text{lat}} = -1$ indicates a lane change to the left, and $A_{\text{lat}} = 0$ means no lane change. These lateral actions are based on the CAV's current lane position y , the lane difference relative to the EMV (l_{EMV}), and the state of neighboring vehicles $\mathbf{N}_{\text{local}}$, allowing the agent to perform lane changes that contribute to efficient DQJL formation.

Transition Function The transition function T^i represents the probabilistic model of how the environment changes in response to the CAV's actions. Given the current state S^i and action A^i , T^i models the transition to the next state. This includes the changes in the CAV's position, speed, and the dynamic states of neighboring vehicles based on both local actions and external factors like traffic flow and EMV behavior. Mathematically, this can be expressed as:

$$T_{\text{CAV}}^i(S_t^i, A_t^i) \sim P(S_{t+1}^i | S_t^i, A_t^i),$$

Observation Space and Function The observation space Ω^i consists of information that the i -th CAV can perceive from the environment. The observation function O^i maps the global state S^i to the partial observation Ω^i available to the CAV. Mathematically, this can be expressed as:

$$\Omega^i = O^i(S^i) \quad \text{where} \quad O^i : S^i \rightarrow \Omega^i$$

The observation space Ω^i is a concatenation of the state of the ego vehicle and the states of all vehicles within a certain radius. If a neighboring vehicle is a CAV, full state information is communicated, including position, velocity, and lane index. For HDVs,

the CAV can only perceive partial information, limited to the position (x, y) and velocity v . Therefore, Ω^i is defined as:

$$\Omega^i = \{x, y, v, \mathbf{N}_{CAV}, \mathbf{N}_{HDV}\},$$

where \mathbf{N}_{CAV} denotes the full state information of neighboring CAVs, including their position (x, y) , velocity v , and \mathbf{N}_{HDV} represents the partial state information of neighboring HDVs, limited to their position (x, y) and velocity v .

This design aligns with the advanced communication and perception capabilities of CAVs, positioning them as the proactive agents in traffic control. By leveraging their ability to exchange comprehensive state information with other CAVs and perceive partial data from HDVs, CAVs can make informed, real-time decisions that optimize traffic flow and ensure smoother interactions with CAVs and HDVs.

3.3.2.2 Human-Driven Vehicles (HDVs)

The POMDP for the i -th HDV agent is defined as:

$$\text{POMDP}^i = (S^i, A^i, T^i, R^i, \Omega^i, O^i, \gamma) \quad (3.5)$$

State Space The state space for the i -th HDV is given by:

$$S^i = \{x, y, v, b_{\text{alert}}\} \quad (3.6)$$

In this formulation, x denotes the longitudinal position of the HDV, while y refers to the lateral position, represented as an integer indicating the lane index. The variable v represents the velocity of the HDV. The boolean variable b_{alert} indicates whether the HDV

has been alerted to the EMV's presence, either through visual or auditory cues such as sirens or traffic signals.

Action Space The action space for the i -th HDV is simplified to account for basic human driving maneuvers:

$$A^i = A_{\text{yield}} \times A_{\text{lat}} \quad (3.7)$$

The longitudinal action space, A_{yield} , is binary, indicating whether the HDV decides to yield (1) or not (0) in response to an EMV alert. The lateral action space, A_{lat} , governs lane-changing behavior. Similar to CAVs, $A_{\text{lat}} = 1$ represents a lane change to the right, $A_{\text{lat}} = -1$ signifies a lane change to the left, and $A_{\text{lat}} = 0$ indicates no lane change. Under normal driving conditions, HDVs do not yield. However, when hearing sirens or observing visual cues from an approaching EMV, the HDVs' actions are locked into $A_{\text{yield}} = 1$, prompting them to find the next available free space to change lanes, pull over, or stop. These simplified actions reflect the limited complexity of human drivers' decision-making when responding to EMVs. It is anticipated that CAVs, being more proactive agents, can learn the yielding patterns of HDVs and adjust accordingly.

Transition Function The transition function T^i for the i -th HDV models how the environment evolves based on the HDV's actions. Given the current state S^i and action A^i , T^i describes the transition to the next state, accounting for changes in the HDV's position, speed, and interactions with other vehicles. Since HDVs rely on limited sensory information, external factors such as CAVs' maneuver and EMV behavior have significant

influence on these transitions. Mathematically, this can be expressed as:

$$T_{\text{HDV}}^i(S_t^i, A_t^i) \sim P(S_{t+1}^i | S_t^i, A_t^i),$$

Observation Space and Function HDVs operate with a simplified observation space, limited to the ego vehicle’s state and nearby vehicle positions and velocities. Lacking communication capabilities, HDVs rely solely on local perceptions from onboard sensors, resulting in restricted and naive decision-making. This limitation underscores the critical role of CAVs in compensating for HDVs’ reduced situational awareness and reactivity.

Despite their mostly passive behavior, HDVs are still modeled as agents for several reasons. First, their actions, such as deciding to yield or not, directly influence the efficiency of DQJL formation and the passage time of the EMV. Modeling HDVs as agents allows the framework to incorporate the stochastic and reactive nature of human drivers, which is critical for robust policy learning by CAVs. Second, this design enables the simulation of realistic interactions between CAVs and HDVs, allowing CAVs to anticipate HDV behavior and adapt accordingly. Finally, HDVs contribute to the learning process by generating reward signals (see Subsubsec. 3.3.2.3), ensuring that the policies learned by CAVs account for both cooperative and uncooperative HDV behaviors. By treating HDVs as agents, the framework effectively captures the dynamics of mixed traffic environments and ensures scalability under varying levels of CAV penetration.

3.3.2.3 Reward Design

The reward structure is designed to encourage both global cooperation and individual efficiency. For each agent i , the reward function combines a shared global reward and an agent-specific local reward:

$$R_{\text{global}} = - \left(\underbrace{\beta_1 \cdot t_{\text{EMV}}}_{\text{Time Penalty}} + \underbrace{\beta_2 \cdot n_{\text{EMV}}^{\text{lane change}}}_{\text{Lane Change Penalty}} + \underbrace{\beta_3 \cdot \left(1 - \frac{d_{\text{clear}}}{L}\right)}_{\text{DQJL Completeness Penalty}} \right) \quad (3.8)$$

$$R^i = \alpha R_{\text{global}} - (1 - \alpha) \cdot R_{\text{local}}^i \quad (3.9)$$

The global reward R_{global} is shared among all agents and reflects system-wide objectives: minimizing EMV passage time, reducing EMV lane changes, and ensuring complete DQJL formation. This shared reward promotes coordination between agents toward common goals.

The local reward R_{local}^i varies by agent type:

1. ****For CAVs****:

$$R_{\text{local}}^{\text{CAV}} = \underbrace{-\eta_1 \cdot n_{\text{CAV}}^{\text{lane change}}}_{\text{Local: CAV Lane Change Penalty}} + \underbrace{-\eta_2 \cdot |a_{\text{long}}|}_{\text{Local: CAV Acceleration Penalty}}$$

The local reward for CAVs penalizes excessive lane changes and sudden acceleration or deceleration, encouraging smoother driving behavior.

2. ****For HDVs****:

$$R_{\text{local}}^{\text{HDV}} = \underbrace{-\eta_3 \cdot n_{\text{HDV}}^{\text{lane change}}}_{\text{Local: HDV Lane Change Penalty}}$$

For HDVs (passive agents), the local reward simply tracks lane-changing penalties.

The parameter $\alpha \in [0, 1]$ balances the trade-off between global coordination and local efficiency. A higher α emphasizes system-wide performance, while a lower α prioritizes individual agent behavior.

3.4 Multi-Agent Learning for DQJLs

To address the challenge of coordinating multiple agents in forming DQJLs, we employ the Multi-Agent Proximal Policy Optimization (MAPPO) algorithm. This section details MAPPO’s adaptation for the DQJL task, starting with preliminaries in Subsec. 3.4.1, an explanation of MAPPO’s alignment with DQJL in Subsec. 3.4.2, the MAPPO-DQJL algorithm in Algorithm S2, and network architectures in Subsec. 3.4.3.

3.4.1 Preliminaries

MAPPO is an on-policy reinforcement learning algorithm designed to optimize individual agent policies while accounting for the collective behavior of all agents. Schulman et al. [146] introduced Proximal Policy Optimization (PPO), which has since become a widely adopted algorithm for model-free reinforcement learning due to its balance of stability and performance. Yu et al. [147] highlight the exceptional performance of multi-agent reinforcement learning in collaborative settings, further emphasizing its potential for diverse applications.

In the context of DQJL formation, this approach enables agents to quickly form DQJLs by learning cooperative strategies. MAPPO operates under centralized training and decentralized execution, making it ideal for this scenario. During centralized training, agents share information and are trained with a global perspective of the environment. This allows the system to leverage full-state information, ensuring that the policies learned reflect the global objective of minimizing EMV passage time while maintaining traffic flow.

In contrast, decentralized execution allows agents to make decisions based on local observations. This ensures scalability and real-world applicability, as agents act indepen-

dently, responding to their immediate environment in real-time. This autonomy is crucial in mixed autonomy settings where communication might be limited, allowing agents to function effectively despite partial observability. The decentralized execution phase ensures robust behavior in dynamic traffic conditions, while the centralized training phase guarantees that these local actions contribute to the broader goal of DQJL formation.

A key feature of MAPPO is its centralized value function estimation, where a centralized critic evaluates each agent’s actions based on the global state of the system. This helps agents understand how their actions contribute to the collective objective. Policy updates using the PPO objective ensure a balance between exploration and exploitation, leading to stable and efficient learning. The reward structure encourages both individual and collective coordination, optimizing DQJL formation and minimizing disruptions to surrounding traffic, thus ensuring the safe and swift passage of EMVs.

3.4.2 MAPPO for DQJL Formation

In our approach to DQJL formation, we adapt MAPPO with parameter sharing for CAVs, designing policy and value networks specifically tailored to the dynamic, interactive nature of traffic systems. All CAV agents utilize a common policy network $\pi_{\theta_{CAV}}(a_i | o_i)$, where θ_{CAV} denotes the shared policy parameters, ensuring that these agents learn a unified, generalizable strategy based on their local observations. HDVs are modeled as passive agents with fixed policy networks $\pi_{\theta_i}(a_i | o_i)$, enabling a unified agent-based representation of the traffic system while maintaining realistic human driving patterns. This design choice not only simplifies state representation but also provides the flexibility to incorporate different HDV behavioral models within the same framework. Our experimental results demonstrate that treating HDVs as agents rather than environmental elements leads to superior performance in mixed-autonomy scenarios.

To foster coordination across all vehicles, we employ a centralized value network $V_\phi(s)$ that evaluates the global state s , which includes information from both active (CAVs) and passive (HDVs) agents. This unified value function, parameterized by ϕ , enables consistent evaluation of vehicle interactions regardless of autonomy level, providing a comprehensive assessment of the traffic situation. The centralized evaluation mechanism guides CAVs toward cooperative behaviors while realistically accounting for HDV responses, ultimately supporting efficient DQJL formation.

The reward function R_i for each CAV reconciles individual-level goals—such as safety and maneuver efficiency—with the broader aim of expediting EMV passage. By balancing local incentives with global objectives, this hierarchical reward structure motivates agents to coordinate their actions in a manner that promotes improved overall traffic flow and reduced disruptions.

To ensure stable learning and robust policy improvement, we employ the clipped PPO objective. This training paradigm maintains a careful equilibrium between exploration and exploitation, controlling volatility in performance as the CAVs refine their shared policy. By combining parameter-sharing among CAVs, a unified agent-based representation for both CAVs and HDVs, and a carefully crafted reward structure, our MAPPO-based framework facilitates the rapid, secure, and cooperative implementation of DQJLs.

3.4.2.1 MAPPO-DQJL Algorithm

We present the pseudocode for our MAPPO-DQJL algorithm in Algorithm S2, followed by a detailed walk-through of its key components.

Centralized Training with Decentralized Execution The algorithm adopts the centralized training and decentralized execution (CTDE) paradigm, which is well-suited for

Algorithm S2: MAPPO-DQJL Training with Parameter Sharing

Input : T : maximum time step of an episode
 N_{bs} : batch size
 η_θ : learning rate for policy networks
 η_ϕ : learning rate for value networks
Output : ϕ : learned parameters for the shared value network
 θ_{CAV} : learned parameters for the shared CAV policy network

- 1 Initialize $\phi, \theta_{CAV}, k \leftarrow 0, B \leftarrow \emptyset$;
- 2 Initialize simulation environment (SUMO), $t \leftarrow 0$, get $\{s_t^i\}_{i \in \mathcal{N}}$;
- 3 **repeat**
 - /* Generate trajectories */
 - 4 **foreach** CAV $i \in \mathcal{N}_{CAV}$ (in parallel) **do**
 - 5 Sample a_t^i from $\pi_{\theta_{CAV}}$;
 - 6 Execute fixed policy for HDVs $j \in \mathcal{N}_{HDV}$;
 - 7 Receive r_t^i and s_{t+1}^i ;
 - 8 $B \leftarrow B \cup \{(s_t^i, a_t^i, s_{t+1}^i, r_t^i)\}$;
 - 9 $t \leftarrow t + 1, k \leftarrow k + 1$;
 - 10 **if** $t == T$ **then**
 - 11 Reset simulation, $t \leftarrow 0$, get $\{s_0^i\}_{i \in \mathcal{N}}$;
 - 12 **if** $k == N_{bs}$ **then**
 - /* Update using shared parameters for CAVs */
 - 13 Compute advantages $\{\hat{A}_t^i\}_{i \in \mathcal{N}_{CAV}}$ using GAE ;
 - 14 Compute returns $\{\hat{R}_t^i\}_{i \in \mathcal{N}_{CAV}}$;
 - 15 Aggregate gradients over CAVs in \mathcal{N}_{CAV} ;
 - 16 $\phi \leftarrow \phi - \eta_\phi \nabla_\phi L_V(\phi)$;
 - 17 $\theta_{CAV} \leftarrow \theta_{CAV} + \eta_\theta \nabla_{\theta_{CAV}} L^{CLIP}(\theta_{CAV})$;
 - 18 $k \leftarrow 0, B \leftarrow \emptyset$;
- 19 **until** Convergence;

the DQJL task. During decentralized execution, each CAV i observes its local state $o_{i,t}$, including neighboring vehicles, and independently selects actions $a_{i,t}$ based on its shared policy $\pi_{\theta_{\text{CAV}}}$. This decentralized approach enables real-time autonomy, scalability, and robust responses to dynamic traffic conditions without requiring communication between agents during deployment.

During centralized training, given our reward design that incorporates both shared global objectives and agent-specific local rewards, a critic evaluates the global state s_t through a value function:

$$V_{\phi}(s_t) = \mathbb{E}_{\pi} \left[\sum_{k=0}^{\infty} \gamma^k \left(R_{\text{global}}(s_{t+k}, \mathbf{a}_{t+k}) + \sum_{i \in \mathcal{N}_{\text{non-EMV}}} R_{\text{local}}^i(s_{t+k}, a_{t+k}^i) \right) \mid s_t \right] \quad (3.10)$$

where R_{global} represents the shared system-wide reward focusing on EMV-related objectives, and R_{local}^i captures the local efficiency of each CAV i .

This centralized value function provides a comprehensive assessment that: 1. Tracks global DQJL formation progress through R_{global} 2. Aggregates individual CAV contributions through $\sum_{i \in \mathcal{N}_{\text{CAV}}} R_{\text{local}}^i$ 3. Accounts for HDV interactions implicitly through state transitions

The value network V_{ϕ} is updated by minimizing the squared error between this estimated value and the observed returns:

$$L_V(\phi) = \mathbb{E}_{\mathcal{B}} \left[\left(V_{\phi}(s_t) - \hat{R}_t \right)^2 \right] \quad (3.11)$$

where \hat{R}_t represents the actual discounted sum of rewards observed during rollouts. This CTDE framework enables agents to learn coordinated behaviors that optimize both system-wide efficiency and individual performance while maintaining scalability in

real-world deployments.

Generalized Advantage Estimation (GAE) In the MAPPO framework, the update of policy networks relies on accurate estimation of the advantage function \hat{A}_t , which measures how much better or worse an action $a_{i,t}$ is relative to the current policy. In our context, this helps the CAVs learn how their actions (e.g., lane changes, acceleration) contribute to efficient DQJL formation. To compute the advantage, we use Generalized Advantage Estimation (GAE), which reduces variance in the policy gradient estimates while maintaining manageable bias.

The advantage function at time t is given by:

$$\hat{A}_t = \sum_{k=0}^{\infty} (\gamma\lambda)^k \delta_{t+k} \quad (3.12)$$

where $\delta_t = r_t + \gamma V_\phi(s_{t+1}) - V_\phi(s_t)$ represents the temporal difference (TD) error, and r_t is the reward received at time t . The parameters γ and λ control the trade-off between emphasizing immediate and future rewards, which in this context ensures that agents focus not only on short-term lane clearing but also long-term efficiency in EMV passage.

Policy Network Update and Parameter Sharing for CAVs Our framework employs PPO with a clipped objective to refine the policy parameters shared among all CAV agents, while HDVs maintain fixed policies that reflect realistic driving behaviors. By consolidating the learning process into a single, unified policy $\pi_{\theta_{\text{CAV}}}$ for all CAVs, we enable these vehicles to collectively learn and improve their decision-making behaviors from one another’s experiences. This parameter sharing is particularly advantageous in DQJL formation, where CAVs must jointly coordinate their maneuvers while accounting

for HDV responses to ensure effective lane-clearing and prompt EMV passage.

The PPO objective with the CLIP function is given by:

$$L^{\text{CLIP}}(\theta) = \mathbb{E}_{\mathcal{B}} \left[\min(r_t(\theta)\hat{A}_t, \text{clip}(r_t(\theta), 1 - \epsilon, 1 + \epsilon)\hat{A}_t) \right], \quad (3.13)$$

where

$$r_t(\theta) = \frac{\pi_{\theta}(a_t | o_t)}{\pi_{\theta_{\text{old}}}(a_t | o_t)}$$

represents the probability ratio between the updated and previous shared policies. By constraining $r_t(\theta)$ to $[1 - \epsilon, 1 + \epsilon]$, the policy avoids large, destabilizing jumps. This controlled adaptation is critical in a DQJL context, where sudden, drastic policy shifts might lead to erratic maneuvers and reduced cooperation among CAVs.

The policy update is performed via gradient ascent:

$$\theta \leftarrow \theta + \alpha_{\pi} \nabla_{\theta} L^{\text{CLIP}}(\theta),$$

with α_{π} as the learning rate. Over successive updates, all CAVs collectively converge toward more reliable and efficient DQJL formation strategies, as knowledge gained from one scenario disseminates through the shared parameters to benefit the entire CAV fleet.

3.4.3 Transformer-based Network Architecture

This study implements a transformer-based architecture for both policy and value networks in our MAPPO-DQJL algorithm. The transformer architecture, introduced by Vaswani et al. [148], is selected for its proven capability in modeling complex dependencies through self-attention mechanisms. In the context of DQJL formation, where vehicles must coordinate across varying distances and time horizons, the transformer's

ability to capture long-range interactions and process information in parallel makes it particularly suitable for real-time decision-making in dense traffic conditions [149, 150].

3.4.3.1 Policy Network

Under our parameter-sharing framework, all CAV agents utilize a single shared policy network π_θ . The network processes each CAV's local observation o_i through the following sequence:

1. Embedding layer transforms observations into a higher-dimensional feature space
2. Positional encodings incorporate spatial and temporal information
3. N transformer encoder layers process the embedded input using self-attention
4. Policy head (fully connected layer) computes action distribution parameters

Formally, for any CAV agent i :

$$\pi_\theta(a_i | o_i) = \text{PolicyHead}\left(\text{TransformerEncoder}\left(\text{PositionalEncoding}\left(\text{Embedding}(o_i)\right)\right)\right),$$

where $\pi_\theta(a_i | o_i)$ represents the probability distribution over actions a_i , conditioned on o_i . The parameter sharing enables efficient knowledge transfer across the CAV fleet. See Subsections B.1.1 for implementation details.

3.4.3.2 Value Network

The centralized value network V_ϕ evaluates the global state s through a similar transformer-based architecture:

$$V_\phi(s) = \text{ValueHead}\left(\text{TransformerEncoder}\left(\text{Embedding}(s)\right)\right).$$

This shared value network provides a unified assessment of how joint actions impact the global traffic state, guiding CAVs toward optimal DQJL formation strategies. See Subsections [B.1.2](#) for implementation details.

3.4.3.3 Transformer Encoder Layer

Each transformer encoder layer maintains the standard architecture: multi-head attention followed by a position-wise feed-forward network, with layer normalization and residual connections after each sub-layer. Detailed implementation specifications and parameter estimations are provided in Subsections [B.1.3](#) and [B.1.4](#), respectively.

3.5 Experimental Setup

In this section, we delineate the methodology used to evaluate the performance of MAPPO-DQJL. Subsection [3.5.1](#) specifies the central research objectives that guide our experimental investigations. Subsection [3.5.2](#) details the evaluation metrics employed to gauge the framework’s effectiveness. Subsection [3.5.3](#) describes the simulation environment utilized in these experiments. Finally, Subsection [3.5.4](#) introduces the benchmarks that serve as comparative baselines for assessing MAPPO-DQJL.

3.5.1 Experimental Objectives

The experiments are designed to address the following key research questions:

- **Effectiveness of MAPPO-DQJL:** To what extent does our MARL-based approach for DQJL formation outperform established benchmarks with respect to EMV passage time and holistic traffic flow optimization?

- **Impact of Penetration Rates:** How does varying CAV penetration rates influence the performance of the proposed framework, particularly regarding DQJL coordination and operational efficiency?
- **Impact of Traffic Density:** Similarly, how does varying traffic density influence the performance of the proposed framework?

These focal points collectively shape the principal objectives of our study. By rigorously examining these questions, we aim to elucidate the complex interplay between DQJL formation strategies, CAV adoption levels, and performance trade-offs, ultimately informing near-term policy decisions and strategic deployment of intelligent traffic management solutions.

3.5.2 Evaluation Metrics

Although a DQJL is typically formed prior to EMV ingress into a given road segment, the underlying agent behaviors remain consistent throughout the EMV's traversal. Consequently, the temporal duration required to establish the DQJL is effectively captured by the EMV's passage time. We employ the following evaluation metrics:

- **EMV Passage Time (t_{EMV}):** This metric represents the duration required for the EMV to traverse the designated road segment once the DQJL is in place, emphasizing the primary objective of expediting emergency response.
- **Number of Lane-changing for EMVs (N_{EMV}^{LC}) and Non-EMVs ($N_{non-EMV}^{LC}$):** We also measure the lane-changing efforts of both EMVs and non-EMVs, including CAVs and HDVs. Slight increments in EMV passage time may substantially diminish the maneuvering burden imposed on non-EMVs. Our analysis focuses on

carefully balancing these trade-offs to minimize overall disruption while maintaining efficient EMV transit.

3.5.3 Simulation Environment

We employ Simulation of Urban Mobility (SUMO) as our simulation environment. SUMO's ability to realistically model fine-grained interactions in mixed traffic scenarios, coupled with its native support for V2X communication and precise vehicle dynamics, provides a high-fidelity platform for examining DQJL formation and its implications on traffic flow. The simulation is conducted on a representative roadway environment, reflecting a typical urban street layout.

To ensure simulation reliability, we conducted a comprehensive calibration and validation process using empirical traffic flow data from the NYC Mobility Report [151]. The calibration focused on key parameters including car-following behavior, lane-changing dynamics, and intersection delays, leveraging Manhattan's peak hour metrics such as average vehicle speeds and traffic volumes. Our model validation against these real-world observations achieved a goodness-of-fit of over 85% for key metrics including average travel times, queue lengths, and throughput. These calibrated parameters were then applied consistently across all experimental scenarios to maintain reliability in our comparative analyses. For vehicle behavior modeling, we utilized SUMO's built-in car-following and lane-changing models (detailed in Subsec. B.2.1 and Subsec. B.2.2), adapting them to implement fixed policies for HDVs. Rather than treating HDVs as purely rule-based environmental elements, we represented them as passive agents, ensuring consistent representation of all vehicle types within our MAPPO framework while preserving SUMO's realistic vehicle dynamics.

To ensure a focused investigation of the interplay between CAVs and HDVs, we

assume homogeneous configurations for each class of vehicle. Specifically, all CAVs share a uniform set of learning parameters, while all HDVs share a common fixed policy derived from realistic driving behaviors.

Road Configurations We adopt three distinct road configurations in SUMO: Two-Lane, Three-Lane, and Four-Lane roadways, each spanning a length of 1500 meters. Traffic flow is varied across different simulation settings, ensuring a realistic depiction of dynamic traffic conditions. The EMV on duty enters the roadway already populated with vehicles on any lane randomly, simulating real-world congestion scenarios. Vehicles continuously enter and leave the roadway as the EMV traverses, and the observation window concludes once the EMV has exited the roadway.

3.5.4 Benchmarks

Although DQJL is a novel concept specifically designed to facilitate EMV passage through congested urban roads, there are other frameworks aimed at improving EMV intra-link movements in similar traffic conditions. Two control frameworks that address tasks closely related to DQJL in heterogeneous traffic environments are as follows:

1. **No Control:** This scenario represents a baseline condition where no specialized control strategy is employed. Non-EMVs adhere strictly to their default car-following and lane-changing behaviors in SUMO, reacting only to immediate traffic conditions without any global coordination. Although vehicles may occasionally yield when the EMV is in close proximity, these responses are purely local and uncoordinated, often resulting in suboptimal clearance times for the EMV.
2. **PPO-based Corridor Clearance (PPO-CC):** Suo et al. [117] introduced a single-agent PPO-based control framework where a CAV acts as a "splitting point" agent

to assist EMVs in clearing corridors. The CAV dynamically adjusts its speed and positioning based on local traffic conditions, creating a corridor for the EMV to pass through with minimal disruption to other vehicles.

3. **MAPPO-DQJL-CAV**: A reduced version of our proposed framework that considers only CAVs as agents, treating HDVs as part of the environment. The agent design for CAVs remains consistent with MAPPO-DQJL. This benchmark evaluates whether the inclusion of HDVs as agents significantly impacts performance.

3.6 Results and Discussion

In this section, we present the results from the simulated experiments. The effects of penetration rate, traffic density, and the adoption of contra-flow lanes on MAPPO-DQJL performance are detailed in Subsec. 3.6.1. Additionally, the contributions of different components within MAPPO-DQJL are analyzed in Subsec. 3.6.2. Environment configurations, MDP parameters, and training hyper-parameters selected to produce the following results are listed in Table B.1.

3.6.1 Sensitivity Studies

Many factors influence the effectiveness of candidate lane-clearing schemes. Among these, two primary determinants stand out: the penetration rate of CAVs and the prevailing traffic density. Variations in CAV penetration rates influence the degree of cooperative behaviors and the system’s capacity to execute sophisticated maneuvers, while shifts in traffic density alter the underlying operational conditions, potentially affecting both safety and efficiency outcomes.

To ensure a fair comparison of performance among the candidate schemes, all other parameters remain consistent across different experimental conditions. Traffic flow is fixed as **15** veh/lane/min for penetration rate study and penetration rate is set as **50%** for traffic density study. All statistics reported in the tables are based on a total of 20 runs per scenario.

3.6.1.1 Penetration Rate

Two-Lane Roadway When the traffic density is set to 15 veh/lane/min, the EMV passage time, the number of EMV lane-change maneuvers, and the number of non-EMVs' lane-change maneuvers are presented Table 3.1.

Method	0%	25%	50%	75%	100%
$t_{EMV}(s)$					
No Control			191.2 ± 9.7		
PPO-CC [117]	190.3 ± 9.7	183.5 ± 10.3	171.5 ± 10.5	152.2 ± 8.9	145.6 ± 7.3
MAPPO-DQJL-CAV	189.8 ± 9.9	175.0 ± 10.0	162.3 ± 10.1	145.7 ± 7.9	143.0 ± 6.5
MAPPO-DQJL	189.6 ± 9.5	170.8 ± 10.8	150.9 ± 11.5	138.4 ± 8.8	133.8 ± 7.6
N_{EMV}^{LC}					
No Control			4.0 ± 0.3		
PPO-CC [117]	1.0 ± 0.0	1.0 ± 0.0	1.0 ± 0.0	1.0 ± 0.0	1.0 ± 0.0
MAPPO-DQJL-CAV	3.9 ± 0.4	2.8 ± 0.4	1.6 ± 0.3	1.3 ± 0.2	1.1 ± 0.2
MAPPO-DQJL	4.0 ± 0.3	1.8 ± 0.3	0.9 ± 0.2	0.7 ± 0.1	0.6 ± 0.1
$N_{non-EMV}^{LC}$					
No Control			20.3 ± 2.7		
PPO-CC [117]	19.3 ± 2.0	17.0 ± 1.8	14.7 ± 1.5	12.1 ± 1.2	9.5 ± 1.0
MAPPO-DQJL-CAV	19.5 ± 2.0	18.0 ± 1.8	16.0 ± 1.6	13.0 ± 1.3	11.0 ± 1.1
MAPPO-DQJL	20.5 ± 1.8	16.9 ± 1.7	14.0 ± 1.4	10.7 ± 1.2	8.3 ± 0.9

Table 3.1: Performance for all methods on evaluation metrics in the Two-Lane Roadway across different penetration rates. Bold values indicate the best performance.

The results presented in Table 3.1 demonstrate that the proposed MAPPO-DQJL framework outperforms all other methods across all non-zero penetration rates with

respective to all metrics. Although MAPPO-DQJL-CAV also leverages multi-agent coordination, its reliance on treating HDVs as part of the environment rather than as learning agents leads to noticeably longer EMV passage times compared to MAPPO-DQJL. This suggests that fully integrating HDVs into the learning process is crucial for achieving more efficient cooperation and faster EMV clearance.

As the CAV penetration rate increases, the passage time for EMVs under MAPPO-DQJL ultimately reduces by approximately 30% relative to the No Control scenario, underscoring the substantial benefits gained from widespread CAV adoption. When comparing MAPPO-DQJL to PPO-CC, the advantage is less pronounced—on the order of 8% at intermediate penetration levels—yet still meaningful. These findings highlight the importance of fully integrated, multi-agent cooperation among CAVs and HDVs to attain near-optimal traffic flow conditions and expedite EMV passage.

A notable observation is that the PPO-CC approach consistently reports a mean of 1.0 ± 0.0 lane changes. This behavior arises from its design: PPO-CC designates a CAV as a stationary “splitting point,” ensuring that the EMV must execute exactly one lane-changing maneuver to travel through the cleared corridor. In contrast, as the penetration rate reaches the 50% mark, MAPPO-DQJL achieves an average lane-change count below 1.0, indicating that for than half times, the EMV can traverse through the corridor without changing lane. This improvement becomes even more pronounced at higher penetration rates, where MAPPO-DQJL consistently outperforms all other methods, demonstrating its efficiency in coordinating maneuvers and reducing unnecessary maneuvers.

On the other hand, the MAPPO-DQJL-CAV variant, which treats HDVs as part of the environment rather than as active learning agents, cannot achieve this level of efficiency. Consequently, the EMV under MAPPO-DQJL-CAV often performs more than one lane-change on average, reflecting a non-ideal scenario where less integrated

coordination with HDVs leads to suboptimal maneuvering behaviors.

The results also indicate that the proposed MAPPO-DQJL method outperforms the other approaches across all non-zero CAV penetration rates. In particular, MAPPO-DQJL-CAV, which does not treat HDVs as learning agents, suffers from a lack of coordination between CAVs and HDVs. This oversight allows PPO-CC, despite its simpler structure, to achieve fewer lane-change maneuvers in certain intermediate scenarios than MAPPO-DQJL-CAV. Nonetheless, at 100% CAV penetration, MAPPO-DQJL not only reduces non-EMV lane-change maneuvers by roughly 60% compared to the No Control baseline, but also maintains about a 10% margin of improvement over PPO-CC. These findings underscore the value of fully integrated cooperation among CAVs and HDVs, enabling more substantial efficiency gains at higher penetration levels.

Fig. 3.3 illustrates the training patterns of MAPPO-DQJL, MAPPO-DQJL-CAV, and PPO-CC across episodes for the Two-Lane Roadway with 15 veh/lane/min under 50% penetration rate. As shown in Fig. 3.3a, PPO-CC converges around 3000 episodes, but t_{EMV} fluctuates around 170s at convergence. MAPPO-DQJL converges near 7500 episodes, achieving the lowest t_{EMV} overall. MAPPO-DQJL-CAV demonstrates a similar learning pattern but stabilizes at a higher t_{EMV} of around 162s. Fig. 3.3b reflects this trend, also highlighting greater fluctuations in MAPPO-DQJL-CAV compared to MAPPO-DQJL.

Three-Lane Roadway Table 3.2 shows the performance achieved by all methods on the Three-Lane Roadway. The outcomes mirror the trends observed in the two-lane scenario, with MAPPO-DQJL consistently yielding superior performance as CAV penetration increases. As shown in Table 3.2, MAPPO-DQJL yields lower EMV passage times than all other methods at every non-zero penetration level. Similar to the two-lane scenario,

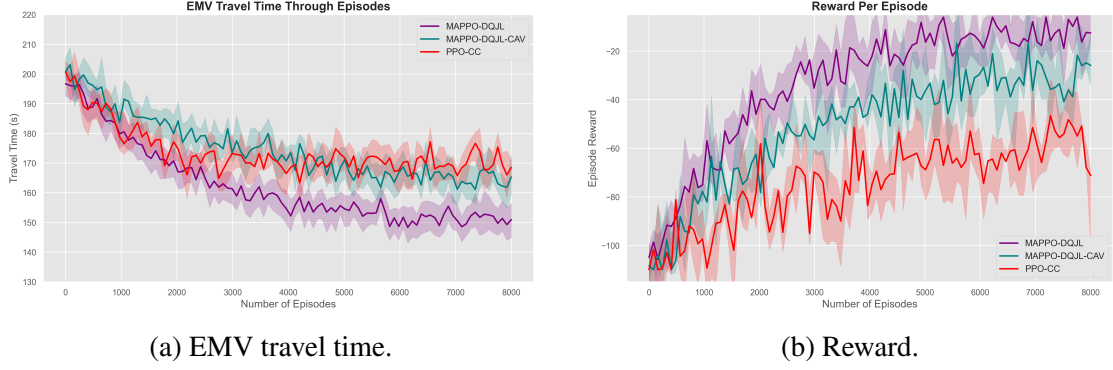


Figure 3.3: Comparison of EMV travel time (a) and reward (b) per episode achieved by learning-based methods.

Method	0%	25%	50%	75%	100%
$t_{EMV} (s)$					
No Control			180.0 ± 9.2		
PPO-CC [117]	179.5 ± 9.5	165.3 ± 10.1	150.4 ± 10.3	138.7 ± 9.1	130.1 ± 8.5
MAPPO-DQJL-CAV	178.8 ± 9.7	159.6 ± 10.5	141.8 ± 10.6	134.2 ± 9.0	127.5 ± 8.0
MAPPO-DQJL	178.4 ± 9.3	156.4 ± 10.8	135.9 ± 10.9	127.8 ± 9.2	125.7 ± 8.7
N_{EMV}^{LC}					
No Control			3.2 ± 0.4		
PPO-CC [117]	1.0 ± 0.0	1.0 ± 0.0	1.0 ± 0.0	1.0 ± 0.0	1.0 ± 0.0
MAPPO-DQJL-CAV	2.9 ± 0.4	2.1 ± 0.3	1.5 ± 0.2	1.2 ± 0.2	1.1 ± 0.2
MAPPO-DQJL	3.1 ± 0.3	1.7 ± 0.3	0.9 ± 0.2	0.5 ± 0.1	0.4 ± 0.1
$N_{non-EMV}^{LC}$					
No Control			27.3 ± 2.1		
PPO-CC [117]	26.8 ± 2.2	21.6 ± 1.8	17.2 ± 1.4	14.6 ± 1.2	12.3 ± 1.0
MAPPO-DQJL-CAV	27.4 ± 2.2	24.5 ± 1.9	19.3 ± 1.5	14.0 ± 1.2	11.5 ± 1.0
MAPPO-DQJL	26.9 ± 1.9	22.0 ± 1.6	16.5 ± 1.4	12.3 ± 1.1	10.2 ± 0.9

Table 3.2: Performance metrics on the Three-Lane Roadway across different penetration rates. Bold values indicate the best performance.

MAPPO-DQJL-CAV remains at a disadvantage due to its limited integration of HDVs. However, the introduction of a third lane provides additional flexibility for non-EMVs to yield, thereby creating more free space and further reducing EMV passage times relative to the two-lane case.

Similarly, the presence of an additional lane provides the EMV with greater lateral flexibility, reducing the number of lane changes required during its traversal. This increased spatial availability allows the EMV to complete its passage with fewer maneuvers, highlighting the benefits of enhanced clearance. However, this improvement comes at the cost of increased lane changes by non-EMVs, as they actively yield space for the EMV. This trend is particularly evident in the evaluation of $N_{\text{non-EMV}}^{\text{LC}}$, where the total number of non-EMV maneuvers increases to accommodate the EMV's passage.

Nevertheless, it is important to note that the rise in $N_{\text{non-EMV}}^{\text{LC}}$ is partially attributable to the increased number of non-EMVs present on the roadway. When normalized by the number of vehicles, $N_{\text{non-EMV}}^{\text{LC}}$ per vehicle is lower compared to other methods. This observation underscores the effectiveness of MAPPO-DQJL in minimizing additional disturbances.

Four-Lane Roadway With the same traffic flow configurations as above, we present the performance metrics in Table 3.3. As indicated in Table 3.3, relative to the three-lane scenario, the EMV passage time under MAPPO-DQJL is further reduced, and the EMV requires even fewer lane changes at high CAV penetration. In this configuration, the extra lane further diminishes the EMV's need to shift lanes. At 100% penetration, MAPPO-DQJL reduces EMV lane changes to approximately 0.4 on average, implying that under most circumstances, the EMV can traverse the segment with virtually no lane-changing. This outcome suggests that the proposed method has effectively reached a peak level of

Method	0%	25%	50%	75%	100%
$t_{EMV}(s)$					
No Control			184.1 ± 9.9		
PPO-CC [117]	179.0 ± 9.2	165.0 ± 9.8	150.5 ± 10.0	128.5 ± 8.8	120.0 ± 8.2
MAPPO-DQJL-CAV	178.8 ± 9.5	150.2 ± 10.2	130.8 ± 10.3	122.0 ± 9.0	115.0 ± 8.5
MAPPO-DQJL	178.5 ± 9.3	147.5 ± 10.5	125.0 ± 10.7	118.5 ± 8.8	113.0 ± 8.0
N_{EMV}^{LC}					
No Control			2.5 ± 0.3		
PPO-CC [117]	1.0 ± 0.0	1.0 ± 0.0	1.0 ± 0.0	1.0 ± 0.0	1.0 ± 0.0
MAPPO-DQJL-CAV	2.2 ± 0.3	1.6 ± 0.3	1.1 ± 0.2	0.9 ± 0.2	0.7 ± 0.1
MAPPO-DQJL	2.4 ± 0.3	1.4 ± 0.3	0.9 ± 0.2	0.6 ± 0.1	0.4 ± 0.1
$N_{non-EMV}^{LC}$					
No Control			34.1 ± 2.7		
PPO-CC [117]	33.7 ± 2.6	27.4 ± 2.3	22.3 ± 2.0	18.5 ± 1.8	15.6 ± 1.3
MAPPO-DQJL-CAV	34.3 ± 2.5	28.6 ± 2.4	21.7 ± 1.9	16.9 ± 1.5	15.8 ± 1.3
MAPPO-DQJL	33.5 ± 2.8	26.6 ± 2.2	19.6 ± 1.8	16.2 ± 1.3	15.1 ± 1.0

Table 3.3: Performance metrics on the Four-Lane Roadway across different penetration rates. Bold values indicate the best performance.

coordination and efficiency in facilitating EMV passage.

Meanwhile, although we observe a slight increase in the total number of lane-change maneuvers for all non-EMVs as their numbers grow, MAPPO-DQJL still ensures that the average number of lane-change maneuvers per non-EMV remains the smallest. In other words, while non-EMVs collectively adjust their positions more frequently to accommodate the EMV, the overall system benefits from greater lane-change efficiency. This pattern reinforces that, from a system-wide perspective, MAPPO-DQJL optimizes the trade-off between EMV clearance and non-EMV maneuvering complexity. In this setting, we observe a 39.8% reduction in EMV passage time and 55.7% decrease in non-EMV lane-changing maneuvers with the adopt of MAPPO-DQJL.

The findings clearly indicate that as the penetration rate of CAVs increases, both EMV passage time and the number of maneuvers for EMV consistently decrease, as

anticipated. This reduction occurs because, in the worst-case scenario, CAV behavior approximates that of HDVs, thereby providing at least the baseline level of performance. Moreover, the diminishing marginal improvement in reward with increasing penetration rates suggests that, beyond a certain threshold of CAV presence in the mixed traffic, the system approaches near-optimal conditions for DQJL formation. Achieving this critical mass of CAVs is therefore key to unlocking substantial gains in traffic efficiency. These results align with the findings of related studies investigating various traffic management tasks in a mixed environment [152, 153, 154, 155, 156, 157], further emphasizing the importance of CAV penetration rates in shaping overall traffic dynamics.

3.6.1.2 Traffic Density

Method	5 veh/lane/min	15 veh/lane/min	25 veh/lane/min
$t_{EMV}(s)$			
No Control	120.3 ± 9.1	171.2 ± 10.7	212.4 ± 13.2
PPO-CC [117]	118.7 ± 9.5	169.8 ± 11.2	202.6 ± 12.5
MAPPO-DQJL-CAV	117.4 ± 9.3	159.7 ± 10.3	191.5 ± 11.4
MAPPO-DQJL	114.9 ± 8.7	149.9 ± 11.8	188.2 ± 10.9
N_{EMV}^{LC}			
No Control	2.2 ± 0.5	4.0 ± 0.3	3.5 ± 0.6
PPO-CC [117]	1.0 ± 0.0	1.0 ± 0.0	1.0 ± 0.0
MAPPO-DQJL-CAV	1.3 ± 0.4	1.6 ± 0.3	2.5 ± 0.5
MAPPO-DQJL	0.5 ± 0.1	0.8 ± 0.2	1.2 ± 0.3
$N_{non-EMV}^{LC}$			
No Control	8.8 ± 1.2	15.0 ± 1.7	21.0 ± 2.2
PPO-CC [117]	9.2 ± 1.1	12.8 ± 1.5	18.5 ± 2.1
MAPPO-DQJL-CAV	9.7 ± 1.2	16.3 ± 1.7	20.9 ± 2.3
MAPPO-DQJL	7.9 ± 1.2	10.9 ± 1.4	16.2 ± 1.4

Table 3.4: Performance metrics on the Two-Lane Roadway across varying traffic densities. Bold values indicate the best performance.

Two-Lane Roadway As indicated in Table 3.4, under moderate traffic conditions (e.g., 15 veh/lane/min), MAPPO-DQJL demonstrates relatively greater time savings compared to fully congested scenarios (25 veh/lane/min). This finding suggests that while MAPPO-DQJL's coordinated strategy excels at reducing EMV passage time and maneuver complexity at moderate densities, its relative benefits diminish as the system approaches full saturation. In other words, while MAPPO-DQJL significantly improves performance under intermediate traffic loads, the advantage it offers naturally tapers off once congestion reaches near-maximum levels.

Under low-density conditions, the EMV performs approximately 0.5 lane-change maneuvers on average, demonstrating the near-elimination of unnecessary lane changes. Even as density increases to 25 veh/lane/min, MAPPO-DQJL maintains fewer EMV maneuvers than any other method, underscoring its capacity to ensure smoother EMV passage. At moderate congestion levels, MAPPO-DQJL's EMV lane-change frequency is only about 20% of that observed with No Control, and even under heavily congested conditions (25 veh/lane/min), it remains approximately one-third. These observations align with earlier findings, suggesting that as spatial flexibility declines, the coordination potential of MAPPO-DQJL diminishes, yet still surpasses that of alternative approaches. Meanwhile, in low-density conditions (5 veh/lane/min), non-EMVs make relatively few lane changes overall, and MAPPO-DQJL still achieves the lowest number. At moderate density (15 veh/lane/min), the values are in line with previous analyses, reaffirming MAPPO-DQJL's advantage. Under heavy congestion (25 veh/lane/min), non-EMVs must undertake more lane changes to accommodate the EMV, but MAPPO-DQJL continues to yield fewer maneuvers than the other methods, demonstrating its enduring benefits even as the system approaches saturation.

Method	5 veh/lane/min	15 veh/lane/min	25 veh/lane/min
$t_{EMV}(s)$			
No Control	94.7 ± 7.4	156.7 ± 10.9	216.2 ± 12.3
PPO-CC [117]	92.9 ± 7.2	150.1 ± 10.4	206.4 ± 11.9
MAPPO-DQJL-CAV	91.3 ± 7.6	141.6 ± 10.5	199.1 ± 11.3
MAPPO-DQJL	89.4 ± 6.9	135.7 ± 10.8	196.3 ± 10.0
N_{EMV}^{LC}			
No Control	1.9 ± 0.2	1.3 ± 0.2	2.9 ± 0.5
PPO-CC [117]	1.0 ± 0.0	1.0 ± 0.0	1.0 ± 0.0
MAPPO-DQJL-CAV	1.4 ± 0.3	1.6 ± 0.2	2.2 ± 0.3
MAPPO-DQJL	0.8 ± 0.1	0.9 ± 0.2	1.4 ± 0.2
$N_{non-EMV}^{LC}$			
No Control	13.7 ± 1.4	21.9 ± 1.8	31.3 ± 2.3
PPO-CC [117]	13.2 ± 1.3	17.2 ± 1.4	25.4 ± 2.0
MAPPO-DQJL-CAV	14.8 ± 1.5	19.2 ± 1.6	27.4 ± 2.1
MAPPO-DQJL	12.9 ± 1.4	16.7 ± 1.3	23.1 ± 2.2

Table 3.5: Performance metrics on the Three-Lane Roadway across varying traffic densities. Bold values indicate the best performance.

Three-Lane Roadway The performance metrics across varying traffic densities on the Three-Lane Roadway, as summarized in Table 3.5, highlight the consistent advantages of MAPPO-DQJL. For t_{EMV} , MAPPO-DQJL demonstrates shorter durations across all densities. At a moderate density of 15 veh/lane/min, these results align closely with prior benchmarks, confirming its robustness. Even as traffic density increases to 25 veh/lane/min, MAPPO-DQJL maintains a relative advantage over competing methods, underscoring its effectiveness in high-density scenarios.

The trends in EMV lane-change maneuvers further emphasize the benefits of MAPPO-DQJL. As traffic density rises, the additional lanes of the roadway contribute to keeping EMV maneuvers low. At 15 veh/lane/min, MAPPO-DQJL’s performance is consistent with earlier analyses, while at higher densities, it continues to effectively limit the EMV’s lane changes compared to other methods.

Similarly, non-EMV lane-change maneuvers exhibit the anticipated trend of increasing with traffic density. At 15 veh/lane/min, MAPPO-DQJL's results align with previously established patterns, demonstrating fewer lane changes than competing methods. Even at 25 veh/lane/min, where maneuver frequencies are heightened, MAPPO-DQJL preserves a distinct advantage, reflecting its capacity to handle high-density traffic scenarios more efficiently.

Additionally, it is noteworthy that MAPPO-DQJL-CAV induces more non-EMV lane changes than both PPO-CC and MAPPO-DQJL. This outcome arises from the fact that MAPPO-DQJL-CAV, by treating HDVs purely as environmental elements rather than learning agents, fails to incorporate the nuanced, diverse behaviors of HDVs into its decision-making process. Consequently, the control framework lacks the sophistication to minimize disruptions effectively, leading to a higher frequency of non-EMV maneuvers.

Four-Lane Roadway As indicated in Table 3.6, the introduction of an additional lane in the four-lane scenario further reduces EMV passage times at low and moderate densities, aligning with previously established trends. Although EMV passage times rise noticeably at 25 veh/lane/min, MAPPO-DQJL still achieves the shortest durations. A similar pattern is evident when examining EMV lane changes: under moderate densities, the EMV can maintain even fewer lane changes, and while maneuver counts increase slightly at high density, MAPPO-DQJL continues to enable the fewest EMV lane changes overall. In parallel, non-EMVs must also perform additional lane changes as density escalates. While MAPPO-DQJL moderates this increase more effectively than other approaches, the underlying trend of heightened complexity at greater densities persists, mirroring the patterns observed in both two-lane and three-lane configurations.

Experimental results for all three scenarios have clearly indicate that, under low-

	5 veh/lane/min	15 veh/lane/min	25 veh/lane/min
$t_{EMV}(s)$			
No Control	84.3 ± 6.9	147.2 ± 10.4	206.7 ± 11.7
PPO-CC [117]	82.4 ± 6.7	140.3 ± 10.1	196.6 ± 10.9
MAPPO-DQJL-CAV	81.6 ± 6.8	131.4 ± 10.2	186.2 ± 10.6
MAPPO-DQJL	78.7 ± 5.9	125.4 ± 10.6	183.1 ± 9.9
N_{EMV}^{LC}			
No Control	1.6 ± 0.3	1.3 ± 0.2	2.3 ± 0.4
PPO-CC [117]	1.0 ± 0.0	1.0 ± 0.0	1.0 ± 0.0
MAPPO-DQJL-CAV	1.1 ± 0.2	1.2 ± 0.2	1.7 ± 0.3
MAPPO-DQJL	0.5 ± 0.1	0.6 ± 0.1	1.1 ± 0.2
$N_{non-EMV}^{LC}$			
No Control	17.4 ± 1.7	26.3 ± 2.1	35.4 ± 2.4
PPO-CC [117]	16.6 ± 1.6	19.9 ± 1.9	28.4 ± 2.2
MAPPO-DQJL-CAV	17.9 ± 1.5	21.3 ± 1.8	29.3 ± 2.3
MAPPO-DQJL	15.2 ± 1.3	16.4 ± 1.5	24.7 ± 2.1

Table 3.6: Performance metrics on the Four-Lane Roadway across varying traffic densities. Bold entries indicate best performance.

density conditions, the performance gap between MAPPO-DQJL and other candidate schemes remains modest, as even conventional approaches can efficiently handle sparse traffic. As density increases and approaches moderate congestion levels, MAPPO-DQJL's advantage becomes most pronounced, significantly outpacing other schemes in reducing EMV passage times. However, once the roadway becomes fully congested, this benefit diminishes. In scenarios of near-total saturation, no scheme can substantially expedite EMV passage, resulting in a vanishing performance gap. This finding underlines the importance of intermediate traffic densities, where MAPPO-DQJL's strategic coordination yields the greatest relative gains over competing approaches. Studies [158, 159, 160], exploring mixed traffic tasks similarly identify "sweet spots" in density. These insights emphasize that operational conditions, not just automation levels, are crucial for realizing the full benefits of advanced traffic management interventions.

Across the entire density sensitivity study, MAPPO-DQJL-CAV consistently underperformed compared to MAPPO-DQJL. This disparity arises because MAPPO-DQJL-CAV treats HDVs purely as part of the environment, rather than as learning agents. Without incorporating HDVs into the coordination process, the control framework cannot anticipate or adapt to the distinct and often stochastic behaviors of each HDV. Consequently, as traffic densities increase, the system struggles to maintain efficient flow, leading to more frequent lane changes and prolonged EMV passage times. In other words, omitting HDVs from the learning process significantly impairs the scheme's overall coordination capabilities, particularly under congested conditions.

This observation reinforces the importance of designing a learning framework that accounts for both CAVs and HDVs as active participants, thereby optimizing system performance across a wide range of traffic scenarios.

3.6.2 Ablation Studies

A range of ablation studies is conducted to clarify the influence of key components in the MAPPO-DQJL framework. By selectively altering certain design choices, we can isolate their effects and better understand the fundamental drivers of performance in DQJL formation.

3.6.2.1 Calibration of α

Reward shaping plays a pivotal role in guiding agent behaviors. By adjusting the balance between global and local rewards, we can observe how different configurations influence EMV passage efficiency and overall traffic stability. All experiments conducted in Subsec. 3.6.1 adopt $\alpha = 0.75$. In this ablation study, we systematically vary the balancing coefficient α in Eq. (3.9) on the Three-Lane Roadway under 15 veh/lane/min traffic density and 50% CAV penetration. Each unique value of α is associated with a separate training phase for the agents, followed by 20 simulation runs to evaluate performance. The results are presented in Table 3.7.

	$\alpha = 0$	$\alpha = 0.25$	$\alpha = 0.5$	$\alpha = 0.75$	$\alpha = 1.0$
t_{EMV} (s)	200.3 ± 11.8	170.7 ± 11.9	150.2 ± 11.3	135.9 ± 10.9	125.4 ± 10.1
N_{EMV}^{LC}	4.1 ± 0.4	2.9 ± 0.3	1.7 ± 0.3	0.9 ± 0.2	0.7 ± 0.1
$N_{non-EMV}^{LC}$	10.2 ± 1.1	13.7 ± 1.6	16.3 ± 1.7	19.7 ± 1.3	23.4 ± 1.9

Table 3.7: Effects of different α values on EMV passage time and lane-change maneuvers on the Three-Lane Roadway with 15 veh/lane/min and 50% CAV penetration rate.

As shown in Table 3.7, increasing α leads to lower t_{EMV} and N_{EMV}^{LC} , as the agents shift their focus toward optimizing global EMV-related objectives. This adjustment in reward composition enhances the EMV’s passage efficiency and reduces its lane-change frequency. However, this improvement comes with a trade-off. As N_{EMV}^{LC} decreases,

$N_{\text{non-EMV}}^{\text{LC}}$ tends to increase. The process of dynamically clearing lanes for the EMV necessitates multiple layers of yielding maneuvers, compelling non-EMVs to adjust their positions more frequently. In other words, while prioritizing the EMV's global objectives streamlines its trajectory, the surrounding traffic must accommodate these changes, resulting in a higher number of lane-change maneuvers by non-EMVs. This provides valuable insight into how EMV operations can cause disruption to overall traffic flow, emphasizing the need for carefully balanced strategies when managing EMV passage under various traffic conditions.

3.6.2.2 Parameter Sharing

Parameter sharing among CAVs facilitates knowledge transfer and promotes consistent strategies across agents. To evaluate the impact of this design choice, we conducted an ablation study comparing our shared policy approach against a variant where each CAV maintains an independent policy network while HDVs retain their fixed policies. This investigation helps understand whether independent learning could potentially lead to better coordination strategies for DQJL formation.

Due to the computational demands of training multiple independent networks, we constrained the experiment to 15 CAVs and 15 HDVs, with HDVs maintaining their fixed behavioral policies throughout. The simulation environment was configured as a Three-Lane Roadway spanning 500 meters, allowing for focused analysis of how parameter sharing affects CAV coordination capability.

See Fig. 3.4 for the learning patterns of CAV agents with and without shared parameters. Without a shared policy network, CAV agents are treated as independent learners, optimizing their policies in isolation. This limits generalization and knowledge transfer, making it harder to converge on optimal strategies for establishing DQJLs.

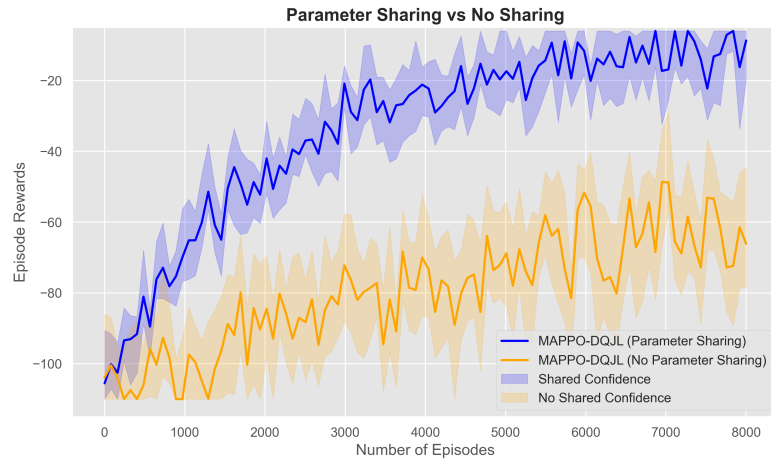


Figure 3.4: Reward convergence with and without parameter sharing for CAVs.

In contrast, treating CAV agents as homogeneous with a shared policy network offers key advantages. Parameter sharing facilitates knowledge transfer, enabling consistent strategies across agents, especially in stochastic environments. It also reduces learning complexity, accelerating convergence, and inherently promotes cooperation by aligning agent objectives. These benefits highlight the efficacy of MAPPO-DQJL’s shared policy design.

3.7 Summary

This study introduces DQJLs as a practical solution for enabling EMVs to navigate congested urban traffic efficiently. Using the MAPPO framework, the proposed system coordinates CAVs and HDVs to improve EMV passage times while minimizing disruptions to overall traffic flow.

Results from SUMO simulations validate the framework’s ability to reduce EMV passage times with minimal lane changes, for both EMVs and non-EMVs. By treating HDVs as dynamic agents rather than passive obstacles, the system accounts for their

stochastic behaviors, enhancing traffic interaction modeling and coordination. The framework scales effectively to multi-lane scenarios, achieving smoother traffic flow and fewer EMV lane changes. Higher CAV penetration rates amplify these benefits, leading to shorter EMV passage times and fewer maneuvers for all vehicles, emphasizing the importance of adopting V2X technologies.

The CTDE approach, combined with a transformer-based architecture, enhances scalability and robustness. This design models complex inter-agent dependencies, ensuring reliable performance in high-density, dynamic traffic conditions. The results demonstrate the framework's capacity to manage real-world traffic complexities while maintaining system efficiency.

DQJLs have clear potential for real-world ITS applications, particularly in congested urban settings. By reducing EMV response times, the proposed approach improves outcomes for ambulances, fire trucks, and law enforcement, safeguarding lives and property. As V2X technologies continue to advance, this framework offers a path toward more cooperative and efficient roadways, transforming EMV assistance into a streamlined, society-wide effort to enhance urban safety and resilience. Future work will focus on incorporating more realistic features, expanding scalability to address higher-dimensional uncertainties, and bridging the sim-to-real gap for practical deployment.

Chapter 4

Intersection-Aware Assessment of EMS Accessibility in NYC: A Data-Driven Approach

4.1 Introduction

Emergency response times in urban areas, particularly in densely populated metropolitan regions such as New York City (NYC), are profoundly influenced by traffic congestion. Research has established that reducing the travel time of emergency vehicles (EMVs)—a critical component of overall emergency response time (ERT)—can significantly improve outcomes for urgent incidents, including emergency medical services (EMS) [161, 162], fires [163, 164], and police activities [165]. However, as New York City continues to undergo rapid urbanization, the growing congestion on its roadways has exacerbated this challenge. Recent reports indicate that the city’s emergency response time for life-threatening situations has increased by 29% over the past decade, reflecting a concerning

trend of slower responses in high-priority cases [166]. According to the Mayor's Management Report, response times in New York City have risen by 82 seconds—16.1% higher than the 8 minute and 28 second average in fiscal year 2019—surpassing even the elevated times seen during the onset of the COVID-19 pandemic in fiscal 2020, despite a 52% increase in civilian fire deaths in fiscal 2023 [167].

Various approaches have been introduced to mitigate delays in EMV travel time, such as traffic signal preemption and route optimization. However, these methods are typically implemented in isolation and fail to address the dynamic and evolving nature of urban traffic congestion. For instance, signal preemption strategies prioritize EMVs by altering traffic signals, but often at the cost of significant disruption to non-EMV traffic. These inefficiencies propagate through the network, creating broader delays and unintended consequences for overall traffic management. Moreover, these traditional methods are static and lack the adaptability needed to respond to real-time fluctuations in traffic conditions and congestion patterns. As a result, their long-term effectiveness is limited, particularly in a complex urban environment like New York City, where traffic patterns are unpredictable and can change rapidly. Addressing these challenges necessitates more integrated and adaptive systems that holistically coordinate traffic management, minimizing disruption to non-EMV traffic while ensuring swift emergency response.

A recent study on emergency response accessibility in NYC identified significant disparities in service coverage, particularly in underserved areas such as Staten Island and parts of Queens [168]. These regions, referred to as "emergency service deserts," experience prolonged response times due to inadequate proximity to fire stations and EMS. The study further highlights a correlation between population density and emergency service accessibility, with less dense areas facing longer delays. While these findings emphasize the need for innovative traffic management solutions to enhance emergency

response across all boroughs, the proposed accessibility model in [168] has been shown to underestimate EMV travel times within the city. An improved EMS accessibility model is therefore essential to accurately identify and address vulnerable areas in NYC.

Building upon these findings, this study aims to develop an EMS accessibility model that incorporates the potential adoption of large-scale traffic signal control (TSC) systems to facilitate EMV passage in congested networks. Using this EMS accessibility model, we can simulate travel times from the nearest medical facility to any location in the city, enabling the identification of vulnerable regions in terms of EMS coverage. Additionally, this model allows for the evaluation of how a TSC scheme, such as *EMVLight* [169], could support these vulnerable areas. By integrating advanced modeling capabilities with insights from the accessibility study, this study is able to demonstrate the potential to significantly enhance emergency response times in NYC's most vulnerable and congested regions.

This study makes the following contributions:

1. It integrates the New York City road network, intersection data, and population distribution into a unified analytical framework.
2. It proposes an EMS accessibility model that accounts for the impact of intersection density along emergency routes.
3. It identifies vulnerable regions using the proposed model, investigates the EMS accessibility and illustrates the potential improvements in accessibility achievable through the incorporation of *EMVLight*.

The structure of this study is as follows. Section 4.2 reviews existing literature on traffic signal controls for EMVs, Intersection delay and EMS accessibility. The datasets employed in this study are introduced in Section 4.3, which also presents the proposed

intersection-aware EMS accessibility model. Section 4.4 details the travel time analysis and the vulnerable regions based on the proposed method. Demographic evaluations are conducted on the result in Section 4.5 and an adoption of *EMVLight* is carried out in Subsec. 4.5.3, highlighting the areas of New York City that stand to benefit the most. Finally, conclusions are summarized in Section 4.6.

4.2 Related Works

This section reviews key literature supporting our study. Subsection 4.2.3 examines advancements in traffic signal control (TSC) for EMVs, Subsection 4.2.2 focuses on intersection delays as a critical factor in EMV travel times and Subsection 4.2.1 explores EMS accessibility and its disparities. Together, these insights provide the foundation for our proposed methodology.

4.2.1 EMS accessibility

The accessibility of EMS is a critical component of public health and safety, particularly in urban areas where rapid response times are essential for saving lives [170, 171, 172, 173, 174, 175]. Studies have developed a variety of methodologies to evaluate and improve EMS accessibility. Novak and Sullivan [176] proposed a link-focused approach for assessing access to emergency services, emphasizing the importance of connectivity within urban road networks. Similarly, Xia et al. [177] utilized big GPS data to measure spatiotemporal accessibility, highlighting the dynamic nature of EMS access influenced by traffic and temporal factors.

Geographic Information Systems (GIS) have played a pivotal role in analyzing and addressing spatial disparities in EMS accessibility [178, 179, 180]. Tansley et al. [181]

employed GIS to assess spatial access to EMS in low- and middle-income countries, revealing significant geographic inequities. Hashtarkhani et al. [182] introduced an age-integrated GIS-based methodology to evaluate EMS accessibility, demonstrating the potential to tailor EMS services to different demographic groups. In Dhaka, Bangladesh, Ahmed et al. [183] examined the impact of traffic variability on EMS access, highlighting the challenges posed by urban congestion in providing equitable emergency healthcare.

Several studies have addressed the influence of environmental and infrastructural factors on EMS accessibility [184, 185, 186]. Green et al. [187] explored city-scale accessibility during flood events, underscoring the importance of resilient infrastructure to maintain EMS operations during natural disasters. Similarly, Yin et al. [188] evaluated the cascading impacts of sea-level rise and coastal flooding on EMS access in Lower Manhattan, New York City, revealing vulnerabilities in emergency response under climate-induced hazards. Albano et al. [189] developed a GIS-based model to estimate the operability of emergency response structures during floods, providing critical insights for urban planning in disaster-prone areas.

Addressing urban-rural disparities has also been a key focus in EMS accessibility research [190, 191, 192]. Luo et al. [193] examined strategies for locating EMS facilities to reduce urban-rural inequalities, while Carr et al. [194] highlighted access challenges in rural areas within the United States. Holguin et al. [195] proposed urban planning methodologies aimed at generating equity in EMS access, emphasizing the need for targeted interventions in underserved regions. The spatiotemporal aspect of EMS accessibility has been further explored in studies like those by Hu et al. [196], who analyzed the impact of traffic on spatial accessibility variations in inner-city Shanghai. Shi et al. [197] conducted a spatial accessibility assessment of urban tourist attractions in Shanghai, demonstrating the need for comprehensive urban planning to address emergency response challenges in

high-density areas.

Chung et al. [168] present a geospatial analysis of emergency service accessibility in New York City, identifying significant disparities in coverage, particularly in Staten Island and parts of Queens. The study introduces an accessibility index that combines spatial proximity, road network connectivity, and response time data to highlight regions with low emergency service availability. Additionally, the authors examine the impact of traffic congestion on EMS response times, emphasizing challenges in densely populated areas.

In summary, EMS accessibility is influenced by a combination of spatial, temporal, and demographic factors [198, 199, 200, 201]. The integration of advanced GIS techniques, real-time traffic data, and tailored urban planning approaches is critical for addressing disparities and ensuring equitable access to emergency services across diverse geographic and socio-economic contexts [202, 203].

4.2.2 Intersections delay

The influence of intersection density and topology on travel time has been a subject of extensive research. Higher intersection densities often lead to increased delays due to frequent stops and interruptions in traffic flow. Ewing and Cervero's meta-analysis [204] established that although higher intersection densities are associated with reduced vehicle miles traveled (VMT), they often result in longer travel times due to frequent interruptions. Al-Dabbagh et al. [205] further emphasize the role of intersection topology, demonstrating how intersection design impacts traffic congestion in urban cities. The *Highway Capacity Manual* (HCM) [206] offers methodologies for assessing urban street performance, highlighting the influence of signalized intersections on travel time [207].

Specific studies have also examined how intersections affect travel times across

different transportation modes [208, 209, 210]. Feng et al. [211] quantified the joint impact of stop locations, signalized intersections, and traffic conditions on bus travel times, highlighting the compounded delays experienced by public transport. Strauss and Miranda-Moreno [212] explored cyclist travel patterns, demonstrating how delays at intersections significantly influence travel times in the Montreal network. Furthermore, Park et al. [213] utilized Bluetooth-based data to measure intersection performance, illustrating how advanced data collection methods can provide detailed insights into intersection-related delays. Ivanov et al. [214] also highlight the importance of intersection geometry and control mechanisms in mitigating delays in high-density areas. These findings collectively underscore the critical role of intersection design and performance in influencing travel time and highlight the need for targeted urban planning interventions [215, 216, 217].

When it comes to EMV travel time, reducing delays at intersections is particularly critical, as every second lost can directly impact emergency outcomes [218, 219, 220]. Therefore, the ability to dynamically manage and optimize intersection performance is essential for ensuring timely emergency response, forming the focus of this study [221, 222, 223].

4.2.3 TSC for EMVs

The optimization of TSC for EMS is paramount in reducing response times and enhancing public safety [224, 225, 226]. Traditional TSC methods, such as signal preemption, temporarily adjust traffic signals to grant EMVs priority passage through intersections [227]. While effective in facilitating EMV movement, these approaches often disrupt the flow of non-EMV traffic, leading to broader network inefficiencies [228]. Advancements in intelligent transportation systems (ITS) have introduced more adap-

tive and dynamic TSC strategies. Bhate et al. [229] proposed an IoT-based intelligent traffic signal system that leverages real-time data to prioritize EMVs, demonstrating significant reductions in response times. Similarly, Noori et al. [83] developed a connected vehicle-based TSC strategy, utilizing vehicle-to-infrastructure communication to enhance EMV preemption efficiency. Predictive control models have also been explored to anticipate EMV arrivals and adjust signal timings accordingly. Qin and Khan [14] investigated control strategies for traffic signal timing transitions during EMV preemption, highlighting methods to minimize disruptions to regular traffic flow. Additionally, Shanmugasundaram et al. [230] introduced a Li-Fi-based automatic traffic signal control system, offering a novel approach to EMV prioritization through high-speed data transmission.

The integration of multi-agent reinforcement learning (MARL) frameworks has further advanced TSC for EMVs [231]. Su et al. [169] presented EMVLight, a decentralized MARL framework that optimizes both EMV routing and traffic signal coordination, effectively reducing response times while maintaining overall traffic efficiency. This approach underscores the potential of machine learning techniques in addressing the complexities of urban traffic management.

Comprehensive reviews by Bin Wan Hussin et al. [232] and Yu et al. [233] provide extensive analyses of existing TSC techniques for EMVs, encompassing traditional methods and emerging technologies. These reviews offer valuable insights into the evolution of TSC strategies and underscore the necessity for continued innovation in this domain.

4.3 Methodology

In this section, we introduce the datasets used for this study in Subsec. 4.3.1 and the EMS accessibility model in Subsec. 4.3.2.

4.3.1 Datasets

In this subsection, we introduce the datasets used for the proposed methodology.

4.3.1.1 Emergency medical services sites

The locations of emergency service sites are sourced from the Homeland Infrastructure Foundation-Level Data (HIFLD) Open Data repository [234, 235]. Given that this study concentrates on optimizing the transit of ambulances and other Emergency Medical Services (EMS) vehicles, we specifically extract the precise locations of hospitals [236] and EMS stations [237] to ensure targeted analysis and effective modeling of emergency response routes. Note that the EMS stations dataset also includes certain fire stations, as these facilities provide EMS services as well. The numbers of sites by each borough is provided in Tab. 4.1 and their locations are represented in Fig. 4.1.

Borough	EMS Stations	Hospitals	Total
Bronx	19	12	31
Brooklyn	76	15	91
Manhattan	28	23	51
Queens	15	10	25
Staten Island	23	6	29
Total NYC	161	66	227

Table 4.1: Number of EMS Stations and Hospitals by boroughs in NYC

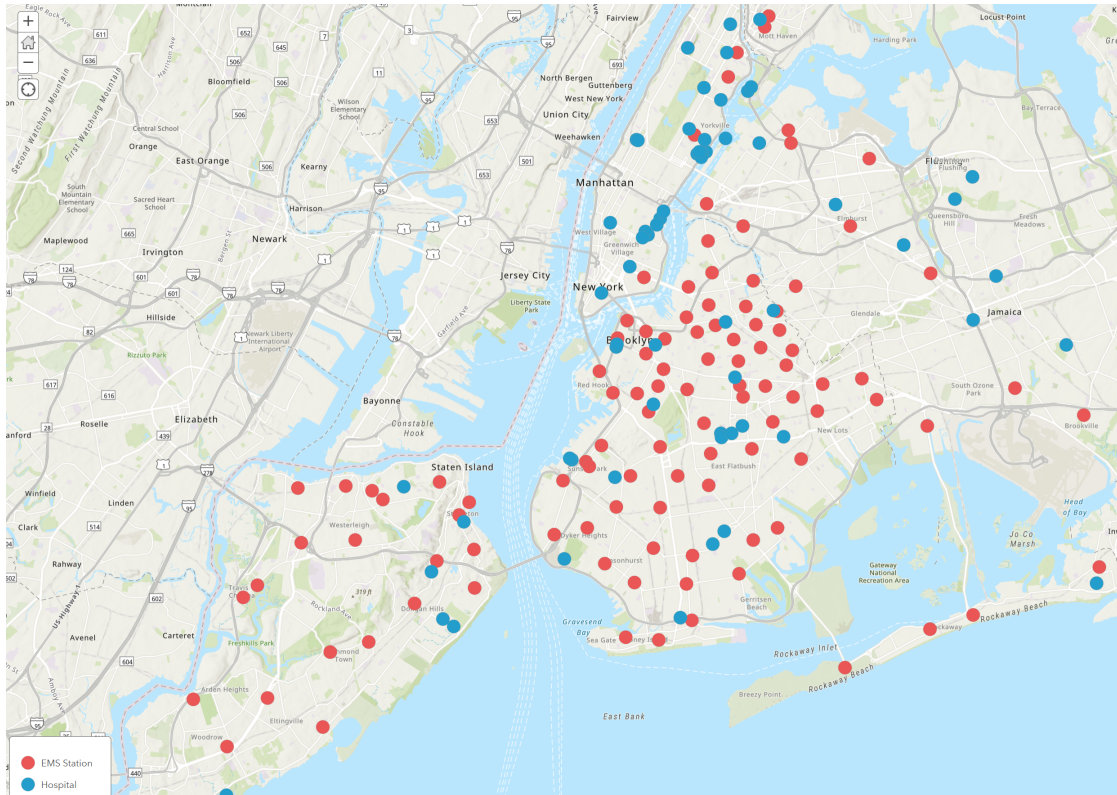


Figure 4.1: EMS Stations (Blue) and Hospitals (Red) in NYC.

4.3.1.2 Road network

OpenStreetMap (OSM) is employed to visualize the streets and intersections of New York City. The road network is represented as a symmetric multigraph, capturing the intricate connections and pathways characteristic of the urban transportation infrastructure. To ensure precision and clarity in the representation, the NYC Street Centerline (CSCL) dataset [238] is utilized. An overview of the network is illustrated in Fig. 4.2. This representation serves as the foundation for analyzing the accessibility of EMS site locations, with travel times along the network serving as a key metric for reachability and service efficiency. By employing this approach, the study offers a realistic depiction of urban mobility and its implications for emergency response performance.

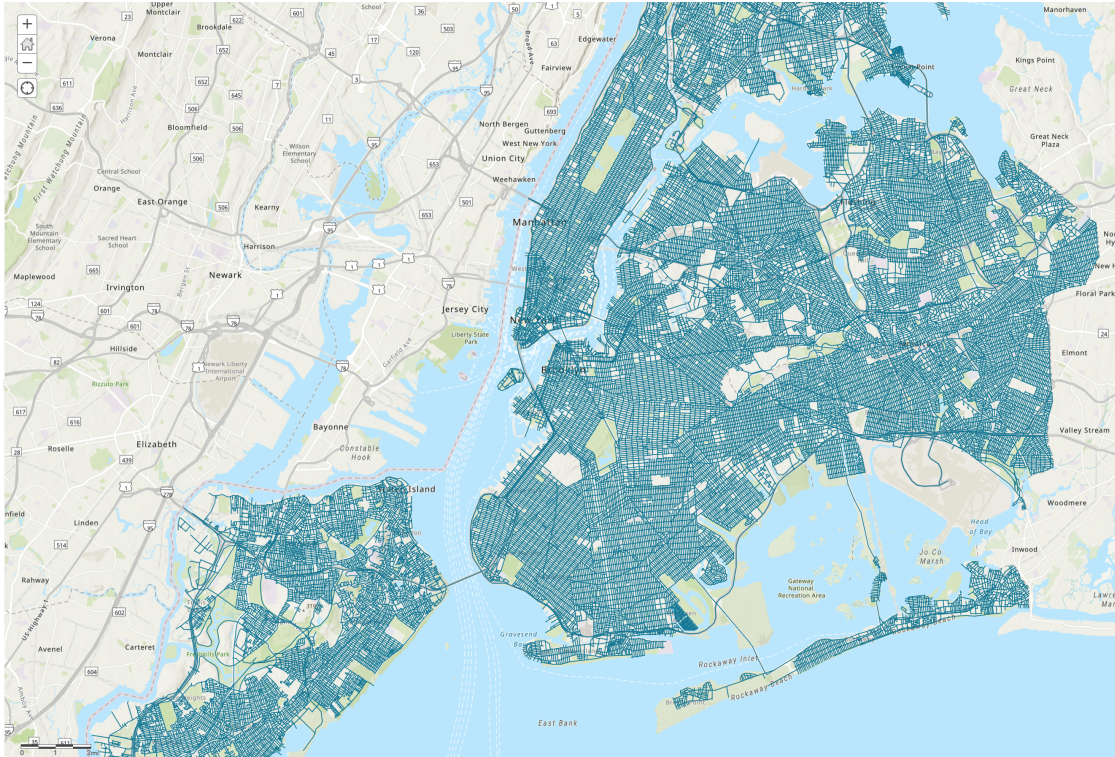


Figure 4.2: All NYC streets following NYC Street Centerline.

4.3.1.3 Signalized intersections

Currently, there is no publicly available open-source dataset that comprehensively identifies all signalized intersections in New York City. However, we have transformed the NYC Street Centerline (CSCL) shapefile to generate an approximate map of signalized intersection locations. Following pre-processing of the CSCL data, we filtered the dataset to include only road types classified as streets or highways and restricted traffic directions to multi-way configurations. Intersection points were derived by extracting line endpoints from the filtered road geometries. To address precision errors and reduce overlap caused by minor positional discrepancies, the coordinates of these endpoints were rounded. Duplicate intersection points were subsequently removed, resulting in a refined and clean dataset of potential signalized intersection locations. Refer to Fig. 4.3 for an illustrative

visualization of the signalized intersection map in New York City, where blue lines represent streets or highways as part of the network in Subsec. 4.3.2.1 and orange dots represent traffic lights.

Given that each signalized intersection can function as an agent within a large-scale TSC system such as *EMVLight*, we regard this map as a realistic near-future representation of the network for facilitating EMV passage in NYC.¹

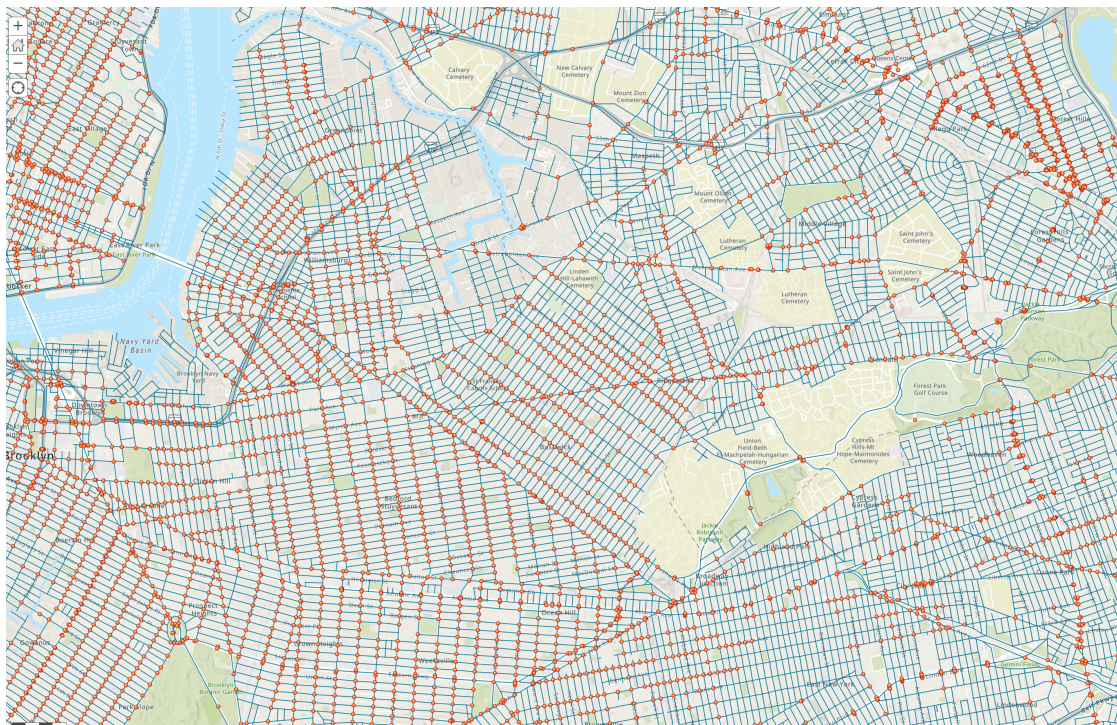


Figure 4.3: Signalized intersections layout in Brooklyn and Queens

4.3.1.4 NYC census data

Census data plays a pivotal role in conducting analyses of accessibility and vulnerability. While Chung [168] employs a five-year average for such assessments, this study utilizes 2023 population data at the census tract level provided by the U.S. Census

¹This intersections map is available at: <https://zenodo.org/records/14280428>

Bureau [239], thereby enhancing temporal precision. The spatial configurations of census tracts are sourced from the U.S. Census Bureau’s dataset [240], with a representative example for Staten Island illustrated in Fig. 4.4. The demographic data are DP05 from American Community Survey (ACS) Demographic and Housing Estimate [241] 2022 5-year estimate data profiles. In subsequent sections of this study, we will undertake a detailed examination of the spatial distribution of various demographic characteristics across New York City. This analysis aims to provide deeper insights into issues surrounding EMS accessibility. To provide an overview of the census data, a population density map illustrating the spatial distribution of the population is presented in Fig. 4.5.

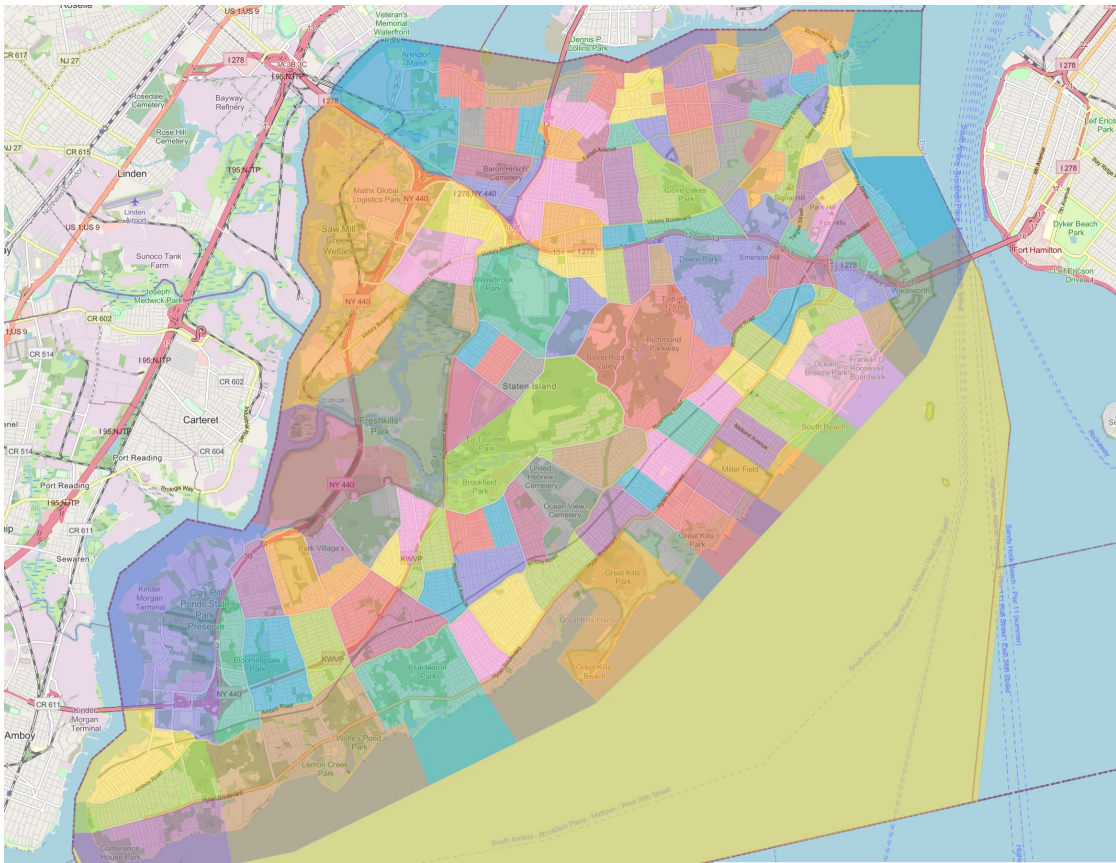


Figure 4.4: Census tracts in Staten Island. Each polygon represents a census tract.

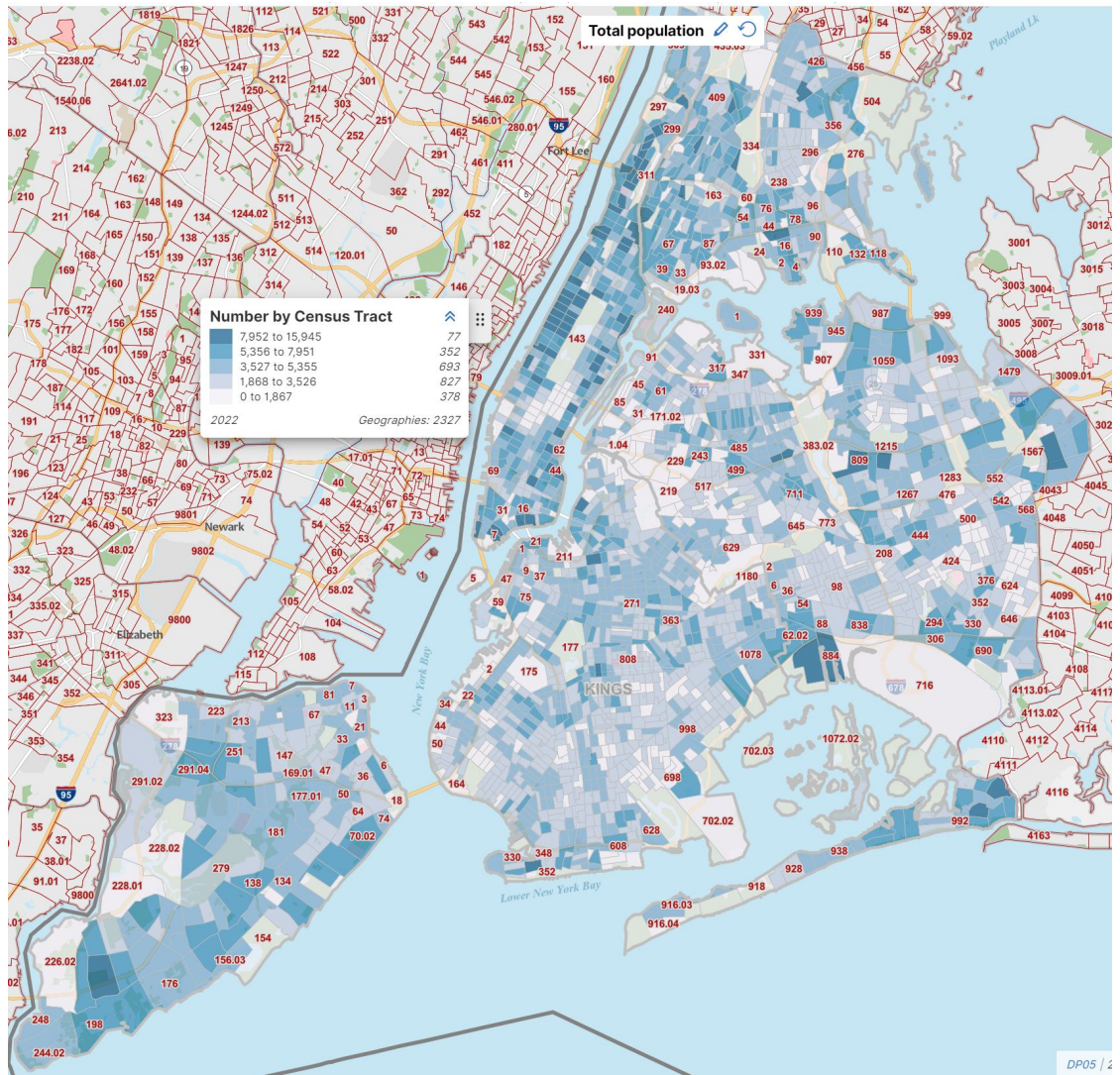


Figure 4.5: Population distribution of NYC census tracts.

4.3.2 Intersection-aware EMS Accessibility Model

Accessibility is commonly defined as the ease of reaching desired destinations, with measures classified into infrastructure-based, location-based, person-based, and utility-based categories [242]. Among these, location-based measures, particularly travel time within a predefined threshold, are widely used for their simplicity and relevance to EMS planning. Travel time thresholds, such as the NFPA 1710 standard of $\tau = 4$

minutes [243], serve as benchmarks for evaluating whether populations can access critical EMS facilities.

This study adopts a travel time-based measure of accessibility, incorporating intersection density to account for delays in densely connected urban areas. Building on the methodology proposed by Chung et al. [168], the following subsections outline the model's graph representation, travel time assignment, and population weighting framework, providing a refined evaluation of EMS accessibility in NYC.

4.3.2.1 Graph representation

The road network is represented as a graph $G = (V, E)$, where V is the set of nodes, each corresponding to either a road intersection or endpoint, and E denotes the set of edges, each representing a distinct road segment connecting two nodes. Attributes associated with each edge, such as road length and speed limit, facilitate the initial computation of travel time across the network under idealized conditions.

4.3.2.2 Travel time assignment

To capture the influence of urban intersection density on travel times, an intersection density metric $I(v)$ is defined for each node $v \in V$. This metric is calculated as the number of intersections within a fixed radius r around the node, normalized by the area of the radius, such that:

$$I(v) = \frac{\text{Number of intersections within radius } r}{\pi r^2}. \quad (4.1)$$

A higher $I(v)$ value implies a denser concentration of intersections, which is expected to contribute to travel delays, particularly affecting emergency response times in congested

urban zones. Based on Leadership in Energy and Environmental Design (LEED) [244], we adopt $r = 800$ m for intersection density evaluations.

To compute travel times in the road network, we follow the graph representation introduced in Subsec. 4.3.2.1. Each edge $e \in E$ is assigned a baseline travel time $T(e)$, calculated as the edge, i.e., road segment, length divided by the speed limit. The default speed limit on most New York City streets is 25 mph, implemented under the Vision Zero initiative [245] to enhance traffic safety. On highways and parkways, the limit is generally higher, ranging from 50 mph to 55 mph depending on signage. The baseline travel time matrix T is then defined as:

$$T_{ij} = \text{Shortest path travel time from node } v_i \text{ to node } v_j, \quad (4.2)$$

where T_{ij} represents the cumulative travel time across all edges along the shortest path between nodes v_i and v_j , under traffic-free conditions (no delays).

To account for delays caused by intersection density, we adjust the travel time for each edge e using a node-based intersection delay design. The delay for an edge e connecting nodes v_m and v_n is modeled as:

$$D_{\text{intersection}}(e) = \alpha \cdot \frac{I(v_m) + I(v_n)}{2}, \quad (4.3)$$

where $I(v_m)$ and $I(v_n)$ are the intersection densities of the nodes at the two ends of the edge e , and α is a calibration factor reflecting the impact of intersection density on delays, in units of [minutes · square meters per intersection]. This design ensures that travel times accurately capture the influence of densely connected nodes at the start and end of each road segment, aligning with the principle that congestion delays are more pronounced in highly interconnected regions.

The adjusted travel time for each edge is then given by:

$$T'(e) = T(e) + D_{\text{intersection}}(e), \quad (4.4)$$

and the corresponding adjusted travel time matrix T' is:

$$T'_{ij} = \text{Shortest path travel time from node } v_i \text{ to node } v_j \text{ incorporating intersection delays.} \quad (4.5)$$

A node v_i is considered accessible to/from an EMS site (EMS station or hospital) s_j if:

$$T'_{ij} \leq \tau, \quad (4.6)$$

where τ is a benchmark travel time, typically set as 4 minutes, aligned with the National Fire Protection Association standards [243].

By integrating both road characteristics and node-based intersection delays, this framework offers a more realistic evaluation of travel times, enabling the identification of vulnerable regions where response times exceed the benchmark τ . While the model operates under the assumption that the EMV can travel unimpeded between nodes—an idealization that does not fully align with real-world conditions—it effectively captures the concept of accessibility and accounts for intersection delays along the route, providing valuable insights regarding EMS accessibility.

4.3.2.3 Population assignment

To accurately gauge the number of residents affected by EMS accessibility, population assignment is also incorporated extending the idea proposed by [168]. Each node $v \in V$ is assigned a population density by intersecting census tracts with node-based Voronoi

polygons[246]. Census tracts provide demographic data, including the population count $P(c)$ and livable area $L(c)$.

For simplicity, the livable area of each census tract in our study is considered synonymous with its total area, which can be acquired directly from [239]. The effective population density $\rho^*(c)$ is defined as:

$$\rho^*(c) = \frac{P(c)}{L(c)}. \quad (4.7)$$

See Table 4.2 for total area, population and population density by each borough.

Borough	$L(c)$ [mi ²]	$P(c)$ [M]	$\rho^*(c)$ [k ppl/mi ²]
Bronx	42.2	1.42	33.65
Brooklyn	69.4	2.57	37.04
Manhattan	22.7	1.63	71.81
Queens	108.7	2.27	20.88
Staten Island	57.5	0.47	8.17
Total NYC	300.5	8.36	27.82

Table 4.2: Total area, population and population density for boroughs and NYC.

The Voronoi region $R(v)$ associated with node v defines the area influenced by that node within the road network. The population assigned to each node v , $P(v)$, is then computed by proportionally weighting the overlap of $R(v)$ with each census tract $c \in C$, as follows:

$$P(v) = \sum_{c \in C} (|R(v) \cap c| \cdot \rho^*(c)), \quad (4.8)$$

where $|R(v) \cap c|$ represents the area of overlap between the Voronoi region $R(v)$ and census tract c . This assignment ensures that each node in the network has a population weighting, allowing for the assessment of accessibility impacts across densely and

sparsely populated areas.

By integrating both intersection-adjusted travel times and population density metrics, the modified EMS model provides a more granular perspective on emergency accessibility in urban environments, particularly highlighting regions where dense intersections may exacerbate response delays.

4.3.2.4 Vulnerability determination

Vulnerability to insufficient EMS coverage is assessed by comparing the shortest adjusted travel time $T'_{i,EMS}$ from each node v_i to the nearest EMS facility against a benchmark threshold τ , following National Fire Protection Association (NFPA) guidelines[243]. Nodes with $T'_{i,EMS} > \tau$ are deemed inaccessible.

Regions are classified as “vulnerable” if they contain clusters of inaccessible nodes. To quantify the impact, population weights are assigned to each inaccessible node, allowing for an aggregate measure of residents underserved by EMS. This population-weighted vulnerability assessment highlights priority areas for potential TSC enhancement.

4.4 Results

In this section, we present travel times using the proposed EMS accessibility model outlined in Subsec.4.4.1. We then compare the simulated EMV travel time with the ground-truth travel time in Subsec. 4.4.2. Vulnerable regions with respect to EMS accessibility are identified in Subsec. 4.4.3.

4.4.1 Travel Time

Table 4.3 summarizes the travel time statistics for EMS stations, hospitals, and a combined category considering EMS stations and hospitals as one type of facility providing comprehensive medical services based on the simulation of the proposed EMS accessibility model. The statistics are presented across different α values, where α is the intersection delay factor introduced in Subsec. 4.3.2, which represents the additional delay induced by intersection density. α is expressed in unit of seconds \cdot square meters for better readability.

Travel times are reported in minutes and include key percentiles (25%, 50%, 75%, 97.5%, and 100%) alongside the average travel time for each category. The 97.5% percentile represents the practically longest travel time while excluding a small number of extreme outliers in the complete simulated travel time distribution.

Travel time to EMS stations are typically shorter due to the higher density and wider distribution of EMS stations compared to hospitals. Hospitals, although fewer in number, extend the range of travel times because of their greater average distance in urban areas. Consequently, the overall travel time to the nearest emergency medical facility is slightly shorter than that to the nearest EMS station, as the inclusion of hospitals increases the number of accessible options.

Figures 4.6 and 4.7 illustrate the travel time distributions for EMS stations and hospital, respectively, under different α values. Each figure consists of subplots representing travel time distributions for $\alpha = 0, 5, 10,$ and $15 \text{ s} \cdot \text{m}^2$. The distributions show an increasing pattern in travel times as α grows, reflecting the impact of intersection-induced delays.

Category	$\alpha(\text{s} \cdot \text{m}^2)$	25%	50%	75%	97.5%	100%	Average
EMS Stations	0	2.15	3.10	4.18	6.60	7.95	4.80
	5	2.28	3.23	4.35	6.85	8.12	4.97
	10	2.50	3.48	4.72	7.28	8.42	5.19
	15	2.95	3.98	5.12	7.98	8.93	5.68
Hospital	0	3.45	5.03	6.82	9.35	10.90	6.70
	5	3.68	5.11	6.93	9.46	11.15	6.95
	10	3.85	5.29	7.12	9.71	11.41	7.22
	15	4.10	5.81	7.60	10.32	11.92	7.50
Overall	0	2.07	2.98	3.92	6.03	7.22	3.92
	5	2.18	3.13	4.08	6.12	7.34	4.09
	10	2.35	3.42	4.47	6.48	7.52	4.19
	15	2.73	3.86	4.99	7.28	8.38	4.41

Table 4.3: Summary of travel time [mins] for EMS stations, hospitals, and combined (Overall) given different α values.

4.4.2 Calibration of α

To validate the correctness of the proposed model’s predicted travel time, which accounts for delays due to intersections, we summarize the EMV travel times recorded in the 911 NYC End-to-End dataset [1]. These travel times are derived from the time difference between agency dispatch and agency arrival and span the period from the week of November 18, 2023, to October 21, 2024. For reference, Fig. 4.8 illustrates the trend of EMV travel time over the past decade, revealing a continuous increase in EMV travel time for NYPD-reported medical emergencies throughout the study period. Notably, EMV travel time for both life-threatening and non-life-threatening emergencies experienced an abrupt decline during the outbreak of Covid-19 in the city due to shelter-in-place, followed by a gradual rise in the post-Covid-19 period.

If we calculate the statistics of the actual EMV travel time T_{actual} for all medical

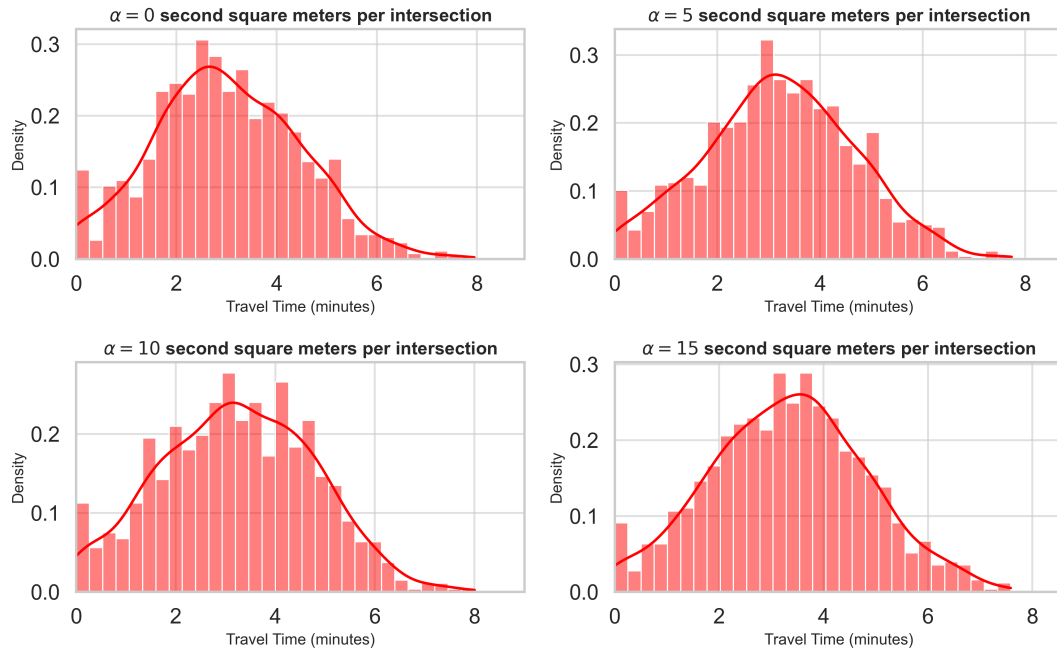


Figure 4.6: Travel time distributions for EMS stations across different α values.

incidents and compare it with the simulated travel time $T_{simulated}$ when $\alpha = 15 \text{ s} \cdot \text{m}^2$, as shown in Table 4.4, we observe that the simulated travel times in Table 4.3 tend to underestimate the actual travel times. This observation aligns with the findings of [168], as both studies assume that EMVs always travel at the speed limit between intersections. Furthermore, we note that for shorter trips, the ratio $T_{actual}/T_{simulated}$ tends to be larger compared to longer trips. This can be attributed to intersection delay factors, which play a proportionally greater role in shorter trips, whereas the simulation-to-reality gap narrows for longer trips due to the influence of extended road segments.

While it may be tempting to scale the intersection delay factor α by the average underestimation ratio ($1.8 \times 15 = 27 \text{ s} \cdot \text{m}^2$), this approach oversimplifies the underlying dynamics of EMV travel times. Firstly, attributing the majority of travel time to

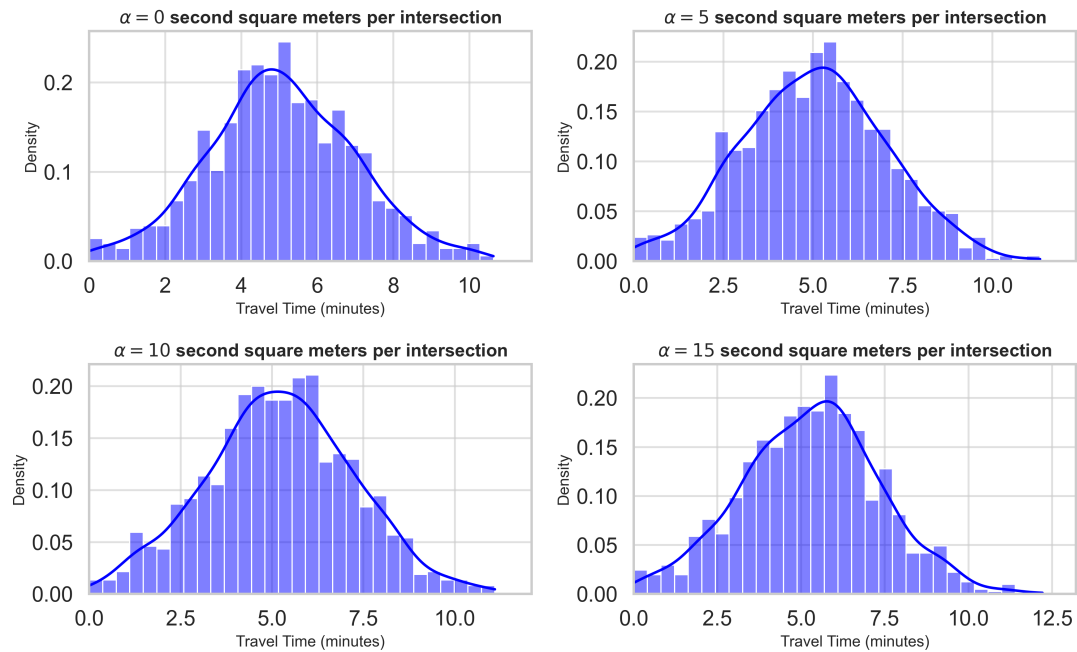


Figure 4.7: Travel time distributions for Hospital across different α values.

intersection delay overlooks the fact that urban travel times are influenced by numerous interacting factors, such as traffic congestion, vehicle acceleration and deceleration, driver behavior, and road geometry [247]. These factors are not uniformly distributed across all trips and vary based on location, time of day, and road conditions. Assigning a higher α uniformly would disproportionately amplify the role of intersections and fail to capture these complexities. For instance, segments with fewer intersections but heavy congestion would still exhibit significant delays, which a simple scaling approach cannot account for.

Secondly, the model assumes that intersection delay is additive rather than multiplicative, meaning the travel time for a road segment is modeled as the sum of its free-flow travel time and an intersection delay component. Scaling α directly would imply a shift

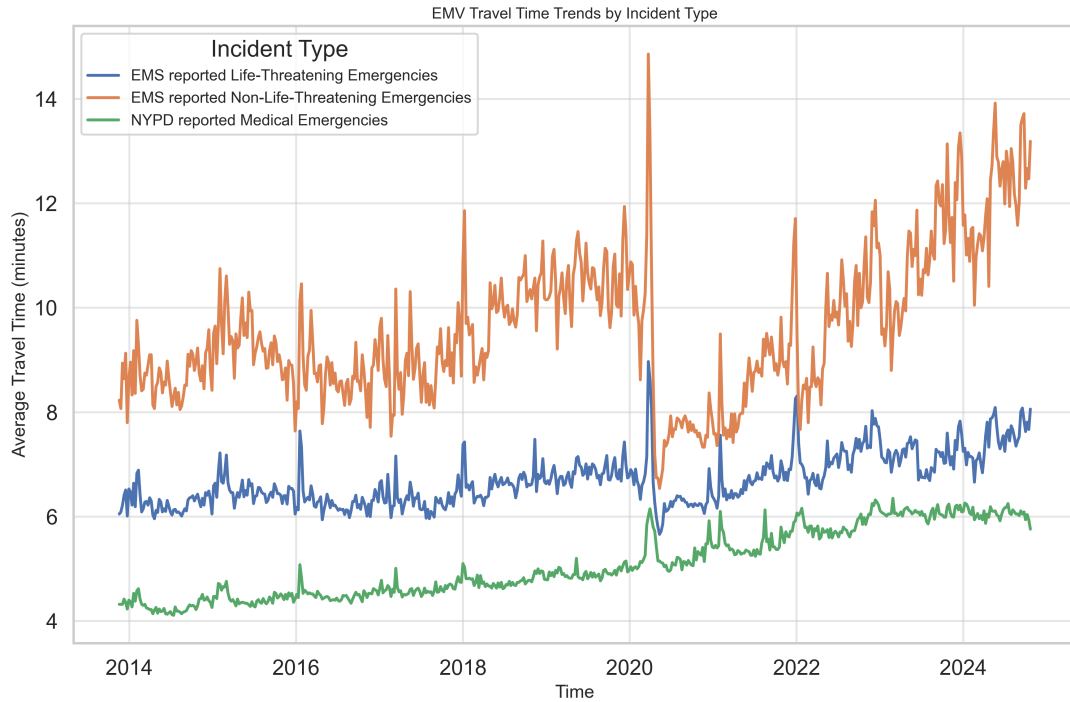


Figure 4.8: EMV travel time trend based on 911 NYC End-to-End.

in this underlying assumption, potentially leading to inconsistent results. Increasing α would exaggerate delays at intersections without considering the diminishing marginal impact of additional intersections, especially in areas where traffic congestion or coordinated signals mitigate delay. This would likely result in unrealistic travel time predictions in regions with high intersection densities but well-managed traffic flow.

Finally, experiments conducted on the Synthetic Grid_{5×5} map in Section 4.5.3 demonstrate that $\alpha = 15 \text{ s} \cdot \text{m}^2$ aligns closely with observed delays in scenarios lacking preemption. This consistency underscores that $\alpha = 15 \text{ s} \cdot \text{m}^2$ provides a reasonable baseline for evaluating EMS accessibility without overestimating intersection effects. While the model underestimates absolute travel times due to idealized assumptions, $\alpha = 15 \text{ s} \cdot \text{m}^2$ strikes a balance, effectively capturing relative differences in EMS accessibility and

	T_{actual} (minutes)	$T_{actual}/T_{simulated}$
25%	6.39	2.34
50%	7.62	1.92
75%	9.40	1.89
97.5%	12.34	1.69
100%	14.86	1.77
Average	7.96	1.80

Table 4.4: Statistics for actual travel time (T_{actual}) based on 911 End-to-End reports. The ratio $T_{actual}/T_{simulated}$ compares actual travel time to simulated travel time for overall medical service when $\alpha = 15 \text{ s} \cdot \text{m}^2$.

identifying vulnerable regions.

4.4.3 Vulnerable regions

Based on the simulated travel time in Subsec. 4.4.1 for the overall EMS accessibility with $\alpha = 15 \text{ s} \cdot \text{m}^2$, we here highlight the EMS accessibility vulnerable regions in NYC, see Fig. 4.9.

We identified four regions within New York City that are particularly vulnerable in terms of EMS accessibility, all exhibiting average EMS travel times exceeding the benchmark of $\tau = 4$ minutes. First, the southern and western parts of Staten Island are characterized by sparse population distribution and a suburban layout with a limited number of medical facilities. This geographic configuration leads to prolonged response times and reduced accessibility for residents. Second, the outer ring of Queens faces a dual challenge of low medical facility density and relatively high intersection density. These geographically expansive areas experience significant gaps in EMS coverage, particularly within densely populated residential neighborhoods. Third, the Upper West Side of Manhattan, a densely populated residential neighborhood, is marked by a dense network

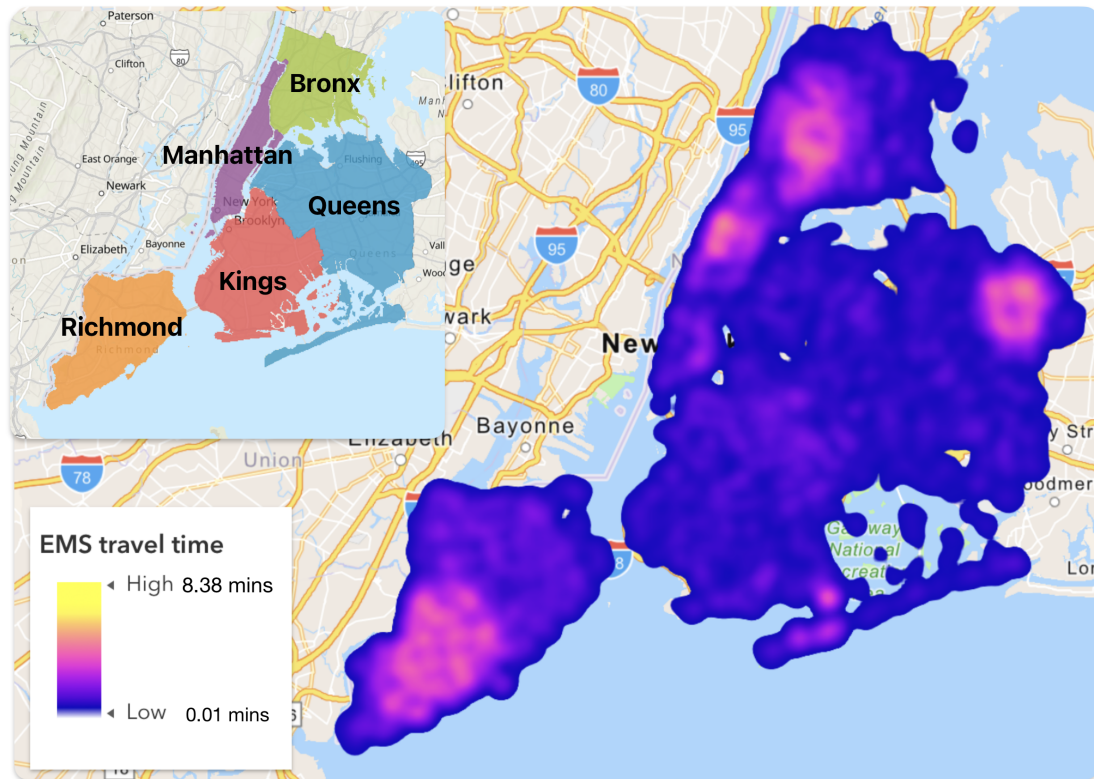


Figure 4.9: EMS travel time heatmap, with heated regions highlighting the vulnerable regions.

of intersections and frequent traffic congestion. These conditions pose substantial barriers to efficient EMS response, further highlighting the region's accessibility challenges. Fourth, large areas of the Bronx, which lack sufficient medical facilities, also suffer from inadequate service coverage. Additionally, minor vulnerable regions with average EMS travel times around $\tau = 4$ minutes are recognized, such as the Rockaway Peninsula. This area, being geographically distant from the city center, faces challenges in accessing general medical services.

4.5 Discussion

In this section, we first conduct a sensitivity study on the value of τ in Subsec. 4.5.1. We examine accessibility' with respect to demographic factors in Subsec. 4.5.2, and then further investigate *EMVLight*'s potential to facilitate these EMS accessibility vulnerable area in Subsec. 4.5.3.

4.5.1 Feasibility of τ

Even though $\tau = 4$ minutes is suggested by NFPA 1710 standards [243] and widely adopted, its feasibility in NYC remains uncertain. Using the population assignment framework proposed in Subsubsec. 4.3.2.3, we evaluate the percentage of the population covered by EMS accessibility as a function of benchmark travel time τ . Fig. 4.10 illustrates the accessibility of emergency services (EMS stations, hospitals, and combined) as a function of τ . The results indicate a rapid increase in population coverage for smaller τ , followed by a plateau as τ increases. At $\tau = 4$ minutes, EMS stations cover approximately 80% of the population, aligning with NFPA 1710 standards, while hospital coverage remains lower, at around 50%.

This disparity underscores the critical role of EMS stations in ensuring rapid response and highlights the need for infrastructure improvements to enhance hospital accessibility. Beyond $\tau = 4$ minutes, additional gains in coverage diminish, making $\tau = 4$ minutes a practical benchmark for EMS station accessibility. When EMS stations and hospitals are considered jointly, 83% of the population can be reached within 4 minutes. However, hospitals, with greater capacity to handle critical emergencies, remain indispensable for specific medical situations. The current allocation of hospitals suggests that a benchmark travel time of $\tau = 5.5$ minutes is more realistic for hospital accessibility in NYC, which

exceeds the NFPA 1710 requirement of 4 minutes. This finding highlights the urgent need for additional hospital locations to ensure equitable and timely access to critical medical care.

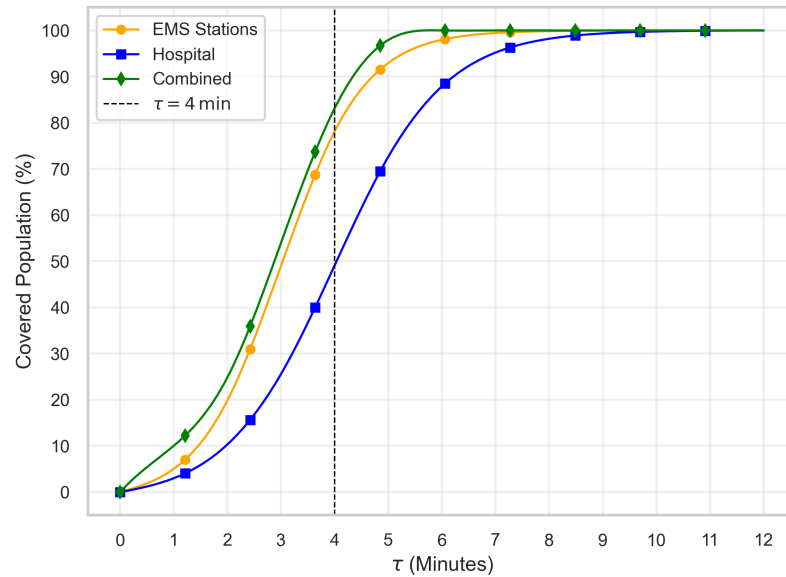


Figure 4.10: Population covered by EMS accessibility as a function of τ .

4.5.2 Demographic analysis

To explore correlations and extend vulnerability analysis to socio-economic dimensions, we compare the identified vulnerable regions with demographic distributions, such as age and median income, derived from the U.S. Census [239]. Figures are available in Appendix C.1.

4.5.2.1 Age

The demographic distribution of NYC reveals significant variations in age structure across census tracts. Fig. C.1 highlights that the 65+ population is concentrated in

Staten Island and southern Brooklyn, where several census tracts have over 1,700 elderly residents. In contrast, the Bronx and parts of northern Manhattan have notably lower concentrations, with many tracts reporting fewer than 338 individuals aged 65+. Fig. C.2, depicting median age, complements this observation, showing that Staten Island and southern Brooklyn exhibit the highest median ages (above 50 years), indicative of older populations. Conversely, the Bronx and northern Brooklyn demonstrate significantly younger median ages, often below 30 years. This spatial dichotomy underscores that demographic aging in Staten Island and southern Brooklyn renders these areas more medically vulnerable, as they are likely to demand greater age-specific medical services.

Overlaying the identified EMS-vulnerable regions with demographic data, particularly the distribution of the population aged 65 and over, reveals several critical insights. The Upper West Side of Manhattan stands out with a notably high concentration of elderly residents, a demographic that is especially reliant on timely emergency medical services. This significant proportion of older adults, combined with the area's existing EMS accessibility challenges, amplifies the region's vulnerability. Similarly, the peripheral areas of Queens exhibit comparable risks, where limited medical infrastructure coincides with a growing elderly population. Staten Island further highlights this intersection of demographic and geographic challenges, particularly in its southern and western census tracts, which feature a high ratio of residents aged 65 and older. As Staten Island is broadly considered an EMS accessibility desert, the substantial presence of seniors in these areas exacerbates the already critical gaps in emergency medical response. These findings underscore the urgent need for targeted interventions to improve EMS accessibility in regions with a high concentration of vulnerable elderly populations.

4.5.2.2 Median Income

We present maps highlighting pronounced socioeconomic disparities across NYC, with Fig. C.3 depicting the median income per census tract and Fig. C.4 illustrating the poverty population ratio per census tract. High-income areas, primarily located in Manhattan (e.g., Upper East Side, Midtown), exhibit median incomes exceeding \$99,680, which align with low poverty ratios (below 10.8%). Conversely, the Bronx stands out as the most economically vulnerable borough, characterized by median incomes below \$34,450 and poverty rates exceeding 34.1%, followed by economically distressed neighborhoods in Brooklyn, such as East New York and Brownsville. This inverse correlation between income and poverty highlights the potential larger medical needs in these underserved areas, particularly in the Bronx and select Brooklyn neighborhoods.

Overlaying the identified EMS-vulnerable regions with median income distribution data reveals critical socioeconomic disparities impacting EMS accessibility. Notably, the peripheral areas of Queens exhibit higher poverty rates compared to surrounding neighborhoods, intensifying the challenges posed by limited medical infrastructure and relatively high intersection densities. In Staten Island, particularly the southern and western regions, residents experience relatively low income levels, compounding the area's designation as an EMS desert and further hindering timely emergency responses. Bronx registers the lowest median household income among New York City's boroughs and also exhibits the most severe EMS accessibility challenge.

4.5.3 Improvement with EMVLight

EMVLight [169] is a state-of-the-art large-scale multi-agent reinforcement learning (MARL) framework designed to optimize real-time TSC for facilitating the efficient

passage of EMVs in congested road networks. By dynamically assigning the roles of pre-emption agents to signalized intersections as EMVs traverse the network, *EMVLight* enables real-time shortest path navigation and coordinated signal control, ensuring seamless EMV mobility through highly congested environments.

Experimental evaluations on synthetic maps (e.g., Synthetic Grid_{5×5}) and real-world maps (e.g., Manhattan, 16 × 3; Hangzhou, 4 × 4) demonstrated that *EMVLight* can reduce EMV travel time (T_{EMV}) by 60% to 80%, depending on whether the network is emergency-capacitated, compared to benchmarks without pre-emption. These results highlight the framework’s ability to substantially enhance EMV traversal efficiency across varying network configurations and densities.

To assess *EMVLight*’s ability to reduce T_{EMV} within the perspective of the EMS accessibility model proposed in Subsec. 4.3.2, we can study the amount of time the EMV takes passing through intersections against the benchmark to estimate the potential intersection delay reduction.

Let us revisit the Synthetic Grid_{5×5} map, shown in Fig. 4.11, where intersections are interconnected through bi-directional links, each consisting of two lanes. For this experiment, we assume that all links have zero emergency capacity. The traffic configuration selected for this study involves northbound and southbound flows transitioning to eastbound and westbound directions, with a non-peak flow of 200 vehicles per lane per hour and a peak flow of 240 vehicles per lane per hour. The origin (O) and destination (D) of the EMV are explicitly labeled on the map to highlight the designated travel route. The traffic flow for this synthetic map spans a duration of 1200 seconds, during which varying congestion levels are simulated. To ensure the network is sufficiently congested, the EMV is dispatched at $t = 600$ s, a point when traffic conditions have reached compactness.

We record the time taken by the EMV as it traverses any of the inner nine intersections,

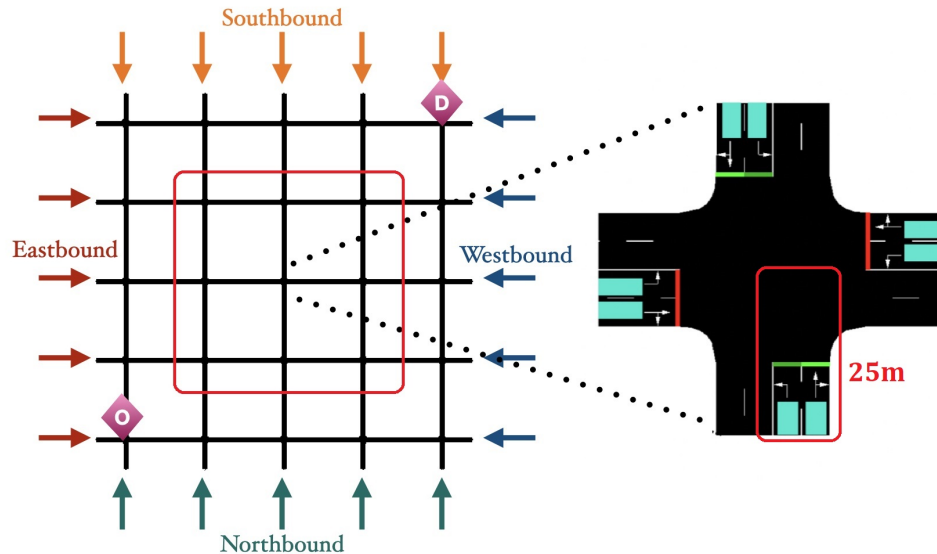


Figure 4.11: Synthetic Grid_{5×5} and the inner 9 intersections are observed for intersection delay.

with the measurement boundaries defined as 25 meters from the center of each intersection in the incoming direction to 25 meters in the outgoing direction. This precise delineation ensures consistency in capturing the traversal times across intersections. The benchmarks for comparison are 1. **Walabi** [41], which is a rule-based control scheme aiming Green Wave for EMVs in SUMO environment, and 2. no pre-emption for EMVs.

After running the simulations 120 times for each scenario, we aggregate and present the time required for the EMV to traverse the observed intersections in Fig. 4.12. The results clearly demonstrate that *EMVLight* reduces intersection delays by approximately 30% compared to the Walabi and achieves a time savings of over 50% relative to no pre-emption scenarios.

The results indicate that incorporating *EMVLight* across the entire city effectively reduces the intersection delay factor, α , by half. By adopting $\alpha = 7.5 \text{ s} \cdot \text{m}^2$, the updated population coverage function, shown in Fig. 4.13, reveals significant improvements in

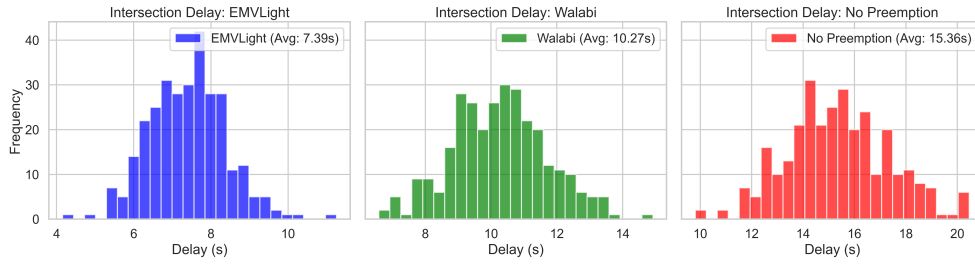


Figure 4.12: Amount of time to pass intersections for EMVs.

EMS accessibility. Approximately 70% of the population gains access to hospitals, and 95% of NYC residents can be served within $\tau = 4$ minutes. These results highlight the transformative potential of *EMVLight* in enhancing emergency service coverage across the city.

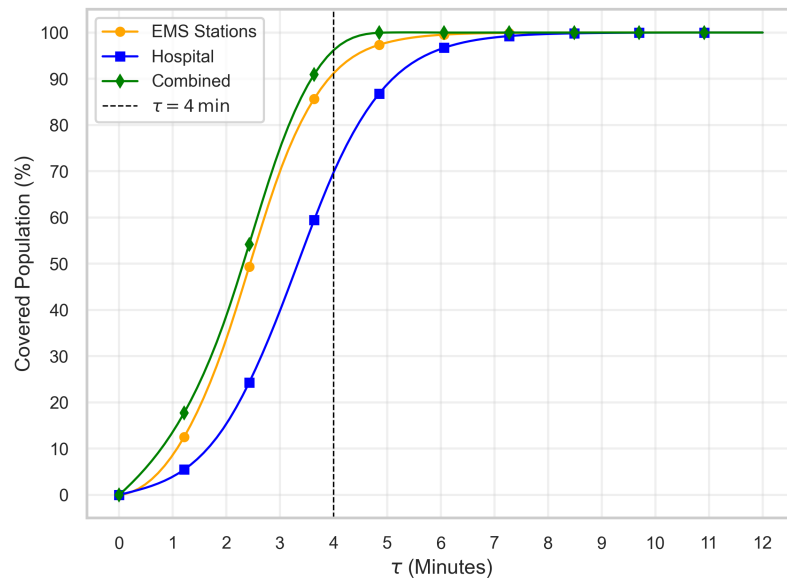


Figure 4.13: Population coverage function against τ with $\alpha = 7.5s \cdot m^2$

4.6 Summary

This study presents an intersection-aware EMS accessibility model to comprehensively evaluate medical emergency service coverage in NYC. By incorporating road network characteristics, intersection delays, and demographic data, the model identifies critical EMS-vulnerable regions, including Staten Island, the peripheral regions of Queens, and parts of Manhattan. These findings emphasize the challenges faced by underserved areas, particularly those with limited medical infrastructure, high intersection densities, or significant demographic vulnerabilities. The analysis further demonstrates the capability of *EMVLight* to significantly improve EMS performance by halving intersection delays, increasing hospital accessibility to 70%, and ensuring 95% of NYC residents are served within the benchmark travel time of $\tau = 4$ minutes.

Despite its contributions, the study is subject to certain limitations. The absence of real-time traffic condition data in the travel time assignment likely underestimates congestion-induced delays, and the assumption of free-flow travel between intersections simplifies the complexity of urban traffic dynamics. These constraints highlight the need for future work to incorporate dynamic traffic data and congestion modeling to refine the accessibility framework. Additionally, the static nature of the EMS station locations in the model does not account for adaptive dispatch strategies, which could further enhance emergency response capabilities in underserved regions.

Nonetheless, this study provides a robust foundation for understanding EMS accessibility and exploring the role of advanced TSC systems like *EMVLight* in improving emergency vehicle navigation. The intersection-aware framework and the integration of demographic and network data offer valuable insights into the spatial and temporal disparities in EMS access. Future studies should focus on validating the model using

real-world traffic data, exploring the scalability of TSC systems across larger urban networks, and assessing the cost-effectiveness of implementing such systems. By addressing these aspects, the findings of this study can inform policy decisions and urban planning strategies aimed at reducing response times and ensuring equitable access to emergency medical services in cities like NYC and beyond.

Chapter 5

Conclusions

This chapter synthesizes the primary findings outlined in Section 5.1 and delves into the limitations and prospective future directions detailed in Section 5.2. Finally, Section 5.3 offers reflective closing remarks on the contributions and implications of the research.

5.1 Research Findings

5.1.1 *EMVLight*

EMVLight, introduced in Chapter 2, demonstrated the feasibility and efficacy of integrating decentralized MARL to simultaneously address EMV routing and traffic signal pre-emption. It effectively tackles two key network-level challenges: (1) coupling dynamic EMV routing with traffic signal control, and (2) reducing EMV travel time while simultaneously mitigating overall congestion. Experimental results highlight that *EMV-Light* achieves a remarkable 42.6% reduction in EMV travel time and a 23.5% decrease in average travel time for all vehicles, significantly outperforming both conventional and

RL-based traffic control methods in synthetic and real-world scenarios.

Many components contribute to the success of *EMVLight*. The incorporation of emergency lane formation highlights the model’s capacity to coordinate between primary pre-emption agents, secondary pre-emption agents, and normal agents to pre-clear links ahead of EMVs effectively. Experimental observations reveal that *EMVLight* often navigates EMVs along longer routes that result in shorter overall travel times. The inclusion of a spatial discount factor, combined with the centralized training and decentralized execution scheme, facilitates optimal trajectory planning across the network during EMV traversal. Additionally, the definition of pressure was modified to align with the agent design, ensuring feasibility in achieving the framework’s goals to reduce disturbance and overall traffic congestion. Another critical component is the use of fingerprints, which, as demonstrated in ablation studies, significantly stabilizes training and improves agent coordination. Furthermore, *EMVLight* explores the trade-off between minimizing EMV travel time and mitigating overall congestion, delegating this decision to traffic managers based on operational priorities.

5.1.2 MAPPO-DQJL

Chapter 3 introduced MAPPO-DQJL, a novel intra-link coordination strategy leveraging the presence of CAVs. This framework dynamically forms lanes to prioritize EMV passage, utilizing V2X communication to coordinate CAVs and indirectly influence HDVs. Modeling the DQJL formation as a POMDP, the framework employs a transformer-based network design and the MAPPO algorithm to train agents to deliver the optimal DQJL establishment strategy for expedited EMV passage with reduced unnecessary maneuvers from non-EMVs.

Extensive experiments on a variety of simulated multi-lane roadway configurations

demonstrated the framework's capacity to clear routes for EMVs while reducing overall traffic disturbances. EMVs changed lanes fewer than once on average across all experimental settings with the proposed methodology. By treating HDVs as agents rather than part of the environment, MAPPO-DQJL significantly enhances performance by enabling CAVs to learn and adapt to HDV behaviors, yielding optimal coordination strategies. The framework achieved up to a 39.8% reduction in EMV passage time and a 55.7% reduction in lane-change maneuvers for non-EMVs, underscoring its scalability and robustness in mixed traffic scenarios.

Notably, the framework's performance improved with higher CAV penetration rates, achieving near-optimal coordination when penetration reached 75% or higher. In multi-lane configurations, MAPPO-DQJL demonstrated that EMVs could navigate segments with fewer than one lane change on average, minimizing disruptions to non-EMVs while expediting emergency responses. Furthermore, it was observed that the benefits of CAV coordination exhibit diminishing returns when penetration rates or traffic density reaches a critical mass, aligning with findings from other CAV applications in tasks similar to DQJL formation.

5.1.3 NYC EMS Accessibility Study

Chapter 4 presented an intersection-aware EMS accessibility model for NYC, integrating road network characteristics, intersection density, and demographic data. The model accounts for delays occurring at intersections and provides valuable insights into travel times assigned to and from EMS facilities. Additionally, it explores the percentage of NYC residents covered within varying benchmark service times.

The study identified vulnerable areas in terms of EMS response times and further analyzed the demographic characteristics of these regions. By incorporating *EMVLight*

into the study, the model demonstrated its potential to reduce intersection delays and improve hospital accessibility.

Results indicated that implementing *EMVLight* could enable over 95% of NYC residents to access hospitals within benchmark travel times, offering actionable insights for urban planners and policymakers to enhance EMS equity and efficiency. Moreover, the study revealed that areas with high intersection densities continue to face delays due to congestion, underscoring the necessity for integrated signal optimization strategies. By analyzing borough-specific response times and population density distributions, the findings emphasize the critical importance of targeted interventions, such as increasing hospital density and optimizing resource allocation in underserved areas.

5.2 Limitations and Future Directions

5.2.1 *EMVLight*

While *EMVLight* effectively integrates routing and pre-emption, several limitations remain. The framework relies on accurate real-time traffic data, which may not always be available or reliable in real-world deployments. Future research could explore integrating predictive traffic models and robust communication systems to address data uncertainty. Additionally, the scalability of *EMVLight* in larger urban networks with more complex traffic patterns warrants further investigation.

A critical consideration for future work lies in the statistical robustness of our experimental results. While our current findings demonstrate improvements in travel times, the statistical significance of these improvements needs more rigorous validation. Future studies should determine the optimal number of experimental runs through power analysis, considering factors such as effect size and desired confidence levels. This

would provide more statistically sound conclusions about the framework's performance improvements, especially regarding travel time reductions which might appear marginal in absolute terms but could have significant cumulative impacts on emergency response efficiency.

Non-trivial future directions for this study include, but are not limited to, the following. First, as an effort to bridge the gap between simulation and reality, we are motivated to develop more sophisticated traffic pattern models that better capture the complex dynamics of mixed traffic with EMVs. Second, we aim to address the challenge of navigating multiple EMVs simultaneously in the same traffic network, which raises both technical and ethical considerations in reward design for pre-emption agents. Third, a fundamental challenge in applying reinforcement learning to transportation systems lies in the extensive trial-and-error nature of the learning process. Future research should focus on developing safe learning frameworks that minimize negative impacts during the learning phase.

5.2.2 MAPPO-DQJL

Despite its success in coordinating DQJLs, MAPPO-DQJL faces challenges in handling extreme traffic densities and low CAV penetration rates. The reliance on centralized training may also limit scalability in real-time applications. Future work should focus on adaptive learning techniques to reduce computational overhead and enhance real-time adaptability.

A key area for enhancement lies in the representation of human-driven vehicles within the framework. Current models may oversimplify the stochastic nature of human driving behaviors and the complex decision-making processes of human drivers. Future work should explore incorporating more sophisticated driver behavior models that account for

varying levels of aggression, risk tolerance, and decision-making patterns. Additionally, the game-theoretic nature of interactions between selfish human drivers, particularly during emergency scenarios, warrants deeper investigation. This could involve developing mechanism design approaches to incentivize cooperative behavior while acknowledging the inherently competitive nature of individual routing choices.

Experimental validation in real-world mixed autonomy environments would provide critical insights for deployment. Additionally, expanding the framework to incorporate multi-lane dynamic lane assignment strategies could further enhance its effectiveness, particularly in environments with asymmetric traffic flows or high vehicle heterogeneity.

Integrating *EMVLight* with MAPPO-DQJL presents a promising avenue for future research, as it combines the strengths of network-wide traffic signal coordination with dynamic intra-link lane-clearing strategies. By leveraging *EMVLight*'s decentralized MARL framework for real-time routing and signal optimization alongside MAPPO-DQJL's capability to manage mixed traffic at the lane level, a unified system could holistically address both macro-level and micro-level challenges of EMV passage. This integration could enable seamless coordination between intersections and road segments, dynamically adapting to traffic patterns while ensuring unobstructed EMV movement. Furthermore, the combined framework would be particularly effective in scenarios with varying CAV penetration rates, where coordination across intersections and individual lanes becomes critical. To achieve this, future work could focus on designing reward mechanisms that align global network efficiency with local lane-level optimization, ensuring that the dual objectives of reducing EMV travel time and minimizing disruptions to non-EMVs are met cohesively. Experimental validation in simulation environments and real-world mixed autonomy networks would be instrumental in demonstrating the practical feasibility and benefits of this integrated approach.

5.2.3 NYC EMS Accessibility Study

Chapter 4 highlighted critical disparities but relied on static data and simplified assumptions about traffic dynamics and intersection delays. Future research could incorporate dynamic traffic simulations and real-time data feeds to refine accessibility models. Expanding the study to include other urban centers with varying demographics and infrastructure would provide a broader understanding of EMS accessibility challenges. Additionally, integrating equity-focused policies, such as targeted investments in underserved areas, could address systemic inequities in EMS coverage.

Another potential direction is to explore the impact of emerging technologies, such as autonomous ambulances or drone-based EMS support, on accessibility metrics. Coupling these innovations with intersection-aware frameworks could revolutionize emergency response strategies, particularly in geographically constrained regions.

5.3 Closing Remarks

This dissertation presents a comprehensive approach to enhancing EMV passage and EMS accessibility in urban environments through innovative methodologies. The integration of MARL-based frameworks, such as *EMVLight* and MAPPO-DQJL, alongside detailed accessibility studies, demonstrates significant potential to improve emergency response efficiency and equity. By addressing the limitations and exploring the proposed future directions, this research lays a robust foundation for advancing emergency traffic management and urban resilience. Furthermore, the findings underscore the transformative potential of integrating cutting-edge technologies with data-driven strategies to create safer, more equitable, and efficient urban transportation systems.

Bibliography

- [1] NYC Open Data. 911 end-to-end data, 2024. Accessed: 2024-11-25.
- [2] INRIX, Inc. Global traffic scorecard, 2024. Accessed: 2024-12-10.
- [3] Jeffrey L. Saver. Time is brain—quantified. *Stroke*, 37(1):263–266, 2006.
- [4] AHA. *Heart Disease and Stroke Statistics*, 2013.
- [5] Andreas Buchenscheit, Florian Schaub, Frank Kargl, and Michael Weber. A vanet-based emergency vehicle warning system. *2009 IEEE Vehicular Networking Conference (VNC)*, pages 1–8, 2009.
- [6] Shamsunnahar Yasmin, Sabreena Anowar, and Richard Tay. Effects of drivers’ actions on severity of emergency vehicle collisions. *Transportation Research Record*, 2318(1):90–97, 2012.
- [7] Jocelyn Berdowski, Robert A Berg, Jan GP Tijssen, and Rudolph W Koster. Global incidences of out-of-hospital cardiac arrest and survival rates: systematic review of 67 prospective studies. *Resuscitation*, 81(11):1479–1487, 2010.
- [8] NYC Analytics. End-to-end response times. <https://www1.nyc.gov/site/fdny/about/resources/data-and-analytics/end-to-end-response-times.page>, 2021.

- [9] L. Lu and S. Wang. Literature review of analytical models on emergency vehicle service: Location, dispatching, routing and preemption control. In *2019 IEEE Intelligent Transportation Systems Conference (ITSC)*, pages 3031–3036, 2019.
- [10] Subash Humagain, Roopak Sinha, Edmund Lai, and Prakash Ranjitkar. A systematic review of route optimisation and pre-emption methods for emergency vehicles. *Transport reviews*, 40(1):35–53, 2020.
- [11] Robert A De Lorenzo and Mark A Eilers. Lights and siren: A review of emergency vehicle warning systems. *Annals of emergency medicine*, 20(12):1331–1335, 1991.
- [12] Pauline Grant. The human factors associated with responding to emergency vehicles. *Edith Cowan University Theses: Doctorates and Masters*, 2017.
- [13] Eric J Nelson and Darcy Bullock. Impact of emergency vehicle preemption on signalized corridor operation: An evaluation. *Transportation research record*, 1727(1):1–11, 2000.
- [14] Xiaolin Qin and Ata M Khan. Control strategies of traffic signal timing transition for emergency vehicle preemption. *Transportation research part C: emerging technologies*, 25:1–17, 2012.
- [15] Yi-Sheng Huang, Yi-Shun Weng, and MengChu Zhou. Design of traffic safety control systems for emergency vehicle preemption using timed petri nets. *IEEE Transactions on Intelligent Transportation Systems*, 16(4):2113–2120, 2015.
- [16] Samuel Coogan and Murat Arcaç. A compartmental model for traffic networks and its dynamical behavior. *IEEE Transactions on Automatic Control*, 60(10):2698–2703, 2015.

- [17] Ali Haghani, Qiang Tian, and Huijun Hu. Simulation model for real-time emergency vehicle dispatching and routing. *Transportation Research Record*, 1882(1):176–183, 2004.
- [18] Ali Haghani, Huijun Hu, and Qiang Tian. An optimization model for real-time emergency vehicle dispatching and routing. In *82nd annual meeting of the Transportation Research Board, Washington, DC*, page 1. Citeseer, 2003.
- [19] S Panahi and MR Delavar. A gis-based dynamic shortest path determination in emergency vehicles. *World applied sciences journal*, 3(1):88–94, 2008.
- [20] Khaled Shaaban, Muhammad Asif Khan, Ridha Hamila, and Mohammad Ghanim. A strategy for emergency vehicle preemption and route selection. *Arabian Journal for Science and Engineering*, 44(10):8905–8913, 2019.
- [21] Hongwei Hsiao, Joonho Chang, and Peter Simeonov. Preventing emergency vehicle crashes: status and challenges of human factors issues. *Human factors*, 60(7):1048–1072, 2018.
- [22] Haoran Su, Yaofeng Desmond Zhong, Biswadip Dey, and Amit Chakraborty. Emvlight: A decentralized reinforcement learning framework for efficient passage of emergency vehicles. *AAAI proceedings*, 2022.
- [23] Jiawen Wang, Wanjing Ma, and Xiaoguang Yang. Development of degree-of-priority based control strategy for emergency vehicle preemption operation. *Discrete dynamics in nature and society*, 2013, 2013.
- [24] Haibo Mu, Yubo Song, and Linzhong Liu. Route-based signal preemption control of emergency vehicle. *Journal of Control Science and Engineering*, 2018:1–11, 04 2018.

- [25] Eil Kwon, Sangho Kim, and Robert Betts. Route-based dynamic preemption of traffic signals for emergency vehicle operations. In *Transportation Research Board 82nd Annual Meeting* *Transportation Research Board*, page 1, 2003.
- [26] Arun Jotshi, Qiang Gong, and Rajan Batta. Dispatching and routing of emergency vehicles in disaster mitigation using data fusion. *Socio-Economic Planning Sciences*, 43(1):1 – 24, 2009.
- [27] Noraimi Azlin Mohd Nordin, Zati Aqmar Zaharudin, Mohd Azdi Maasar, and Nor Amalina Nordin. Finding shortest path of the ambulance routing: Interface of a-star algorithm using c programming. In *2012 IEEE Symposium on Humanities, Science and Engineering Research*, pages 1569–1573. IEEE, 2012.
- [28] Athanasios K. Ziliaskopoulos and Hani S. Mahmassani. Time-dependent, shortest-path algorithm for real-time intelligent vehicle highway system applications. In *Transportation Research Record 1408*, pages 94–100, 1993.
- [29] Giuseppe Musolino, Antonio Polimeni, Corrado Rindone, and Antonino Vitetta. Travel time forecasting and dynamic routes design for emergency vehicles. *Procedia-Social and Behavioral Sciences*, 87:193–202, 2013.
- [30] Songsang Koh, Bo Zhou, Hui Fang, Po Yang, Zaili Yang, Qiang Yang, Lin Guan, and Zhigang Ji. Real-time deep reinforcement learning based vehicle navigation. *Applied Soft Computing*, 96:106694, 2020.
- [31] Elise D Miller-Hooks and Hani S Mahmassani. Least expected time paths in stochastic, time-varying transportation networks. *Transportation science*, 34(2):198–215, 2000.

- [32] Song Gao and Ismail Chabini. Optimal routing policy problems in stochastic time-dependent networks. *Transportation Research Part B: Methodological*, 40(2):93–122, 2006.
- [33] Seongmoon Kim, Mark E Lewis, and Chelsea C White. Optimal vehicle routing with real-time traffic information. *IEEE Transactions on Intelligent Transportation Systems*, 6(2):178–188, 2005.
- [34] YY Fan, RE Kalaba, and JE Moore II. Shortest paths in stochastic networks with correlated link costs. *Computers & Mathematics with Applications*, 49(9-10):1549–1564, 2005.
- [35] Lixing Yang and Xuesong Zhou. Constraint reformulation and a lagrangian relaxation-based solution algorithm for a least expected time path problem. *Transportation Research Part B: Methodological*, 59:22–44, 2014.
- [36] He Huang and Song Gao. Optimal paths in dynamic networks with dependent random link travel times. *Transportation Research Part B: Methodological*, 46(5):579–598, 2012.
- [37] Song Gao and He Huang. Real-time traveler information for optimal adaptive routing in stochastic time-dependent networks. *Transportation Research Part C: Emerging Technologies*, 21(1):196–213, 2012.
- [38] Samitha Samaranyake, Sebastien Blandin, and Alexandre Bayen. A tractable class of algorithms for reliable routing in stochastic networks. *Transportation Research Part C: Emerging Technologies*, 20(1):199–217, 2012.

- [39] Yu Marco Nie, Xing Wu, and Tito Homem-de Mello. Optimal path problems with second-order stochastic dominance constraints. *Networks and Spatial Economics*, 12(4):561–587, 2012.
- [40] Barrett W Thomas and Chelsea C White III. The dynamic shortest path problem with anticipation. *European journal of operational research*, 176(2):836–854, 2007.
- [41] Laura Bieker-Walz, Yun-Pang Flötteröd, and Alexander Sohr. Modelling of emergency vehicles route choice with use of trajectory data. In *2019 6th International Conference on Models and Technologies for Intelligent Transportation Systems (MT-ITS)*, pages 1–8. IEEE, 2019.
- [42] M. Asaduzzaman and K. Vidyasankar. A priority algorithm to control the traffic signal for emergency vehicles. In *2017 IEEE 86th Vehicular Technology Conference (VTC-Fall)*, pages 1–7, 2017.
- [43] Jiaming Wu, Balázs Kulcsár, Soyoung Ahn, and Xiaobo Qu. Emergency vehicle lane pre-clearing: from microscopic cooperation to routing decision making. *Transportation research part B: methodological*, 141:223–239, 2020.
- [44] Mehdi Hosseinzadeh, Bruno Sinopoli, Ilya Kolmanovsky, and Sanjoy Baruah. Mpc-based emergency vehicle-centered multi-intersection traffic control. *IEEE Transactions on Control Systems Technology*, 2022.
- [45] Baher Abdulhai, Rob Pringle, and Grigoris J Karakoulas. Reinforcement learning for true adaptive traffic signal control. *Journal of Transportation Engineering*, 129(3):278–285, 2003.

- [46] LA Prashanth and Shalabh Bhatnagar. Reinforcement learning with function approximation for traffic signal control. *IEEE Transactions on Intelligent Transportation Systems*, 12(2):412–421, 2010.
- [47] Samah El-Tantawy, Baher Abdulhai, and Hossam Abdelgawad. Multiagent reinforcement learning for integrated network of adaptive traffic signal controllers (marlin-atssc): methodology and large-scale application on downtown toronto. *IEEE Transactions on Intelligent Transportation Systems*, 14(3):1140–1150, 2013.
- [48] Elise Van der Pol and Frans A Oliehoek. Coordinated deep reinforcement learners for traffic light control. *Proceedings of Learning, Inference and Control of Multi-Agent Systems (at NIPS 2016)*, 2016.
- [49] Hua Wei, Nan Xu, Huichu Zhang, Guanjie Zheng, Xinshi Zang, Chacha Chen, Weinan Zhang, Yanmin Zhu, Kai Xu, and Zhenhui Li. Colight: Learning network-level cooperation for traffic signal control. In *Proceedings of the 28th ACM International Conference on Information and Knowledge Management*, pages 1913–1922, 2019.
- [50] Guanjie Zheng, Yuanhao Xiong, Xinshi Zang, Jie Feng, Hua Wei, Huichu Zhang, Yong Li, Kai Xu, and Zhenhui Li. Learning phase competition for traffic signal control. In *Proceedings of the 28th ACM International Conference on Information and Knowledge Management*, pages 1963–1972, 2019.
- [51] Hua Wei, Chacha Chen, Guanjie Zheng, Kan Wu, Vikash Gayah, Kai Xu, and Zhenhui Li. Presslight: Learning max pressure control to coordinate traffic signals in arterial network. In *Proceedings of the 25th ACM SIGKDD International Conference on Knowledge Discovery & Data Mining*, pages 1290–1298, 2019.

- [52] Pravin Varaiya. Max pressure control of a network of signalized intersections. *Transportation Research Part C: Emerging Technologies*, 36:177–195, 2013.
- [53] Li Li and Saif Eddin Jabari. Position weighted backpressure intersection control for urban networks. *Transportation Research Part B: Methodological*, 128:435–461, 2019.
- [54] Michael W. Levin, Jeffrey Hu, and Michael Odell. Max-pressure signal control with cyclical phase structure. *Transportation Research Part C: Emerging Technologies*, 120:102828, 2020.
- [55] Xingmin Wang, Yafeng Yin, Yiheng Feng, and Henry X. Liu. Learning the max pressure control for urban traffic networks considering the phase switching loss. *Transportation Research Part C: Emerging Technologies*, 140:103670, 2022.
- [56] Daniel A. Lazar, Samuel Coogan, and Ramtin Pedarsani. Routing for traffic networks with mixed autonomy. *IEEE Transactions on Automatic Control*, 66(6):2664–2676, 2021.
- [57] Chacha Chen, Hua Wei, Nan Xu, Guanjie Zheng, Ming Yang, Yuanhao Xiong, Kai Xu, and Zhenhui Li. Toward a thousand lights: Decentralized deep reinforcement learning for large-scale traffic signal control. *Proceedings of the AAAI Conference on Artificial Intelligence*, 34(04):3414–3421, Apr. 2020.
- [58] Xinshi Zang, Huaxiu Yao, Guanjie Zheng, Nan Xu, Kai Xu, and Zhenhui Li. Metalight: Value-based meta-reinforcement learning for traffic signal control. *Proceedings of the AAAI Conference on Artificial Intelligence*, 34(01):1153–1160, Apr. 2020.

- [59] Mohammad Aslani, Mohammad Saadi Mesgari, and Marco Wiering. Adaptive traffic signal control with actor-critic methods in a real-world traffic network with different traffic disruption events. *Transportation Research Part C: Emerging Technologies*, 85:732–752, 2017.
- [60] Bingyu Xu, Yaowei Wang, Zhaozhi Wang, Huizhu Jia, and Zongqing Lu. Hierarchically and cooperatively learning traffic signal control. In *Proceedings of the AAAI Conference on Artificial Intelligence*, volume 35, pages 669–677, 2021.
- [61] Tianshu Chu, Jie Wang, Lara Codecà, and Zhaojian Li. Multi-agent deep reinforcement learning for large-scale traffic signal control. *IEEE Transactions on Intelligent Transportation Systems*, 2019.
- [62] Jinming Ma and Feng Wu. Feudal multi-agent deep reinforcement learning for traffic signal control. In *Proceedings of the 19th International Conference on Autonomous Agents and Multiagent Systems (AAMAS)*, pages 816–824, Auckland, New Zealand, May 2020.
- [63] Zhaobin Mo, Wangzhi Li, Yongjie Fu, Kangrui Ruan, and Xuan Di. Cvlight: Decentralized learning for adaptive traffic signal control with connected vehicles. *Transportation Research Part C: Emerging Technologies*, 141:103728, 2022.
- [64] Mohammad Noaen, Atharva Naik, Liana Goodman, Jared Crebo, Taimoor Abrar, Zahra Shakeri Hossein Abad, Ana L.C. Bazzan, and Behrouz Far. Reinforcement learning in urban network traffic signal control: A systematic literature review. *Expert Systems with Applications*, 199:116830, 2022.
- [65] Hua Wei, Guanjie Zheng, Vikash Gayah, and Zhenhui Li. A survey on traffic signal control methods. *arXiv preprint arXiv:1904.08117*, 2019.

- [66] J. LeBrun, Chen-Nee Chuah, D. Ghosal, and M. Zhang. Knowledge-based opportunistic forwarding in vehicular wireless ad hoc networks. In *2005 IEEE 61st Vehicular Technology Conference*, volume 4, pages 2289–2293 Vol. 4, 2005.
- [67] Akash Agarwal and Praveen Paruchuri. V2v communication for analysis of lane level dynamics for better ev traversal. In *arXiv.org*, page 0, 06 2016.
- [68] Insaf Ismath, Tharaka Samarasinghe, Dileeka Dias, Madara Wimalarathna, Waruna Rasanga, Nalin Jayaweera, and Yohan Nugera. Emergency vehicle traversal using dsrc/wave based vehicular communication. In *2019 IEEE Intelligent Vehicles Symposium (IV)*, pages 1981–1986, 06 2019.
- [69] G. J. Hannoun, P. Murray-Tuite, K. Heaslip, and T. Chantem. Facilitating emergency response vehicles’ movement through a road segment in a connected vehicle environment. *IEEE Transactions on Intelligent Transportation Systems*, 20(9):3546–3557, 9 2019.
- [70] Gaby Joe Hannoun, Pamela Murray-Tuite, Kevin Heaslip, and Thidapat Chantem. Sequential optimization of an emergency response vehicle’s intra-link movement in a partially connected vehicle environment. *Transportation research record*, 2675(11):413–423, 2021.
- [71] Haoran Su, Kejian Shi, Joseph. Y. J. Chow, and Li Jin. Dynamic queue-jump lane for emergency vehicles under partially connected settings: A multi-agent deep reinforcement learning approach, 2021.
- [72] DOT Federal Highway Administration. Use of freeway shoulders for travel — guide for planning, evaluating, and designing part-time shoulder use as a traffic

management strategy. <https://ops.fhwa.dot.gov/publications/fhwahop15023/ch1.htm>, 2020. Accessed: 2022-04-27.

- [73] Jiaqi Ma, Jia Hu, David K. Hale, and Joe Bared. Dynamic hard shoulder running for traffic incident management. *Transportation Research Record*, 2554(1):120–128, 2016.
- [74] L. Adacher, G. Oliva, and F. Pascucci. Decentralized route guidance architectures with user preferences in urban transportation networks. *Procedia - Social and Behavioral Sciences*, 111:1054–1062, 2014. Transportation: Can we do more with less resources? – 16th Meeting of the Euro Working Group on Transportation – Porto 2013.
- [75] Yanyan Chen, Michael G. H. Bell, Dongzhu Wang, and Klaus Bogenberger. Risk-averse time-dependent route guidance by constrained dynamic a* search in decentralized system architecture. *Transportation Research Record*, 1944(1):51–57, 2006.
- [76] Yunyue He, Zhong Liu, Jianmai Shi, Yishan Wang, Jiaming Zhang, and Jinyuan Liu. K-shortest-path-based evacuation routing with police resource allocation in city transportation networks. *PLOS ONE*, 10(7):1–23, 07 2015.
- [77] Paul Johnson, Duc Nguyen, and ManWo Ng. Large-scale network partitioning for decentralized traffic management and other transportation applications. *Journal of Intelligent Transportation Systems*, 20(5):461–473, 2016.
- [78] Alireza Mostafizi, Charles Koll, and Haizhong Wang. A decentralized and coordinated routing algorithm for connected and autonomous vehicles. *IEEE Transactions on Intelligent Transportation Systems*, pages 1–13, 2021.

- [79] M.L. Fredman and R.E. Tarjan. Fibonacci heaps and their uses in improved network optimization algorithms. In *25th Annual Symposium on Foundations of Computer Science, 1984.*, pages 338–346, 1984.
- [80] Janusz Gajda, Ryszard Sroka, Marek Stencel, Andrzej Wajda, and Tadeusz Zeglen. A vehicle classification based on inductive loop detectors. In *IMTC 2001. Proceedings of the 18th IEEE Instrumentation and Measurement Technology Conference. Rediscovering Measurement in the Age of Informatics (Cat. No. 01CH 37188)*, volume 1, pages 460–464. IEEE, 2001.
- [81] Andreas Buchenscheit, Florian Schaub, Frank Kargl, and Michael Weber. A vanet-based emergency vehicle warning system. In *2009 IEEE Vehicular Networking Conference (VNC)*, pages 1–8. IEEE, 2009.
- [82] Yinsong Wang, Zhizhou Wu, Xiaoguang Yang, and Luoyi Huang. Design and implementation of an emergency vehicle signal preemption system based on cooperative vehicle-infrastructure technology. *Advances in Mechanical Engineering*, 5:834976, 2013.
- [83] Hamed Noori, Liping Fu, and Sajad Shiravi. A connected vehicle based traffic signal control strategy for emergency vehicle preemption. In *Transportation Research Board 95th Annual Meeting*, pages 16–6763, 2016.
- [84] Jakob Foerster, Nantas Nardelli, Gregory Farquhar, Triantafyllos Afouras, Philip HS Torr, Pushmeet Kohli, and Shimon Whiteson. Stabilising experience replay for deep multi-agent reinforcement learning. In *International conference on machine learning*, pages 1146–1155. PMLR, 2017.

- [85] Pablo Alvarez Lopez, Michael Behrisch, Laura Bieker-Walz, Jakob Erdmann, Yun-Pang Flötteröd, Robert Hilbrich, Leonhard Lücken, Johannes Rummel, Peter Wagner, and Evamarie Wießner. Microscopic traffic simulation using sumo. In *2018 21st International Conference on Intelligent Transportation Systems (ITSC)*, pages 2575–2582. IEEE, 2018.
- [86] German Aerospace Center. Sumo sublane model. <https://sumo.dlr.de/docs/Simulation/SublaneModel.html>, 2022.
- [87] German Aerospace Center. Sumo emergency vehicle simulation. <https://sumo.dlr.de/docs/Simulation/Emergency.html>, 2022.
- [88] Chacha Chen. Synthesized Hangzhou Dataset, howpublished=https://github.com/traffic-signal-control/sample-code/tree/master/data/hangzhou_4x4_gudang_18041610_1h.
- [89] Francesco Corman, Andrea D’Ariano, Dario Pacciarelli, and Marco Pranzo. Evaluation of green wave policy in real-time railway traffic management. *Transportation Research Part C: Emerging Technologies*, 17(6):607–616, 2009.
- [90] Roger P Roess, Elena S Prassas, and William R McShane. *Traffic engineering*. Pearson/Prentice Hall, 2004.
- [91] New York City Government. *New York End-To-End Response Times*, 2019.
- [92] New York City Government. *Emergency Response Incidents*, 2014.
- [93] Rich Calder. Nyc response times to fires, medical emergencies soaring - along with fire deaths, 9 2023.

- [94] Guangwei Zhou and Albert Gan. Performance of transit signal priority with queue jumper lanes. *Transportation Research Record*, 1925(1):265–271, 2005.
- [95] Burak Cesme, Selman Z Altun, and Barrett Lane. Queue jump lane, transit signal priority, and stop location evaluation of transit preferential treatments using microsimulation. *Transportation Research Record*, 2533(1):39–49, 2015.
- [96] Chenyu You, Guang Li, Yi Zhang, Xiaoliu Zhang, Hongming Shan, Mengzhou Li, Shenghong Ju, Zhen Zhao, Zhuiyang Zhang, Wenxiang Cong, et al. Ct super-resolution gan constrained by the identical, residual, and cycle learning ensemble (gan-circle). *IEEE transactions on medical imaging*, 39(1):188–203, 2019.
- [97] Chenyu You, Qingsong Yang, Hongming Shan, Lars Gjestebj, Guang Li, Shenghong Ju, Zhuiyang Zhang, Zhen Zhao, Yi Zhang, Wenxiang Cong, et al. Structurally-sensitive multi-scale deep neural network for low-dose ct denoising. *IEEE access*, 6:41839–41855, 2018.
- [98] Qing Lyu, Chenyu You, Hongming Shan, and Ge Wang. Super-resolution mri through deep learning. *arXiv preprint arXiv:1810.06776*, 2018.
- [99] Qing Lyu, Chenyu You, Hongming Shan, Yi Zhang, and Ge Wang. Super-resolution mri and ct through gan-circle. In *Developments in X-ray tomography XII*, volume 11113, pages 202–208. SPIE, 2019.
- [100] Chenyu You, Linfeng Yang, Yi Zhang, and Ge Wang. Low-dose ct via deep cnn with skip connection and network-in-network. In *Developments in X-Ray tomography XII*, volume 11113, pages 429–434. SPIE, 2019.
- [101] Chenyu You, Junlin Yang, Julius Chapiro, and James S Duncan. Unsupervised wasserstein distance guided domain adaptation for 3d multi-domain liver segmen-

- tation. In *Interpretable and Annotation-Efficient Learning for Medical Image Computing: Third International Workshop, IMIMIC 2020, Second International Workshop, MIL3ID 2020, and 5th International Workshop, LABELS 2020, Held in Conjunction with MICCAI 2020, Lima, Peru, October 4–8, 2020, Proceedings 3*, pages 155–163. Springer, 2020.
- [102] Indranil Guha, Syed Ahmed Nadeem, Chenyu You, Xiaoliu Zhang, Steven M Levy, Ge Wang, James C Torner, and Punam K Saha. Deep learning based high-resolution reconstruction of trabecular bone microstructures from low-resolution ct scans using gan-circle. In *Medical imaging 2020: biomedical applications in molecular, structural, and functional imaging*, volume 11317, pages 204–214. SPIE, 2020.
- [103] Long Cheng, Chenyu You, Yani Guan, and Yiyi Yu. Body activity recognition using wearable sensors. In *2017 Computing Conference*, pages 756–765. IEEE, 2017.
- [104] Long Cheng and Chenyu You. Hybrid non-linear dimensionality reduction method framework based on random projections. In *2016 IEEE International Conference on Cloud Computing and Big Data Analysis (ICCCBDA)*, pages 43–48. IEEE, 2016.
- [105] Nuo Chen, Fenglin Liu, Chenyu You, Peilin Zhou, and Yuexian Zou. Adaptive bi-directional attention: Exploring multi-granularity representations for machine reading comprehension. In *ICASSP 2021-2021 IEEE International Conference on Acoustics, Speech and Signal Processing (ICASSP)*, pages 7833–7837. IEEE, 2021.

- [106] Chenyu You, Nuo Chen, and Yuexian Zou. Mrd-net: Multi-modal residual knowledge distillation for spoken question answering. In *IJCAI*, pages 3985–3991, 2021.
- [107] Fenglin Liu, Xian Wu, Chenyu You, Shen Ge, Yuexian Zou, and Xu Sun. Aligning source visual and target language domains for unpaired video captioning. *IEEE Transactions on Pattern Analysis and Machine Intelligence*, 44(12):9255–9268, 2021.
- [108] Long Cheng, Chenyu You, and Liguo Chen. Identification of power line outages based on pmu measurements and sparse overcomplete representation. In *2016 IEEE 17th International Conference on Information Reuse and Integration (IRI)*, pages 343–349. IEEE, 2016.
- [109] Long Cheng, Chenyu You, and Yani Guan. Random projections for non-linear dimensionality reduction. *International Journal of Machine Learning and Computing*, 6(4):220–225, 2016.
- [110] Guang Li, Shouhua Luo, Chenyu You, Matthew Getzin, Liang Zheng, Ge Wang, and Ning Gu. A novel calibration method incorporating nonlinear optimization and ball-bearing markers for cone-beam ct with a parameterized trajectory. *Medical physics*, 46(1):152–164, 2019.
- [111] Peter T. Savolainen, Tapan K. Datta, Indrajit Ghosh, and Timothy J. Gates. Effects of dynamically activated emergency vehicle warning sign on driver behavior at urban intersections. *Transportation Research Record*, 2149(1):77–83, 2010.
- [112] Jamal Nahofti Kohneh, Pamela Murray-Tuite, Thidapat Chantem, and Ryan Gerdes. A connected emergency response system to facilitate the movement

- of multiple emergency response vehicles through two-way roadways. *Journal of Transportation Engineering, Part A: Systems*, 150(5):04024019, 2024.
- [113] Jiaming Wu, Balázs Kulcsár, Soyoungh Ahn, and Xiaobo Qu. Emergency vehicle lane pre-clearing: From microscopic cooperation to routing decision making. *Transportation Research Part B: Methodological*, 141:223–239, 2020.
- [114] Fenglin Liu, Chenyu You, Xian Wu, Shen Ge, Xu Sun, et al. Auto-encoding knowledge graph for unsupervised medical report generation. *Advances in Neural Information Processing Systems*, 34:16266–16279, 2021.
- [115] Chenyu You, Lianyi Han, Aosong Feng, Ruihan Zhao, Hui Tang, and Wei Fan. Megan: memory enhanced graph attention network for space-time video super-resolution. In *Proceedings of the IEEE/CVF winter conference on applications of computer vision*, pages 1401–1411, 2022.
- [116] Fenglin Liu, Bang Yang, Chenyu You, Xian Wu, Shen Ge, Zhangdaihong Liu, Xu Sun, Yang Yang, and David Clifton. Retrieve, reason, and refine: Generating accurate and faithful patient instructions. *Advances in Neural Information Processing Systems*, 35:18864–18877, 2022.
- [117] Dajiang Suo, Vindula Jayawardana, and Cathy Wu. Model-free learning of corridor clearance: A near-term deployment perspective. *IEEE Transactions on Intelligent Transportation Systems*, 2024.
- [118] Fenglin Liu, Xuancheng Ren, Guangxiang Zhao, Chenyu You, Xuwei Ma, Xian Wu, and Xu Sun. Rethinking and improving natural language generation with layer-wise multi-view decoding. *arXiv preprint arXiv:2005.08081*, 2020.

- [119] Hongjian Zhou, Fenglin Liu, Boyang Gu, Xinyu Zou, Jinfa Huang, Jinge Wu, Yiru Li, Sam S Chen, Peilin Zhou, Junling Liu, et al. A survey of large language models in medicine: Progress, application, and challenge. *arXiv preprint arXiv:2311.05112*, 2023.
- [120] John Anderson Garcia Henao, Arno Depotter, Danielle V Bower, Herkus Bajercius, Plamena Teodosieva Todorova, Hugo Saint-James, Aurélie Pahud de Mortanges, Maria Cecilia Barroso, Jianchun He, Junlin Yang, et al. A multiclass radiomics method-based who severity scale for improving covid-19 patient assessment and disease characterization from ct scans. *Investigative radiology*, 58(12):882–893, 2023.
- [121] Fenglin Liu, Tingting Zhu, Xian Wu, Bang Yang, Chenyu You, Chenyang Wang, Lei Lu, Zhangdaihong Liu, Yefeng Zheng, Xu Sun, et al. A medical multimodal large language model for future pandemics. *NPJ Digital Medicine*, 6(1):226, 2023.
- [122] Zhuotong Cai, Jingmin Xin, Siyuan Dong, Chenyu You, Peiwen Shi, Tianyi Zeng, Jiazhen Zhang, John A Onofrey, Nanning Zheng, and James S Duncan. Unsupervised domain adaptation by cross-prototype contrastive learning for medical image segmentation. In *2023 IEEE International Conference on Bioinformatics and Biomedicine (BIBM)*, pages 819–824. IEEE, 2023.
- [123] Paul Young Joun Ha, Sikai Chen, Jiqian Dong, Runjia Du, Yujie Li, and Samuel Labi. Leveraging the capabilities of connected and autonomous vehicles and multi-agent reinforcement learning to mitigate highway bottleneck congestion. *arXiv preprint arXiv:2010.05436*, 2020.

- [124] Sai Krishna Sumanth Nakka, Behdad Chalaki, and Andreas A. Malikopoulos. A multi-agent deep reinforcement learning coordination framework for connected and automated vehicles at merging roadways. In *2022 American Control Conference (ACC)*, pages 3297–3302, 2022.
- [125] Chenyu You, Weicheng Dai, Yifei Min, Fenglin Liu, David Clifton, S Kevin Zhou, Lawrence Staib, and James Duncan. Rethinking semi-supervised medical image segmentation: A variance-reduction perspective. *Advances in neural information processing systems*, 36:9984–10021, 2023.
- [126] Junling Liu, Peilin Zhou, Yining Hua, Dading Chong, Zhongyu Tian, Andrew Liu, Helin Wang, Chenyu You, Zhenhua Guo, Lei Zhu, et al. Benchmarking large language models on cmexam-a comprehensive chinese medical exam dataset. *Advances in Neural Information Processing Systems*, 36:52430–52452, 2023.
- [127] Xiangyi Yan, Shanlin Sun, Kun Han, Thanh-Tung Le, Haoyu Ma, Chenyu You, and Xiaohui Xie. After-sam: Adapting sam with axial fusion transformer for medical imaging segmentation. In *Proceedings of the IEEE/CVF Winter Conference on Applications of Computer Vision*, pages 7975–7984, 2024.
- [128] Kun Han, Shanlin Sun, Thanh-Tung Le, Xiangyi Yan, Haoyu Ma, Chenyu You, and Xiaohui Xie. Hybrid neural diffeomorphic flow for shape representation and generation via triplane. In *Proceedings of the IEEE/CVF Winter Conference on Applications of Computer Vision*, pages 7707–7717, 2024.
- [129] Jun Ma, Yuting He, Feifei Li, Lin Han, Chenyu You, and Bo Wang. Segment anything in medical images. *Nature Communications*, 15(1):654, 2024.

- [130] Zihan Guo, Yan Wu, Lifang Wang, and Junzhi Zhang. Coordination for connected and automated vehicles at non-signalized intersections: A value decomposition-based multiagent deep reinforcement learning approach. *IEEE Transactions on Vehicular Technology*, 72(3):3025–3034, 2022.
- [131] Guillen-Perez Antonio and Cano Maria-Dolores. Multi-agent deep reinforcement learning to manage connected autonomous vehicles at tomorrow’s intersections. *IEEE Transactions on Vehicular Technology*, 71(7):7033–7043, 2022.
- [132] Wei Zhou, Dong Chen, Jun Yan, Zhaojian Li, Huilin Yin, and Wanchen Ge. Multi-agent reinforcement learning for cooperative lane changing of connected and autonomous vehicles in mixed traffic. *Autonomous Intelligent Systems*, 2(1):5, 2022.
- [133] Haotian Shi, Yang Zhou, Keshu Wu, Xin Wang, Yangxin Lin, and Bin Ran. Connected automated vehicle cooperative control with a deep reinforcement learning approach in a mixed traffic environment. *Transportation Research Part C: Emerging Technologies*, 133:103421, 2021.
- [134] Dong Chen, Mohammad R. Hajidavalloo, Zhaojian Li, Kaian Chen, Yongqiang Wang, Longsheng Jiang, and Yue Wang. Deep multi-agent reinforcement learning for highway on-ramp merging in mixed traffic. *IEEE Transactions on Intelligent Transportation Systems*, 24(11):11623–11638, 2023.
- [135] Qinghao Liang, Rongtao Jiang, Brendan D Adkinson, Matthew Rosenblatt, Saloni Mehta, Maya L Foster, Siyuan Dong, Chenyu You, Sahand Negahban, Harrison H Zhou, et al. Rescuing missing data in connectome-based predictive modeling. *Imaging Neuroscience*, 2:1–16, 2024.

- [136] Yuwei Cao, Hao Peng, Angsheng Li, Chenyu You, Zhifeng Hao, and Philip S Yu. Multi-relational structural entropy. *arXiv preprint arXiv:2405.07096*, 2024.
- [137] Chenyu You, Yifei Mint, Weicheng Dai, Jasjeet S Sekhon, Lawrence Staib, and James S Duncan. Calibrating multi-modal representations: A pursuit of group robustness without annotations. In *2024 IEEE/CVF Conference on Computer Vision and Pattern Recognition (CVPR)*, pages 26140–26150. IEEE, 2024.
- [138] Xinyuan Zhang, Cong Zhao, Feixiong Liao, Xinghua Li, and Yuchuan Du. Online parking assignment in an environment of partially connected vehicles: A multi-agent deep reinforcement learning approach. *Transportation Research Part C: Emerging Technologies*, 138:103624, 2022.
- [139] Praveen Palanisamy. Multi-agent connected autonomous driving using deep reinforcement learning. In *2020 International Joint Conference on Neural Networks (IJCNN)*, pages 1–7, 2020.
- [140] Leandro Parada, Eduardo Candela, Luis Marques, and Panagiotis Angeloudis. Safe and efficient manoeuvring for emergency vehicles in autonomous traffic using multi-agent proximal policy optimisation. *Transportmetrica A: Transport Science*, pages 1–29, 2023.
- [141] Chenyu You, Weicheng Dai, Fenglin Liu, Yifei Min, Nicha C Dvornek, Xiaoxiao Li, David A Clifton, Lawrence Staib, and James S Duncan. Mine your own anatomy: Revisiting medical image segmentation with extremely limited labels. *IEEE Transactions on Pattern Analysis and Machine Intelligence*, 2024.

- [142] Shanlin Sun, Kun Han, Chenyu You, Hao Tang, Deying Kong, Junayed Naushad, Xiangyi Yan, Haoyu Ma, Pooya Khosravi, James S Duncan, et al. Medical image registration via neural fields. *Medical Image Analysis*, 97:103249, 2024.
- [143] Xiaoshuang Huang, Hongxiang Li, Meng Cao, Long Chen, Chenyu You, and Dong An. Cross-modal conditioned reconstruction for language-guided medical image segmentation. *IEEE Transactions on Medical Imaging*, 2024.
- [144] Pamul Yadav, Ashutosh Mishra, and Shiho Kim. A comprehensive survey on multi-agent reinforcement learning for connected and automated vehicles. *Sensors*, 23(10):4710, 2023.
- [145] Joris Dinneweth, Abderrahmane Boubezoul, René Mandiau, and Stéphane Espié. Multi-agent reinforcement learning for autonomous vehicles: a survey. *Autonomous Intelligent Systems*, 2(1):27, 11 2022.
- [146] John Schulman, Filip Wolski, Prafulla Dhariwal, Alec Radford, and Oleg Klimov. Proximal policy optimization algorithms. *arXiv preprint arXiv:1707.06347*, 2017.
- [147] Chao Yu, Akash Velu, Eugene Vinitzky, Jiaxuan Gao, Yu Wang, Alexandre Bayen, and Yi Wu. The surprising effectiveness of ppo in cooperative multi-agent games. *Advances in Neural Information Processing Systems*, 35:24611–24624, 2022.
- [148] A Vaswani. Attention is all you need. *Advances in Neural Information Processing Systems*, 2017.
- [149] Emilio Parisotto, Francis Song, Jack Rae, Razvan Pascanu, Caglar Gulcehre, Siddhant Jayakumar, Max Jaderberg, Raphael Lopez Kaufman, Aidan Clark, Seb Noury, et al. Stabilizing transformers for reinforcement learning. In *International conference on machine learning*, pages 7487–7498. PMLR, 2020.

- [150] Lili Chen, Kevin Lu, Aravind Rajeswaran, Kimin Lee, Aditya Grover, Misha Laskin, Pieter Abbeel, Aravind Srinivas, and Igor Mordatch. Decision transformer: Reinforcement learning via sequence modeling. *Advances in neural information processing systems*, 34:15084–15097, 2021.
- [151] New York City Department of Transportation. New york city mobility report, 2019.
- [152] Cathy Wu, Aboudy Kreidieh, Kanaad Parvate, Eugene Vinitsky, and Alexandre M Bayen. Flow: Architecture and benchmarking for reinforcement learning in traffic control. *arXiv preprint arXiv:1710.05465*, 10, 2017.
- [153] Arian Houshmand, Salomón Wollenstein-Betech, and Christos G. Cassandras. The penetration rate effect of connected and automated vehicles in mixed traffic routing. In *2019 IEEE Intelligent Transportation Systems Conference (ITSC)*, pages 1755–1760, 2019.
- [154] Jishi Yu Ding, Huei Peng, Yi Zhang, and Li Li. Penetration effect of connected and automated vehicles on cooperative on-ramp merging. *IET Intelligent Transport Systems*, 14(1):56–64, 2020.
- [155] Juan Argote-Cabañero, Eleni Christofa, and Alexander Skabardonis. Connected vehicle penetration rate for estimation of arterial measures of effectiveness. *Transportation Research Part C: Emerging Technologies*, 60:298–312, 2015.
- [156] Zhiyuan Du, Baisravan HomChaudhuri, and Pierluigi Pisu. Coordination strategy for vehicles passing multiple signalized intersections: A connected vehicle penetration rate study. In *2017 American control conference (ACC)*, pages 4952–4957. IEEE, 2017.

- [157] Bidoura Khondaker and Lina Kattan. Variable speed limit: A microscopic analysis in a connected vehicle environment. *Transportation Research Part C: Emerging Technologies*, 58:146–159, 2015.
- [158] Raphael E Stern, Shumo Cui, Maria Laura Delle Monache, Raktim Bhadani, Michael Bunting, Miles Churchill, Nathan Hamilton, Hannah Pohlmann, Fang-Chieh Wu, Benedetto Piccoli, and Daniel B Work. Dissipation of stop-and-go waves via control of autonomous vehicles: Field experiments. *Transportation Research Part C: Emerging Technologies*, 89:205–221, 2018.
- [159] Meng Wang, Winnie Daamen, Serge P Hoogendoorn, and Bart Van Arem. Rolling horizon control framework for driver assistance systems. part i: Mathematical formulation and non-cooperative systems. *Transportation Research Part C: Emerging Technologies*, 59:597–615, 2015.
- [160] Shanshan Feng, Shanbao Bao, and Henry X Liu. How do the benefits of automated vehicles vary across different traffic conditions? *Journal of Intelligent Transportation Systems*, 25(2):169–183, 2021.
- [161] Thomas H Blackwell and Jay S Kaufman. Response time effectiveness: comparison of response time and survival in an urban emergency medical services system. *Academic Emergency Medicine*, 9(4):288–295, 2002.
- [162] Hannah Schuster, Axel Polleres, and Johannes Wachs. Stress-testing road networks and access to medical care. *Transportation Research Part A: Policy and Practice*, 181:104017, 2024.
- [163] Henrik Jaldell. How important is the time factor? saving lives using fire and rescue services. *Fire technology*, 53(2):695–708, 2017.

- [164] Neil Challands. The relationships between fire service response time and fire outcomes. *Fire technology*, 46(3):665–676, 2010.
- [165] Jordi Blanes i Vidal and Tom Kirchmaier. The effect of police response time on crime clearance rates. *The Review of Economic Studies*, 85(2):855–891, 2018.
- [166] Leila Merrill. Don't get sick or injured: Report finds nyc response times hit record high, 2024. Accessed: 2024-10-09.
- [167] Emily Crane. Nyc response times to fires, medical emergencies soaring, 2023. Accessed: 2024-10-09.
- [168] Sukhwan Chung, Madison Smith, Andrew Jin, Luke Hogewood, Maksim Kitsak, Jeffrey Cegan, and Igor Linkov. Access to emergency services: A new york city case study. *Transportation Research Interdisciplinary Perspectives*, 25:101111, 2024.
- [169] Haoran Su, Yaofeng D Zhong, Joseph YJ Chow, Biswadip Dey, and Li Jin. Emv-light: A multi-agent reinforcement learning framework for an emergency vehicle decentralized routing and traffic signal control system. *Transportation Research Part C: Emerging Technologies*, 146:103955, 2023.
- [170] Linfeng Yang, Rajarshi P Ghosh, J Matthew Franklin, Simon Chen, Chenyu You, Raja R Narayan, Marc L Melcher, and Jan T Liphardt. Nuset: A deep learning tool for reliably separating and analyzing crowded cells. *PLoS computational biology*, 16(9):e1008193, 2020.
- [171] Haoyu Ma, Tianlong Chen, Ting-Kuei Hu, Chenyu You, Xiaohui Xie, and Zhangyang Wang. Undistillable: Making a nasty teacher that cannot teach students. *arXiv preprint arXiv:2105.07381*, 2021.

- [172] Haoyu Ma, Tianlong Chen, Ting-Kuei Hu, Chenyu You, Xiaohui Xie, and Zhangyang Wang. Good students play big lottery better. *arXiv preprint arXiv:2101.03255*, 3:4, 2021.
- [173] Chenyu You, Nuo Chen, Fenglin Liu, Dongchao Yang, and Yuexian Zou. Towards data distillation for end-to-end spoken conversational question answering. *arXiv preprint arXiv:2010.08923*, 2020.
- [174] Chenyu You, Nuo Chen, and Yuexian Zou. Contextualized attention-based knowledge transfer for spoken conversational question answering. *arXiv preprint arXiv:2010.11066*, 2020.
- [175] Weiyuan Xu, Peilin Zhou, Chenyu You, and Yuexian Zou. Semantic transportation prototypical network for few-shot intent detection. In *Interspeech*, pages 251–255, 2021.
- [176] David C Novak and James L Sullivan. A link-focused methodology for evaluating accessibility to emergency services. *Decision Support Systems*, 57:309–319, 2014.
- [177] Tianqi Xia, Xuan Song, Haoran Zhang, Xiaoya Song, Hiroshi Kanasugi, and Ryosuke Shibasaki. Measuring spatio-temporal accessibility to emergency medical services through big gps data. *Health & place*, 56:53–62, 2019.
- [178] Chenyu You, Qiwen Wang, and Chao Sun. sbilsan: Stacked bidirectional self-attention lstm network for anomaly detection and diagnosis from system logs. In *Intelligent Systems and Applications: Proceedings of the 2021 Intelligent Systems Conference (IntelliSys) Volume 3*, pages 777–793. Springer, 2022.
- [179] Haoyu Ma, Yifan Huang, Hao Tang, Chenyu You, Deying Kong, and Xiaohui Xie. Sparse logits suffice to fail knowledge distillation. In *ICLR 2022 Workshop on*

PAIR²Struct: Privacy, Accountability, Interpretability, Robustness, Reasoning on Structured Data, 2022.

- [180] Aosong Feng, Chenyu You, Shiqiang Wang, and Leandros Tassioulas. Kergnns: Interpretable graph neural networks with graph kernels. In *Proceedings of the AAAI conference on artificial intelligence*, volume 36, pages 6614–6622, 2022.
- [181] Gavin Tansley, Nadine Schuurman, Ofer Amram, and Natalie Yanchar. Spatial access to emergency services in low-and middle-income countries: a gis-based analysis. *PloS one*, 10(11):e0141113, 2015.
- [182] Soheil Hashtarkhani, Behzad Kiani, Robert Bergquist, Nasser Bagheri, Reza VafaeiNejad, and Mahmood Tara. An age-integrated approach to improve measurement of potential spatial accessibility to emergency medical services for urban areas. *The International journal of health planning and management*, 35(3):788–798, 2020.
- [183] Shakil Ahmed, Alayne M Adams, Rubana Islam, Shaikh Mehdi Hasan, and Rocco Panciera. Impact of traffic variability on geographic accessibility to 24/7 emergency healthcare for the urban poor: a gis study in dhaka, bangladesh. *PloS one*, 14(9):e0222488, 2019.
- [184] Nuo Chen, Chenyu You, and Yuexian Zou. Self-supervised dialogue learning for spoken conversational question answering. *arXiv preprint arXiv:2106.02182*, 2021.
- [185] Chenyu You, Nuo Chen, and Yuexian Zou. Knowledge distillation for improved accuracy in spoken question answering. In *ICASSP 2021-2021 IEEE International*

Conference on Acoustics, Speech and Signal Processing (ICASSP), pages 7793–7797. IEEE, 2021.

- [186] Haoyu Ma, Yifan Huang, Tianlong Chen, Hao Tang, Chenyu You, Zhangyang Wang, and Xiaohui Xie. Stingy teacher: Sparse logits suffice to fail knowledge distillation, 2022.
- [187] Daniel Green, Dapeng Yu, Ian Pattison, Robert Wilby, Lee Boshier, Ramila Patel, Philip Thompson, Keith Trowell, Julia Draycon, Martin Halse, et al. City-scale accessibility of emergency responders operating during flood events. *Natural Hazards and Earth System Sciences*, 17(1):1–16, 2017.
- [188] Jie Yin, Dapeng Yu, Ning Lin, and Robert L Wilby. Evaluating the cascading impacts of sea level rise and coastal flooding on emergency response spatial accessibility in lower manhattan, new york city. *Journal of Hydrology*, 555:648–658, 2017.
- [189] Raffaele Albano, Aurelia Sole, J Adamowski, and L Mancusi. A gis-based model to estimate flood consequences and the degree of accessibility and operability of strategic emergency response structures in urban areas. *Natural Hazards and Earth System Sciences*, 14(11):2847–2865, 2014.
- [190] Chenyu You, Ruihan Zhao, Fenglin Liu, Siyuan Dong, Sandeep Chinchali, Ufuk Topcu, Lawrence Staib, and James Duncan. Class-aware adversarial transformers for medical image segmentation. *Advances in neural information processing systems*, 35:29582–29596, 2022.

- [191] Chenyu You, Nuo Chen, Fenglin Liu, Shen Ge, Xian Wu, and Yuexian Zou. End-to-end spoken conversational question answering: Task, dataset and model. *arXiv preprint arXiv:2204.14272*, 2022.
- [192] Chenyu You, Yuan Zhou, Ruihan Zhao, Lawrence Staib, and James S Duncan. Sim-cvd: Simple contrastive voxel-wise representation distillation for semi-supervised medical image segmentation. *IEEE Transactions on Medical Imaging*, 41(9):2228–2237, 2022.
- [193] Weicong Luo, Jing Yao, Richard Mitchell, Xiaoxiang Zhang, and Wenqiang Li. Locating emergency medical services to reduce urban-rural inequalities. *Socio-Economic Planning Sciences*, 84:101416, 2022.
- [194] Brendan G Carr, Charles C Branas, Joshua P Metlay, Ashley F Sullivan, and Carlos A Camargo Jr. Access to emergency care in the united states. *Annals of emergency medicine*, 54(2):261–269, 2009.
- [195] Juan Holguin, Diego Escobar, and Carlos Moncada. Access to emergency medical services: an urban planning methodology for the generation of equity. *Global Journal of Health Science*, 10(6):181, 2018.
- [196] Wenyan Hu, Jinkai Tan, Mengya Li, Jun Wang, and Fahui Wang. Impact of traffic on the spatiotemporal variations of spatial accessibility of emergency medical services in inner-city shanghai. *Environment and Planning B: Urban Analytics and City Science*, 47(5):841–854, 2020.
- [197] Yong Shi, Qian Yao, Jiahong Wen, Jianchao Xi, Hai Li, and Qingwei Wang. A spatial accessibility assessment of urban tourist attractions emergency response in shanghai. *International Journal of Disaster Risk Reduction*, 74:102919, 2022.

- [198] Kun Han, Yifeng Xiong, Chenyu You, Pooya Khosravi, Shanlin Sun, Xiangyi Yan, James S Duncan, and Xiaohui Xie. Medgen3d: A deep generative framework for paired 3d image and mask generation. In *International Conference on Medical Image Computing and Computer-Assisted Intervention*, pages 759–769. Springer, 2023.
- [199] Zhuotong Cai, Tianyi Zeng, Eléonore V Lieffrig, Jiazhen Zhang, Fuyao Chen, Takuya Toyonaga, Chenyu You, Jingmin Xin, Nanning Zheng, Yihuan Lu, et al. Cross-attention for improved motion correction in brain pet. In *International Workshop on Machine Learning in Clinical Neuroimaging*, pages 34–45. Springer, 2023.
- [200] Tianyi Zeng, Jiazhen Zhang, Eléonore V Lieffrig, Zhuotong Cai, Fuyao Chen, Chenyu You, Mika Naganawa, Yihuan Lu, and John A Onofrey. Fast reconstruction for deep learning pet head motion correction. In *International Conference on Medical Image Computing and Computer-Assisted Intervention*, pages 710–719. Springer, 2023.
- [201] Chenyu You, Weicheng Dai, Yifei Min, Lawrence Staib, and James S Duncan. Implicit anatomical rendering for medical image segmentation with stochastic experts. In *International Conference on Medical Image Computing and Computer-Assisted Intervention*, pages 561–571. Springer, 2023.
- [202] Jun Ma, Yuanzhi Zhu, Chenyu You, and Bo Wang. Pre-trained diffusion models for plug-and-play medical image enhancement. In *International Conference on Medical Image Computing and Computer-Assisted Intervention*, pages 3–13. Springer, 2023.

- [203] Chenyu You, Weicheng Dai, Yifei Min, Lawrence Staib, Jas Sekhon, and James S Duncan. Action++: Improving semi-supervised medical image segmentation with adaptive anatomical contrast. In *International Conference on Medical Image Computing and Computer-Assisted Intervention*, pages 194–205. Springer, 2023.
- [204] Reid Ewing and Robert Cervero. Travel and the built environment: A meta-analysis. *Journal of the American Planning Association*, 76(3):265–294, 2010.
- [205] Marwan Salim Mahmood Al-Dabbagh, Ali Al-Sherbaz, and Scott Turner. The impact of road intersection topology on traffic congestion in urban cities. In *Intelligent Systems and Applications: Proceedings of the 2018 Intelligent Systems Conference (IntelliSys) Volume 1*, pages 1196–1207. Springer, 2019.
- [206] Transportation Research Board. *Highway Capacity Manual*. National Research Council, Washington, D.C., 2010.
- [207] Fenglin Liu, Bang Yang, Chenyu You, Xian Wu, Shen Ge, Zhangdaihong Liu, Xu Sun, Yang Yang, and David A Clifton. Retrieval-augmented and knowledge-grounded language models for faithful clinical medicine. *arXiv preprint arXiv:2210.12777*, 2022.
- [208] Fenglin Liu, Bang Yang, Chenyu You, Xian Wu, Shen Ge, Adelaide Woicik, and Sheng Wang. Graph-in-graph network for automatic gene ontology description generation. In *Proceedings of the 28th ACM SIGKDD Conference on Knowledge Discovery and Data Mining*, pages 1060–1068, 2022.
- [209] Nuo Chen and Chenyu You. Exploring and exploiting multi-granularity representations for machine reading comprehension. *arXiv preprint arXiv:2208.08750*, 2022.

- [210] Chenyu You, Ruihan Zhao, Lawrence H Staib, and James S Duncan. Momentum contrastive voxel-wise representation learning for semi-supervised volumetric medical image segmentation. In *International Conference on Medical Image Computing and Computer-Assisted Intervention*, pages 639–652. Springer, 2022.
- [211] Wei Feng, Miguel Figliozzi, and Robert L Bertini. Quantifying the joint impacts of stop locations, signalized intersections, and traffic conditions on bus travel time. *Public Transport*, 7:391–408, 2015.
- [212] Jillian Strauss and Luis F Miranda-Moreno. Speed, travel time and delay for intersections and road segments in the montreal network using cyclist smartphone gps data. *Transportation research part D: transport and environment*, 57:155–171, 2017.
- [213] SeJoon Park, Amirali Saeedi, David S Kim, and J David Porter. Measuring intersection performance from bluetooth-based data utilized for travel time data collection. *Journal of Transportation Engineering*, 142(5):04016014, 2016.
- [214] Vladimir Ivanov, Vitaly Silyanov, and Grigory Kramarev. Assessing the traffic capacity of urban road intersections. *Frontiers in Built Environment*, 8:968846, 2022.
- [215] Kun Han, Shanlin Sun, Xiangyi Yan, Chenyu You, Hao Tang, Junayed Naushad, Haoyu Ma, Deying Kong, and Xiaohui Xie. Diffeomorphic image registration with neural velocity field. In *Proceedings of the IEEE/CVF Winter Conference on Applications of Computer Vision*, pages 1869–1879, 2023.
- [216] Xiangyi Yan, Junayed Naushad, Shanlin Sun, Kun Han, Hao Tang, Deying Kong, Haoyu Ma, Chenyu You, and Xiaohui Xie. Representation recovering for self-

- supervised pre-training on medical images. In *Proceedings of the IEEE/CVF winter conference on applications of computer vision*, pages 2685–2695, 2023.
- [217] Nuo Chen, Linjun Shou, Ming Gong, Jian Pei, Chenyu You, Jianhui Chang, Daxin Jiang, and Jia Li. Bridge the gap between language models and tabular understanding. *arXiv preprint arXiv:2302.09302*, 2023.
- [218] Siyuan Dong, Gilbert Hangel, Wolfgang Bogner, Georg Widhalm, Karl Rössler, Siegfried Trattig, Chenyu You, Robin de Graaf, John A Onofrey, and James S Duncan. Multi-scale super-resolution magnetic resonance spectroscopic imaging with adjustable sharpness. In *International Conference on Medical Image Computing and Computer-Assisted Intervention*, pages 410–420. Springer, 2022.
- [219] Chenyu You, Jinlin Xiang, Kun Su, Xiaoran Zhang, Siyuan Dong, John Onofrey, Lawrence Staib, and James S Duncan. Incremental learning meets transfer learning: Application to multi-site prostate mri segmentation. In *International Workshop on Distributed, Collaborative, and Federated Learning*, pages 3–16. Springer, 2022.
- [220] Siyuan Dong, Gilbert Hangel, Eric Z Chen, Shanhui Sun, Wolfgang Bogner, Georg Widhalm, Chenyu You, John A Onofrey, Robin de Graaf, and James S Duncan. Flow-based visual quality enhancer for super-resolution magnetic resonance spectroscopic imaging. In *MICCAI Workshop on Deep Generative Models*, pages 3–13. Springer, 2022.
- [221] Shanlin Sun, Thanh-Tung Le, Chenyu You, Hao Tang, Kun Han, Haoyu Ma, Deying Kong, Xiangyi Yan, and Xiaohui Xie. Hybrid-csr: Coupling explicit and implicit shape representation for cortical surface reconstruction. *arXiv preprint arXiv:2307.12299*, 2023.

- [222] Junling Liu, Chao Liu, Peilin Zhou, Qichen Ye, Dading Chong, Kang Zhou, Yueqi Xie, Yuwei Cao, Shoujin Wang, Chenyu You, et al. Llmrec: Benchmarking large language models on recommendation task. *arXiv preprint arXiv:2308.12241*, 2023.
- [223] Yuwei Cao, Liangwei Yang, Chen Wang, Zhiwei Liu, Hao Peng, Chenyu You, and Philip S Yu. Multi-task item-attribute graph pre-training for strict cold-start item recommendation. In *Proceedings of the 17th ACM Conference on Recommender Systems*, pages 322–333, 2023.
- [224] Suet-Ying Lam, Qingcheng Zeng, Kexun Zhang, Chenyu You, and Rob Voigt. Large language models are partially primed in pronoun interpretation. *arXiv preprint arXiv:2305.16917*, 2023.
- [225] Chenyu You, Weicheng Dai, Yifei Min, Lawrence Staib, and James S Duncan. Bootstrapping semi-supervised medical image segmentation with anatomical-aware contrastive distillation. In *International conference on information processing in medical imaging*, pages 641–653. Springer, 2023.
- [226] Bang Yang, Fenglin Liu, Zheng Li, Qingyu Yin, Chenyu You, Bing Yin, and Yuexian Zou. Multimodal prompt learning for product title generation with extremely limited labels. *arXiv preprint arXiv:2307.01969*, 2023.
- [227] Carl J Obeck. Traffic signal control for emergency vehicles, 5 1991. US Patent 5,014,052.
- [228] NMZ Hashim, AS Jaafar, NA Ali, L Salahuddin, NR Mohamad, and MA Ibrahim. Traffic light control system for emergency vehicles using radio frequency. *Traffic*, 3(7):43–52, 2013.

- [229] Shubhankar Vishwas Bhate, Prasad Vilas Kulkarni, Shubham Dhanaji Lagad, Mahesh Dnyaneshwar Shinde, and Shivprasad Patil. Iot based intelligent traffic signal system for emergency vehicles. In *2018 Second international conference on inventive communication and computational technologies (ICICCT)*, pages 788–793. IEEE, 2018.
- [230] R Shanmughasundaram, S Prasanna Vadanam, and Vivek Dharmarajan. Li-fi based automatic traffic signal control for emergency vehicles. In *2018 Second International Conference on Advances in Electronics, Computers and Communications (ICA ECC)*, pages 1–5. IEEE, 2018.
- [231] Guang Li, Xue Chen, Chenyu You, Xinhai Huang, Zhenhao Deng, and Shouhua Luo. A nonconvex model-based combined geometric calibration scheme for micro cone-beam ct with irregular trajectories. *Medical Physics*, 50(5):2759–2774, 2023.
- [232] Wan Mohd Hafiz bin Wan Hussin, Marshima Mohd Rosli, and Rosmawati Nordin. Review of traffic control techniques for emergency vehicles. *Indonesian Journal of Electrical Engineering and Computer Science*, 13(3):1243–1251, 2019.
- [233] Weiqi Yu, Weichen Bai, Wenjing Luan, and Liang Qi. State-of-the-art review on traffic control strategies for emergency vehicles. *IEEE Access*, 10:109729–109742, 2022.
- [234] Xiangyi Yan, Junayed Naushad, Chenyu You, Hao Tang, Shanlin Sun, Kun Han, Haoyu Ma, James S Duncan, and Xiaohui Xie. Localized region contrast for enhancing self-supervised learning in medical image segmentation. In *International Conference on Medical Image Computing and Computer-Assisted Intervention*, pages 468–478. Springer, 2023.

- [235] Guang Li, Longyin Ji, Chenyu You, Shuai Gao, Langrui Zhou, Keshu Bai, Shouhua Luo, and Ning Gu. Marganvac: metal artifact reduction method based on generative adversarial network with variable constraints. *Physics in Medicine & Biology*, 68(20):205005, 2023.
- [236] Homeland Infrastructure Foundation-Level Data (HIFLD). Hospitals and emergency medical services locations, 2024. Accessed: 2024-11-11.
- [237] Homeland Infrastructure Foundation-Level Data (HIFLD). Ems stations locations, 2024. Accessed: 2024-11-11.
- [238] New York City Office of Technology and Innovation. Nyc street centerline (cscl), 2014. Accessed: 2024-11-16.
- [239] USC Bureau. Census. gov. *Retrieved April, 25:2023*, 2023.
- [240] U.S. Census Bureau. 2023 census tracts shapefiles, 2023. Accessed: 2024-11-11.
- [241] U.S. Census Bureau. Acs 5-year estimates data profiles: Selected social characteristics in the united states, 2021, 2021. Accessed: 2024-11-11.
- [242] Karst T Geurs and Bert van Wee. Accessibility evaluation of land-use and transport strategies: Review and research directions. *Journal of Transport Geography*, 12(2):127–140, 2004.
- [243] National Fire Protection Association (NFPA). NFPA 1710: Standard for the Organization and Deployment of Fire Suppression Operations, Emergency Medical Operations, and Special Operations to the Public by Career Fire Departments. <https://www.nfpa.org/codes-and-standards/all-codes-and-standards/list-of-codes-and-standards/detail?code=1710>, 2020. Accessed: 2024-11-13.

- [244] LEED User. Intersection density as a proxy for community connectivity, 2023. Accessed: 2024-11-23.
- [245] New York City Department of Transportation. Vision zero: Speed limit reduction, 2014. Accessed: 2024-11-27.
- [246] Peter A Burrough, Rachael McDonnell, and C Lloyd. 8.11 nearest neighbours: Thiessen (dirichlet/voroni) polygons. *Principles of Geographical Information Systems*, pages pp–160, 2015.
- [247] Xiaodong Zhang and Masao Kuwahara. Modeling vehicle delays at intersections in urban traffic networks. *Transportation Research Part C: Emerging Technologies*, 15(6):359–371, 2007.
- [248] Laura Bieker-Walz, Michael Behrisch, and Marek Junghans. Analysis of the traffic behavior of emergency vehicles in a microscopic traffic simulation. *EPiC Series in Engineering*, 2:1–13, 2018.

Appendix A

Appendix for Chapter 1

In this appendix, we present the implementation details of the proposed EMVLight framework in Section A.1, the hyper-parameters selected for all RL-based methods in Section A.2, and the implementation of the emergency lane in SUMO in Section A.3.

A.1 Implementation Details

MDP time step. Although MDP step length can be arbitrarily small enough for optimality, traffic signal phases should be maintained a minimum amount of time so that vehicles and pedestrians can safely cross the intersections. To avoid rapid switching between the phases, we set our MDP time step length to be 5 seconds.

Implementation details for Non-emergency-capacitated/Emergency capacitated Synthetic Grid_{5×5}

- dimension of $s_{\mathcal{V}_i}^t$: $5 \times (8 + 8 + 4 + 2) = 110$
- dimension of $\tilde{s}_{\mathcal{V}_i}^t$: $5 \times (8 + 8 + 4 + 2) = 110$
- dimension of $\pi_{\mathcal{N}_i}^{t-1}$: $4 \times 8 = 32$

- Policy network $\pi_{\theta_i}(a_i^t | s_{\mathcal{V}_i}^t, \pi_{\mathcal{N}_i}^{t-1})$: $\text{concat} [110 \xrightarrow{\text{FC}} 128\text{ReLU}, 32 \xrightarrow{\text{FC}} 64\text{ReLU}] \rightarrow 64\text{LSTM} \xrightarrow{\text{FC}} 8\text{Softmax}$
- Value network $V_{\phi_i}(\tilde{s}_{\mathcal{V}_i}^t, \pi_{\mathcal{N}_i}^{t-1})$: $\text{concat} [110 \xrightarrow{\text{FC}} 128\text{ReLU}, 32 \xrightarrow{\text{FC}} 64\text{ReLU}] \rightarrow 64\text{LSTM} \xrightarrow{\text{FC}} 1\text{Linear}$
- Each link is $200m$. The free flow speed of the EMV is $12m/s$ and the free flow speed for non-EMVs is $6m/s$.
- Temporal discount factor γ is 0.99 and spatial discount factor α is 0.90.
- Initial learning rates η_{ϕ} and η_{θ} are both $1e-3$ and they decay linearly. Adam optimizer is used.
- MDP step length $\Delta t = 5s$ and for secondary pre-emption reward weight β is 0.5.
- Regularization coefficient is 0.01.

Implementation details for Manhattan_{16×3} The implementation is similar to the synthetic network implementation, with the following differences:

- Initial learning rates η_{ϕ} and η_{θ} are both $5e-4$.
- Since the avenues and streets are both one-directional, the number of actions of each agent are adjusted accordingly.
- Avenues and streets length are based on real Manhattan block size with each block of $80m \times 274m$.

Implementation details for Hangzhou_{4×4} The implementation is similar to the synthetic network implementation, with the following differences:

- Initial learning rates η_{ϕ} and η_{θ} are both $5e-4$.

- Streets length are based on real map of Hangzhou Gudang district.

A.2 Hyperparameters

We provide the the choice of hyper-parameters for RL-based methods in Table.A.1.

Hyper-parameters	CDRL	PL	CL	EMVLight
temporal discount		0.99		
batch size	32	128	128	128
buffer size	1e5	1e4	1e4	1e4
sample size	2048	1000	1000	1000
η and decay	0.5&0.975	0.8&0.95	0.8&0.95	0.8&0.95
optimizer	Adam	RMSprop	RMSprop	Adam
Learning rate	0.00025	1e-3	1e-3	1e-3
# Conv layers	1	-	3	-
# MLP layers	1	4	3	1
# MLP units	(168,168)	(32,32)	(32,32)	(192,1)
MLP Activation		ReLU		
Initialization		Random Normal		
step length ΔT		5 seconds		

Table A.1: Hyper-parameters selected for RL-based methods.

A.3 Emergency Lane in SUMO

With increased lateral resolution after enabling the sublane model, SUMO is able to simulates the virtual lane, i.e. emergency lane, formation for emergency traffic. Vehicles can drive between lanes under this mode. At the same time, we define the EMV as a *blue light device* to incorporate with the sublane model. Thus, we can observe that non-EMVs on the left would pull over towards the left side, i.e. `latAlignment="left"`, and non-EMVs on the right would pull over towards the right side, i.e., `latAlignment="right"`. When the EMV is traveling on the emergency lane, these vehicles do not perform lane changes and they do not move onto the emergency lane. After the EMV leaves this segments, these

vehicles resume normal driving and move back with their previous lateral alignment. These two SUMO built-in modules together is able to achieve our proposed emergency lane. See Fig. A.1 below from [248].

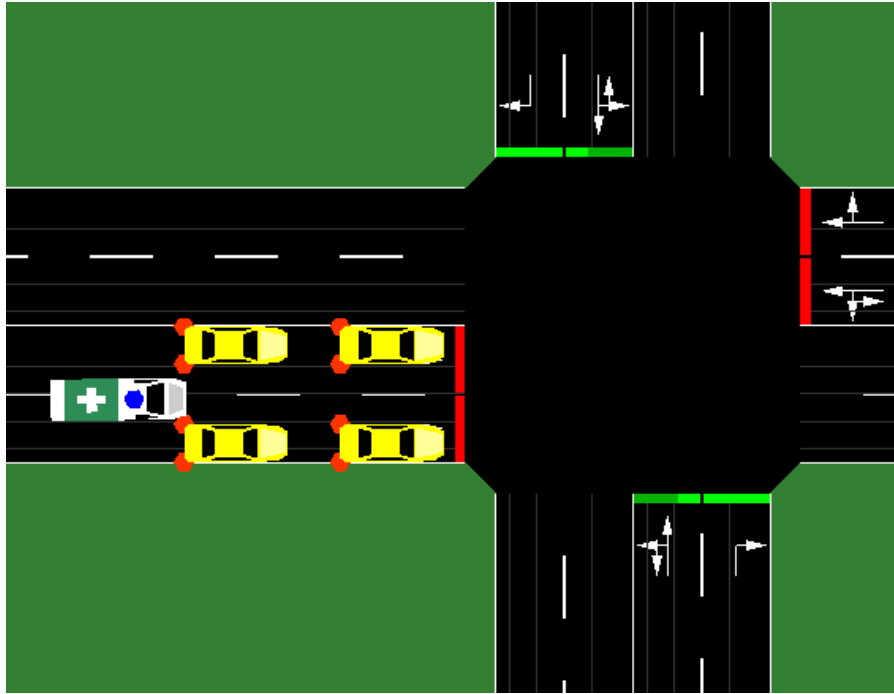


Figure A.1: A blue light device approaching an intersection with the sublane model activated.

Appendix B

Appendix for Chapter 2

In this appendix, we provide a comprehensive description of the network architectures for CAVs in Section B.1, along with the SUMO configurations and MAPPO-DQJL parameters detailed in Section B.2.

B.1 Network Details for CAVs

B.1.1 Policy Network

$$\pi_{\theta}(a_i | o_i) = \text{PolicyHead}(\text{TransformerEncoder}(\text{PositionalEncoding}(\text{Embedding}(o_i)))).$$

Architecture Overview (CAVs):

- **Input:** Observation o_i
- **Embedding Layer:** Dimension $d_{\text{model}} = 256$

- **Positional Encoding:** Spatial and temporal context
- **Transformer Encoder:**
 - Number of Layers: $N = 6$
 - Attention Heads: $h = 8$
 - Hidden Dimension: $d_{\text{hidden}} = 528$
 - Feed-Forward Dimension: $d_{\text{ff}} = 1024$
 - Activation: ReLU, Dropout Rate: 0.1
- **Policy Head:** Fully connected layer producing action probabilities

B.1.2 Centralized Value Network

$$V_{\phi}(s) = \text{ValueHead}(\text{TransformerEncoder}(\text{Embedding}(s))).$$

Architecture Overview (CAVs):

- **Input:** Global state s
- **Embedding Layer:** Dimension $d_{\text{model}} = 256$
- **Transformer Encoder:**
 - Number of Layers: $M = 6$
 - Attention Heads: $h = 8$
 - Hidden Dimension: $d_{\text{hidden}} = 512$
 - Feed-Forward Dimension: $d_{\text{ff}} = 2048$

- Activation: ReLU, Dropout Rate: 0.1

- **Value Head:** Fully connected layer producing a scalar value

B.1.3 Transformer Encoder Layer

Each transformer encoder layer operates over representations of dimension $d_{\text{model}} = 256$ (as adopted in the policy network design for CAVs) and comprises:

- **Multi-Head Attention:**
 - Number of Heads: $h = 8$
 - Key/Value Dimension per Head: $d_k = d_v = \frac{d_{\text{model}}}{h} = 32$

The output of the multi-head attention is projected back to $d_{\text{model}} = 256$.

- **Feed-Forward Network:** Two fully connected layers with $d_{\text{ff}} = 4096$ and ReLU activation.
- **Residual Connections:** Applied after both the multi-head attention and feed-forward sub-layers, improving gradient flow and stability.
- **Layer Normalization:** Applied to each sub-layer's output (after residual addition) to stabilize training dynamics.

B.1.4 Number of Parameters

Most parameters arise from the Transformer Encoder layers, each MHA and FFN sub-layers. For both the policy and value networks, MHA (with 8 heads and $d_{\text{model}} = 256$) requires four linear transformations (queries, keys, values, and output), each 256×256 , yielding about $4 \times 256 \times 256 \approx 262,000$ parameters per layer. In the policy network,

the FFN has $d_{\text{ff}} = 1024$, contributing $2 \times 256 \times 1024 \approx 524,000$ parameters per layer. Thus, each encoder layer adds roughly 786,000 parameters; for 6 layers, this is about 4.7 million parameters, plus a smaller amount for embeddings and the policy head.

In the value network, with $d_{\text{ff}} = 2048$, each layer's FFN has about $2 \times 256 \times 2048 \approx 1,048,000$ parameters. Combined with MHA, each layer adds approximately 1.31 million parameters; over 6 layers, around 7.9 million parameters in total, again plus modest contributions from embeddings and the value head.

B.2 SUMO Configurations

B.2.1 Car-Following Model

In SUMO, the car-following behavior of vehicles is modeled using the Intelligent Driver Model (IDM), which governs how a vehicle adjusts its speed based on the proximity and dynamics of the vehicle ahead. The acceleration $a(t)$ of a vehicle is defined as:

$$a(t) = a_{\text{max}} \left(1 - \left(\frac{v(t)}{v_0} \right)^4 - \left(\frac{s^*(v(t), \Delta v)}{s(t)} \right)^2 \right),$$

where a_{max} is the maximum achievable acceleration, $v(t)$ is the current speed, and v_0 denotes the desired (free-flow) speed. The variable $s(t)$ represents the current gap between the vehicle and the one immediately in front, while Δv is the speed difference between these two vehicles.

The desired gap $s^*(v(t), \Delta v)$ is given by:

$$s^*(v(t), \Delta v) = s_0 + v(t)T + \frac{v(t)\Delta v}{2\sqrt{a_{\text{max}}b}},$$

where s_0 is the minimum safety gap, T the desired time headway, and b the comfortable deceleration. By maintaining a safe following distance and adjusting speed in response to the leading vehicle, IDM ensures realistic and safe traffic flow dynamics.

In the context of DQJL formation, IDM serves as a baseline safety constraint. Both HDVs and CAVs adhere to IDM-based accelerations and distance requirements, guaranteeing that their interactions remain safe and well-coordinated even under dynamic and congested traffic conditions.

B.2.2 Lane-Changing Model

The lane-changing behavior in SUMO employs a rule-based framework that assesses both safety and incentive conditions prior to executing a maneuver. Safety is paramount, ensuring that a vehicle can merge into the target lane without inducing hazardous situations. The safety condition, accounting for deceleration capabilities and reaction times, is expressed as:

$$v(t) + bT \leq v_{\text{leader}}(t) \quad \text{and} \quad v_{\text{follower}}(t) + bT \leq v(t),$$

where $v_{\text{leader}}(t)$ and $v_{\text{follower}}(t)$ are the speeds of the leading and following vehicles in the target lane, respectively. The parameter b denotes the comfortable deceleration, while T represents the driver's reaction time or headway. These inequalities guarantee that both the merging vehicle and those in the target lane can safely adjust their speeds if necessary.

In addition to satisfying the safety condition, the lane change must offer a tangible incentive. A vehicle will opt to change lanes only if the anticipated speed in the target lane is substantially higher than in its current lane. This incentive criterion ensures that

maneuvers are not only safe, but also yield an improvement in travel efficiency, thereby supporting the formation of DQJLs without compromising overall traffic stability.

B.2.3 Parameters, Coefficients and Training Hyper-parameters for MAPPO-DQJL

Parameter	Description	Value	Units
<i>Car-Following (IDM) Parameters</i>			
s_0	Minimum safety gap	2.5	m
T	Desired time headway	1.2	s
v_0	Desired (free-flow) speed	20.0	m/s
a_{\max}	Maximum acceleration	1.5	m/s ²
b	Comfortable deceleration	2.5	m/s ²
<i>Lane-Changing Model Parameters (Same b and T as IDM)</i>			
<i>Global Reward Coefficients</i>			
α	Global-vs-Local reward balance	0.75	–
β_1	EMV time penalty weight	0.02	1/s
β_2	EMV lane-change penalty weight	1.0	1/(#lane changes)
β_3	DQJL completeness reward weight	1.0	1/m
<i>Local Reward Coefficients (CAVs)</i>			
η_1	CAV lane-change penalty weight	1.0	1/(#lane changes)
η_2	CAV acceleration penalty weight	0.2	1/(m/s ²)
<i>Local Reward Coefficients (HDVs)</i>			
η_3	HDV yield reward weight	1.0	1/(yield action)
<i>MDP and Discount Factor</i>			
γ	Future reward weighting	0.99	–
MDP Timestep	Simulation step per action	0.5	s
<i>Training Hyper-parameters</i>			
Learning Rate	Policy and Value Function Optimizer	1×10^{-4}	–
Batch Size	Number of samples per update	64	–
Horizon	Steps per rollout before update	1024	steps
PPO Epochs	Number of PPO update epochs per batch	10	–
Clip Range	PPO clip range for policy updates	0.2	–
GAE λ	Advantage estimation parameter	0.95	–

Table B.1: Parameter summary for MAPPO-DQJL simulations

Appendix C

Appendix for Chapter 3

C.1 Demographic maps

In this section, we present detailed population distribution maps based on data from the 2023 US Census [239]. Fig. C.1 illustrates the distribution of residents aged 65 years or older across NYC, while Fig. C.2 shows the median age for all census tracts. Fig. C.3 depicts the median income across NYC census tracts, and Fig. C.4 provides the poverty ratio distribution among residents in all census tracts.

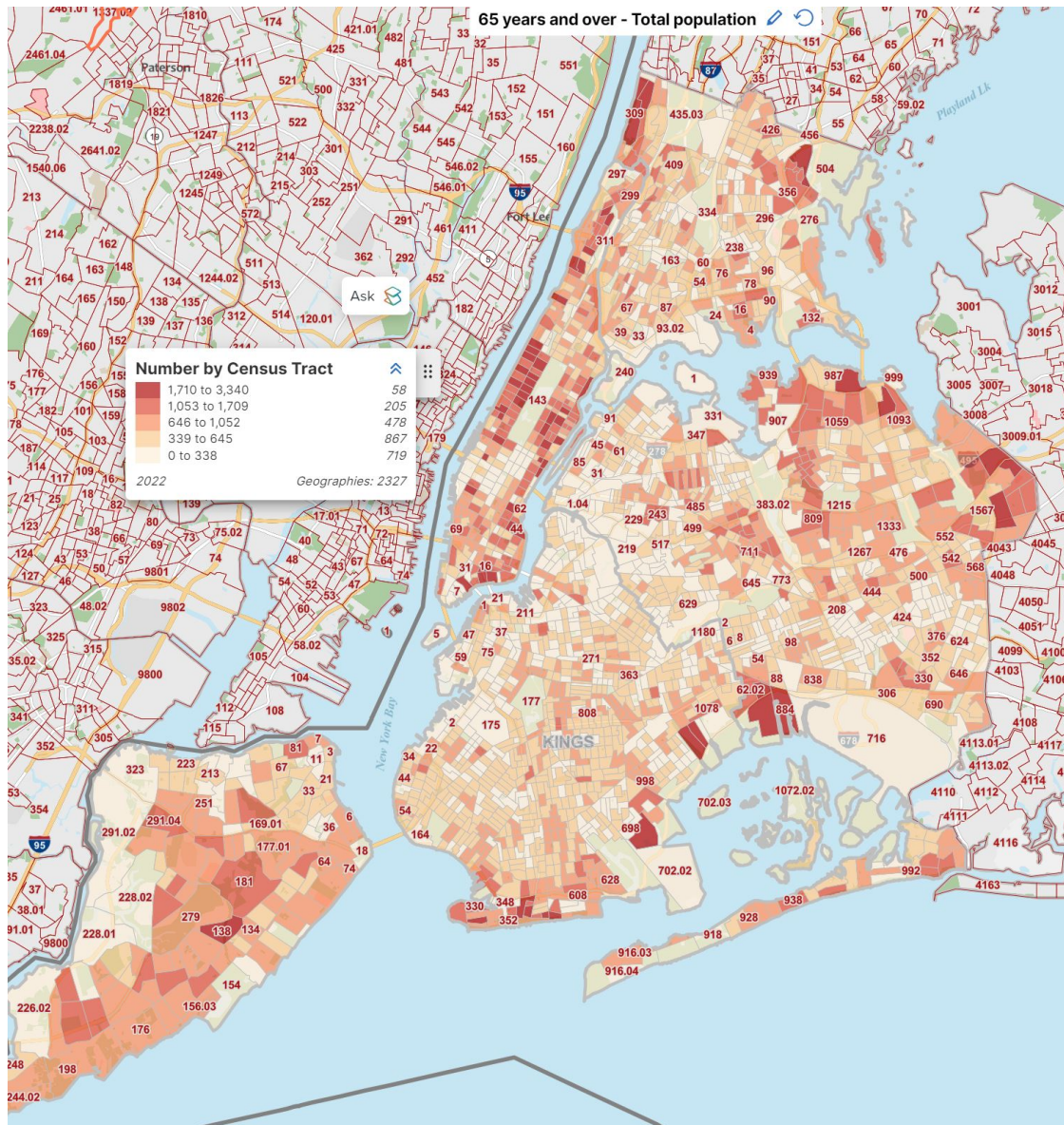


Figure C.1: Population of 65+ years old distribution of NYC census tracts

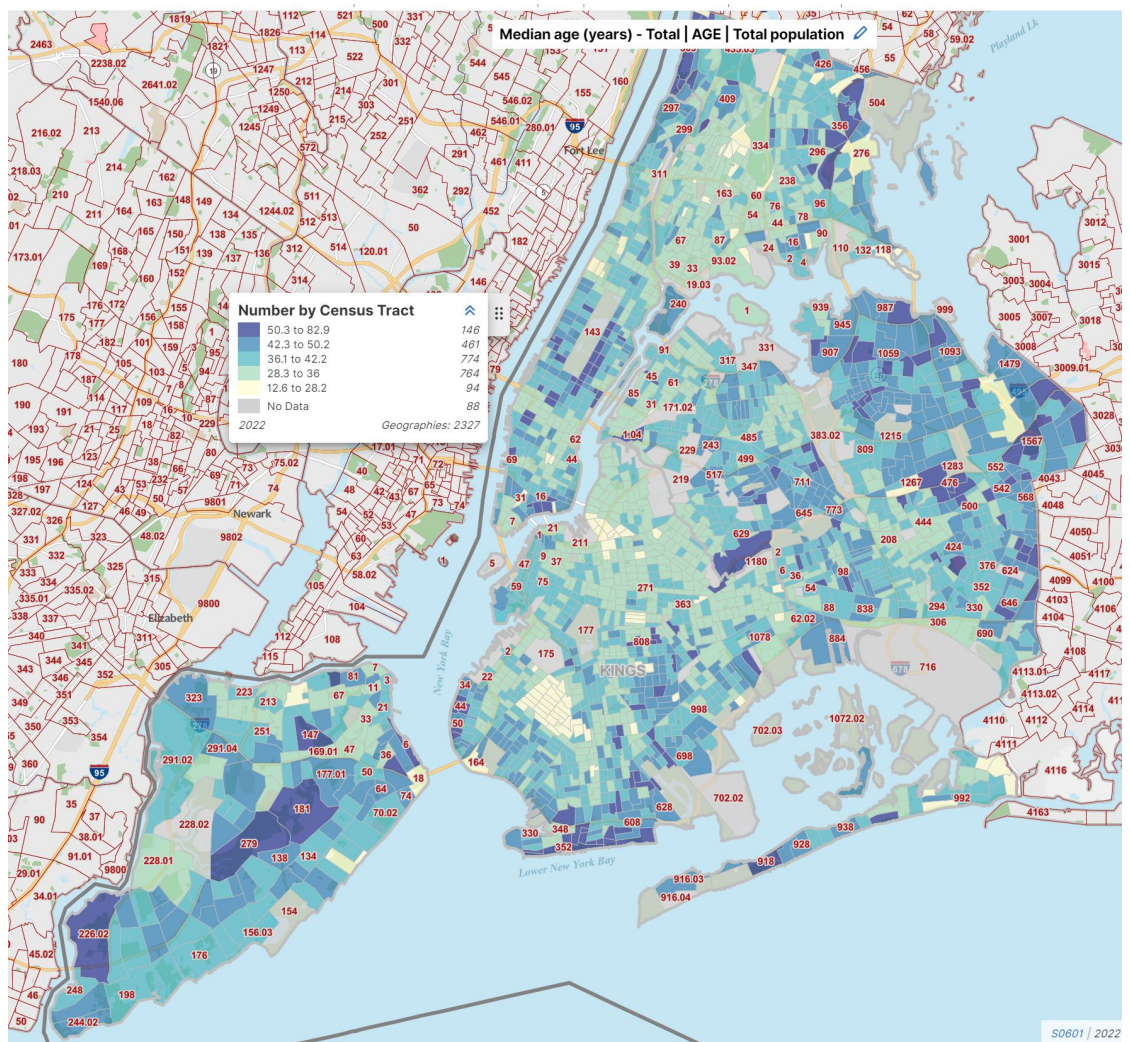


Figure C.2: Median age distribution of NYC census tracts.

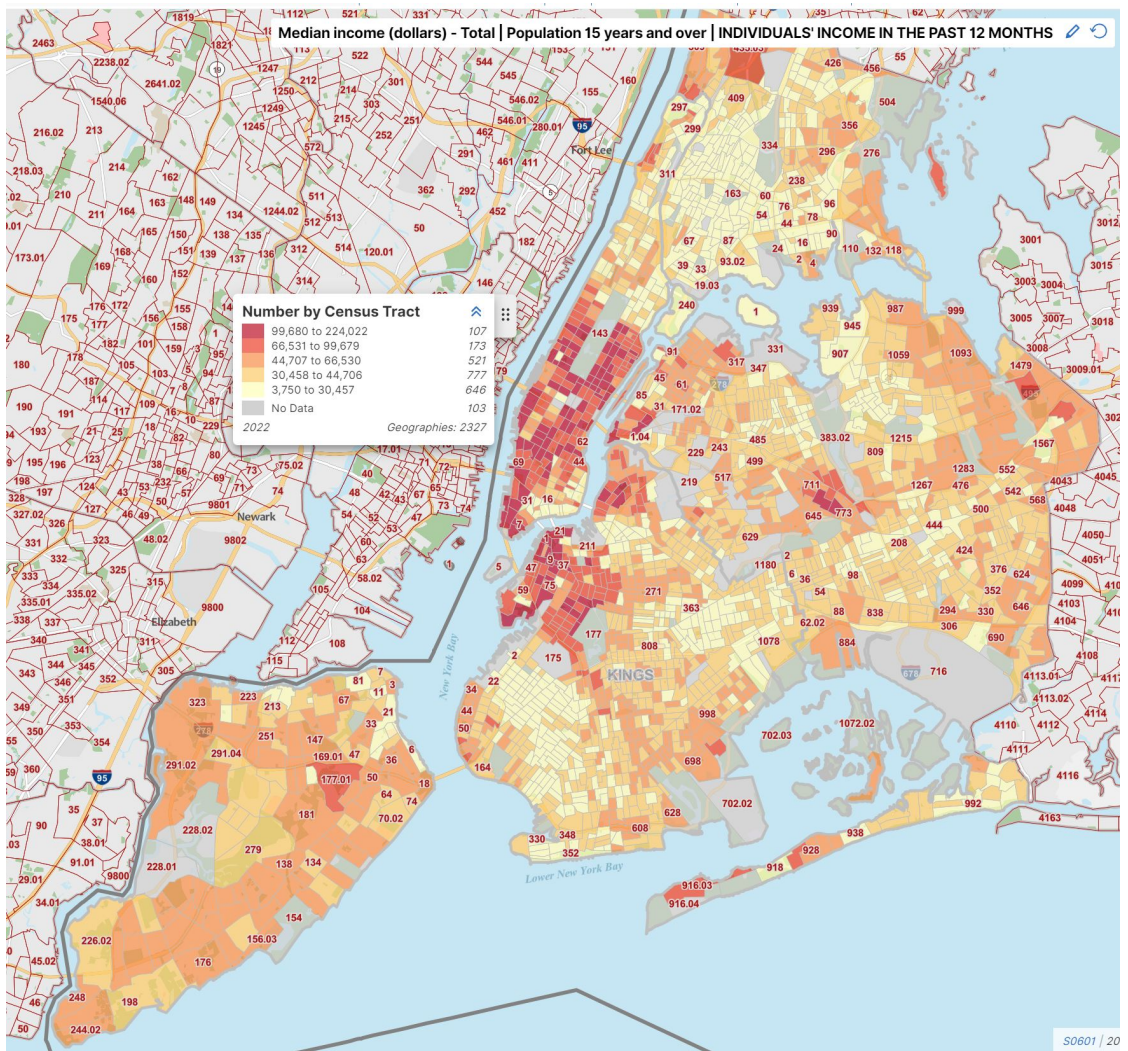


Figure C.3: Median income distribution of NYC census tracts

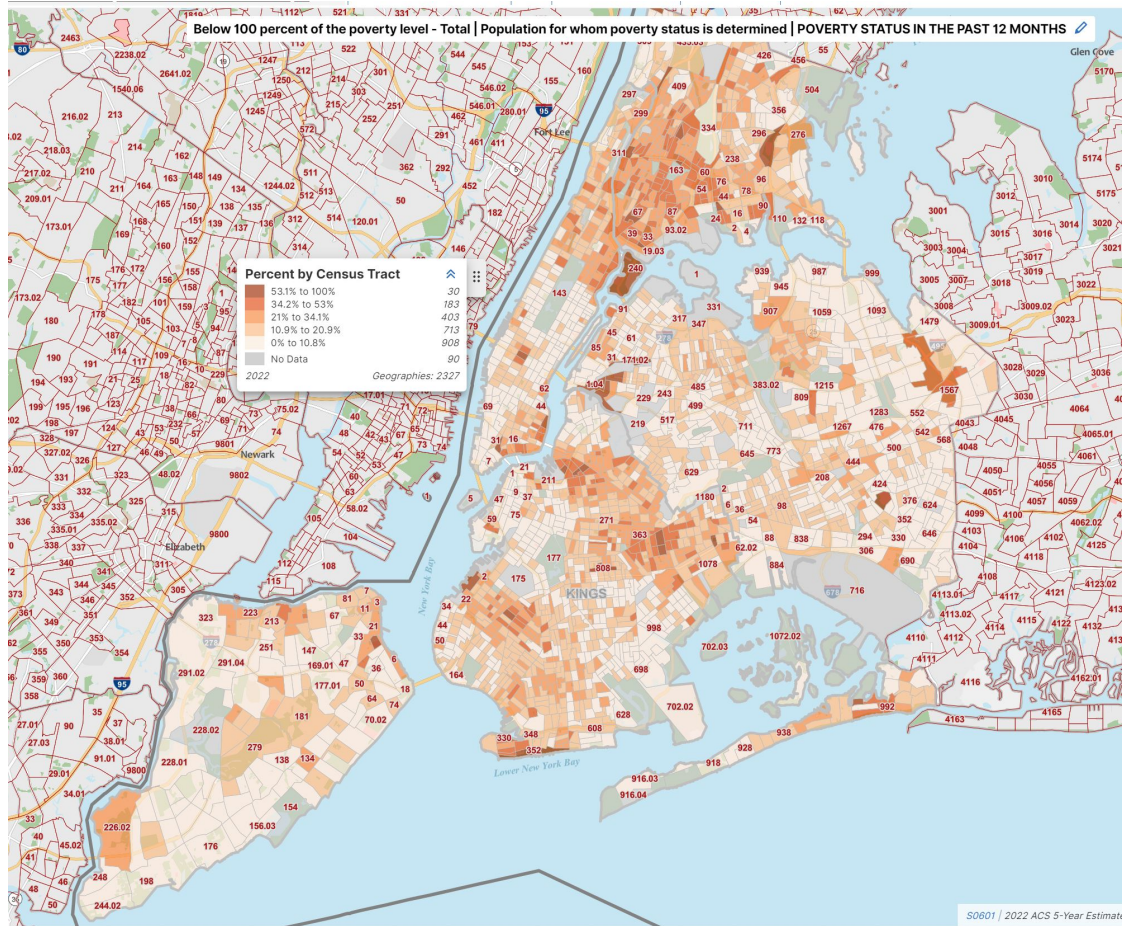


Figure C.4: Poverty percentage distribution of NYC census tracts